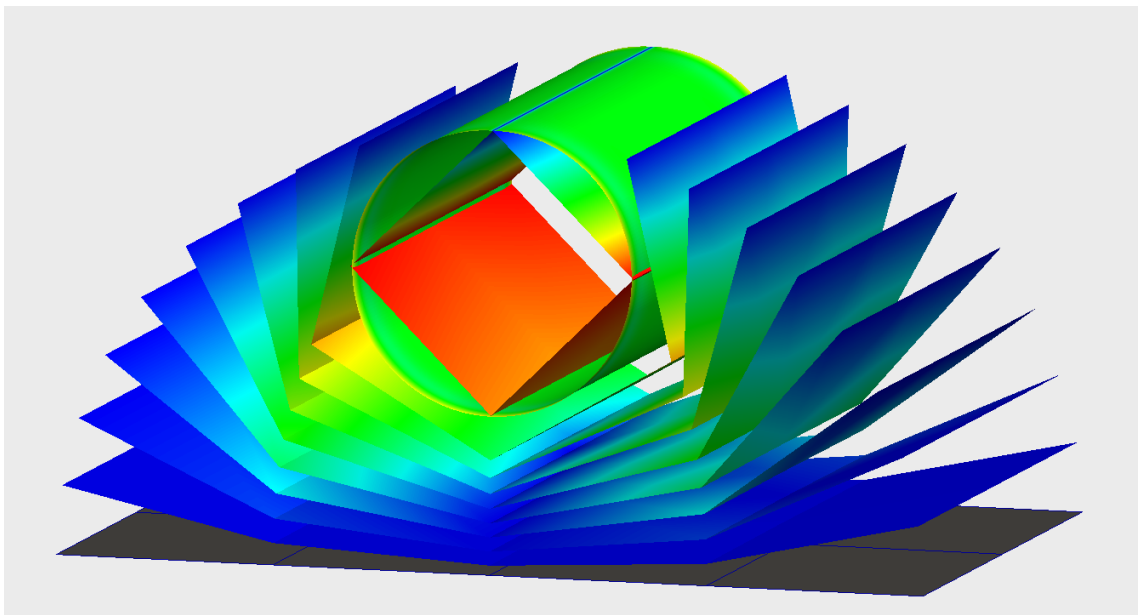# Kirchhoff Plates and Large Deformations
## – Modelling and C$^1$-continuous Discretization

Jens Rückert

Dissertation submitted to the

**Department of Mathematics**

at

**Chemnitz University of Technology**

in accordance with the requirements for the degree Dr. rer. nat.

Advisor: Prof. Dr. Arnd Meyer

Chemnitz,   24th April 2013

# Contents

# Acknowledgement

## Financial support

## Personal thanks

First and foremost I like to express my deep gratitude to my supervisor Prof. Dr. Arnd Meyer. He aroused my interest first for the FEM and later for plate deformations and he was always willing to give me advice and help. He offered me the opportunity to further my personal development and expertise. In addition, due to him, I was able to participate in different scientific conferences in Germany and abroad.

During my years at the university he was the most important person. Without him I would not have been able to develop this dissertation. Thank you, very much.

Furthermore I am much obliged to Prof. Dr. Bernd Luderer and to Dipl.-Math. Martin Stöcker for their efforts and their time spent in the revision of this thesis and for their advice.

Although they are not named separately, I thank all my colleagues at the Department of Mathematics for the inspiring discussions and explanations, by what I got an better overview of the mechanical background.

Moreover I owe a debt of gratitude to the members of staff of Fraunhofer ITWM in Kaiserslautern, who were partners in the mentioned BMBF project *GeoMec*. Particularly, I am indebted to Dr. Joachim Linn, whose suggestions and advice broadened my prospectives concerning my research.

Last but not least, I would express my sincerest gratitude to my whole family and my friends, who all gave me the support which I needed to author this work. Especially, I thank my parents Ines and Willy Rückert, which are the best parents I could imagine. Without them, I would not be the man, who I am, today. In addition I want to mention my parents-in-law, who gave me the opportunity to shorten my duty stroke enormously in the last months. Finally, my special thanks I extend to my wife Nadja, for her patience, for her continuing support and not at least for her great, infinite and unconditional love. At the end, my warmest words

are dedicated thankfully to my little daughter Arja, who brings unlimited pleasure and happiness into my life.

# 1 Introduction

In this thesis we present our research as a result of the joint project GeoMec (grant 05M10OCC) supported by the German Federal Ministry of Education and Research (BMBF). In this project, large deformations of plates and shells are investigated from different points of views. In that way, one project partner was examining a mathematical theory, where large deformations can be calculated very fast, possibly with low accuracy. Such methods are used, for example, in the animation of movements, which becomes an integral part in modern animation movies or in the computer game industry. Here, the main focus is on the simulation of movements in a way that it "looks good" but not necessarily expressing the full mechanical truth.

By contrast to that we pursue the goal of mechanical accuracy as best as possible. For this approach much more aspects have to be taken into account. So, the deformation is based on the minimization of the deformation energy. This especially concerns to some industrial project partners in automotive engineering. Here, for instance, the bending of car headliners during the manufacturing process is of interest.

For elasticity and deformations of plates or shells a very large number of literature exists. The roots of linear plate theory go back far into the past. First approaches have been made in the 17th century, but with some shortcomings (see [3]). Then in 1850 Kirchhoff has published his linear plate theory and is considered as the founder of modern plate theory. Quite nearly a century later, some extensions have been made by Reissner (1944/45) and Mindlin (1951) to include transverse shear. In the late seventies and eighties of the last century first non-linear plate theories were established for example by Ciarlet (see [9]). For that only linear material laws and so only small deformations were considered. A first approach for the calculation of large deformation of plates was the von Kármán plate. Due to the rapid development in the computer industry for the last 20 years, it is possible to compute more complex problems considering non-linear theories and non-linear material laws. Several approaches are found in [7]. In [14] the differential geometry is introduced in a similar way as here, following by a restriction to linearized strain. Here, the well known split of the total energy into a change of metric part and a change of curvature part is used. Furthermore, the resulting theory is only adopted to a cylindrical shell. Another approach one can find in [2]. Here, instead of the normal of the shell mid surface an arbitrary direction vector is considered first and a non-linear system of equations representing the equilibrium of forces is established. By the identification of the direction vector as the normal of the deformed mid surface the Kirchhoff hypothesis is assumed again. In the end the theory is constrained to linearized strain.

For our approach the Kirchhoff hypothesis is considered, too. By contrast with the theories in the cited articles, we do not linearize the strain tensor and maintain these non-linearities for its derivatives. Hence, the usual Kirchhoff assumption is the one and only restriction. No other simplifications are done.

Therefore, at the beginning we consider the well-established 3D-theory for large deformations. We discuss the inherent differential geometry and define the basic principles like the deformation gradient, the right Cauchy-Green deformation tensor or the Lagrangian strain tensor.

The equilibrium of forces corresponds to a minimum of an appropriate energy functional, which is considered here. Its first derivative leads to the weak formulation of the non-linear boundary value problem. For its solution we have to apply some linearizations such as Newton's method.

In the third chapter Newton's method is explained and the incremental Newton algorithm is given for the approximation of a resulting deformation. In this algorithm the second derivative of the energy functional plays an important role. For the full 3D case it can be calculated comparatively easy.

We discuss the differential geometry for a shell and its simplification to a plate in the fourth chapter. Generally, in the shell theory the displacement of the mid surface is considered and then amplified to the whole plate. In our research the Kirchhoff assumption is used for that. As a result a strain tensor of lower rank (rank 2) occurs (mapping the tangential space into itself).

Furthermore, the emerging displacement vector depends on the displacement vector of the mid surface. Therefore, in Chapter 5 we establish the resulting energy functional, which only depends on this mid surface displacement vector. The boundary conditions are considered for hard and soft clamped shells.

For examining the weak formulation of the plate deformation problem the first derivative of the energy functional is determined, which is now more complicated than in the full 3D-theory.

For the resulting energy functional the thickness dependence is not eliminable as usually in using linear strain, but the unknown vector function $\boldsymbol{U}$ only depends on $(\eta^1, \eta^2)$, thus not on the thickness parameter $\tau$. Therefore, we can use the 2D-FEM for its approximation on the mid surface and we have to integrate numerically over thickness direction $\tau$. So, in Chapter 6 we deduce the second derivative of the energy functional and take a closer examination of the difficulties in its calculation. With this second derivative the Newton algorithm is established, which is integrated into the F.E.-solution process. The method and both kinds of considered $C^1$-elements, the BFS- and the reduced HCT-element, are explained. A very short excursion in the field of efficient solvers follows, before we go into details of the implementation. A short discussion about the use of Newton's method in the approximation process brings Chapter 6 to an end.

After that we present two deflection examples, one using the BFS-elements and one the reduced HCT-elements. Subsequently we take a closer look to bending problems, which was the main focus of this work. For that, in the seventh chapter four examples of bending-dominated large plate deformations are presented, using

BFS-elements. These are followed by further two bending-dominated examples using reduced HCT-elements, simulating really large deformations.

This thesis ends up with a reflection of the main results of our work and a prospect of further key aspects of research.

# 2 The deformation problem in the three-dimensional space

In the following we consider vectors or vector fields written as bold capital or lower case letters, respectively. Furthermore a vector is also called a first-order tensor. Then we understand second-order tensors as linear maps of first-order tensors onto first-order tensors, again. For the beginning a pair of first-order tensors such as $\boldsymbol{A}^1\boldsymbol{A}^2$ is understood as a second-order tensor. In general a second-order tensor is any linear combination of such pairs.

Below, some linear operations for the tensor calculus are defined:

(1) The mapping properties, applying a second-order tensor onto a (three-dimensional) vector function $\boldsymbol{U}$ or the other way around, respectively:

$$(\boldsymbol{A}^1\boldsymbol{A}^2)\cdot\boldsymbol{U} = \boldsymbol{A}^1(\boldsymbol{A}^2\cdot\boldsymbol{U})$$
$$\boldsymbol{U}\cdot(\boldsymbol{A}^1\boldsymbol{A}^2) = \boldsymbol{A}^2(\boldsymbol{A}^1\cdot\boldsymbol{U}).$$

(2) The tensor multiplication as a linear mapping of a second-order tensor onto a second-order tensor, again:

$$(\boldsymbol{A}^1\boldsymbol{A}^2)\cdot(\boldsymbol{A}^3\boldsymbol{A}^4) = (\boldsymbol{A}^2\cdot\boldsymbol{A}^3)(\boldsymbol{A}^1\boldsymbol{A}^4).$$

(3) The trace of a second-order tensor is a scalar function

$$\mathrm{tr}(\boldsymbol{A}^1\boldsymbol{A}^2) = \boldsymbol{A}^1\cdot\boldsymbol{A}^2.$$

(4) The transpose of a second-order tensor is given by

$$(\boldsymbol{A}^1\boldsymbol{A}^2)^\top = (\boldsymbol{A}^2\boldsymbol{A}^1).$$

(5) The double contraction of second-order tensors is a scalar function

$$(\boldsymbol{A}^1\boldsymbol{A}^2):(\boldsymbol{A}^3\boldsymbol{A}^4) = \mathrm{tr}\left((\boldsymbol{A}^1\boldsymbol{A}^2)\cdot(\boldsymbol{A}^3\boldsymbol{A}^4)\right)$$
$$= (\boldsymbol{A}^2\cdot\boldsymbol{A}^3)(\boldsymbol{A}^1\cdot\boldsymbol{A}^4).$$

In general, the definitions in (1) to (5) are true for every second-order tensor, because all five definitions above are linear operations.

In the same way we use fourth-order tensors mapping second-order tensors onto second-order tensors via the double contraction (5).

Note that in general a fourth-order tensor is a linear combination of such four-tuple of vectors or of pairs of second-order tensors.

Throughout this paper capital letters are used for second-order tensors, displayed in a flowing font. Vectors are written in bold and matrices in underlined letters. Due to the fact that we consider large deformations, we have to distinguish between the undeformed and the deformed configuration of the considered body using capital and lower case letters, respectively. This is mainly used for the basis vectors.

## 2.1 General differential geometry of deformation in the three-dimensional space

In this section basic facts of differential geometry for the three-dimensional Euclidean space are presented, following [19].

A domain $\Omega_0$ in the Euclidean space is parametrized as

$$\Omega_0 = \{\boldsymbol{X}(\eta) : \eta \in \mathcal{P} \subset \mathbb{R}^3\}, \tag{2.1}$$

where $\boldsymbol{X}$ denotes the position of a material point in the undeformed body under consideration. Herein, $\eta = (\eta^1, \eta^2, \eta^3)$ is a given, possibly curvilinear coordinate system. $\eta^1, \eta^2$ and $\eta^3$ are called the coordinates of the point $\boldsymbol{X}$.

Note that

$$\boldsymbol{X} \longleftrightarrow \eta = (\eta^1, \eta^2, \eta^3) \tag{2.2}$$

is a unique map between the position of a point and its coordinates.

Thus, for every point $\boldsymbol{X}$ in the domain $\Omega_0$ (2.1) the vectors

$$\boldsymbol{G}_i = \frac{\partial}{\partial \eta^i} \boldsymbol{X}, \ \ i = 1, \ldots, 3, \tag{2.3}$$

form the co-variant tensor basis.

The elements of the matrix

$$\underline{G} = (G_{ij})_{i,j=1}^3, \ \ G_{ij} = \boldsymbol{G}_i \cdot \boldsymbol{G}_j, \ \ i, j = 1, \ldots, 3, \tag{2.4}$$

are called metric coefficients of the tensor basis.

At any co-variant tensor basis $\boldsymbol{G}_i$ there exists a contra-variant tensor basis $\boldsymbol{G}^j$ defined in such a way that

$$\boldsymbol{G}_i \cdot \boldsymbol{G}^j = \delta_i^j, \ \ i, j = 1, \ldots, 3.$$

$\delta_i^j$ describes the so-called Kronecker-symbol. Let $G^{ij} = \boldsymbol{G}^i \cdot \boldsymbol{G}^j$, then the equality $\underline{G}^{-1} = (G^{ij})_{i,j=1}^3$, is true.

From now on we use the Einstein summation convention. For this, the indices in this chapter run from 1 to 3. Later on, when the shell theory is considered, the indices will run from 1 to 2, only.

So, the gradient operator is defined by

$$\text{Grad} = \boldsymbol{G}^i \frac{\partial}{\partial \eta^i}. \tag{2.5}$$

If we apply the gradient operator (2.5) to a given function $\mu(\eta)$, we obtain a first-order tensor $\text{Grad } \mu = \boldsymbol{G}^i \frac{\partial}{\partial \eta^i} \mu$. In the same way, we have a second-order tensor $\text{Grad } \boldsymbol{U}(\eta) = \boldsymbol{G}^i \frac{\partial}{\partial \eta^i} \boldsymbol{U} = \boldsymbol{G}^i \boldsymbol{U}_{,i}$, if we apply (2.5) to the vector function $\boldsymbol{U}(\eta) \in \Omega_0$. Here and in the following we use the abbreviation $\boldsymbol{U}_{,i}$ for the partial derivatives $\frac{\partial}{\partial \eta^i} \boldsymbol{U}, \; i = 1, \ldots, 3$.

Let a deformation be described by the isomorphism

$$\omega : \Omega_0 \mapsto \Omega, \quad \boldsymbol{x} = \omega(\boldsymbol{X}). \tag{2.6}$$

Then we introduce a vector field $\boldsymbol{U}$ of displacement vectors. The position of a material point in the deformed body can now be identified as

$$\boldsymbol{x} = \boldsymbol{X} + \boldsymbol{U} : \Omega_0 \mapsto \Omega. \tag{2.7}$$

Here $\Omega$ denotes the deformed domain.

The displacement vector $\boldsymbol{U}$ is a vector function at the point $\boldsymbol{X}$ out of the undeformed domain $\Omega_0$ (2.1). Due to the dependency of the point $\boldsymbol{X}$ on $\eta$, the function $\boldsymbol{U}$ depends on $\eta$ as well. So $\boldsymbol{x}(\eta)$ is a parametrization of the deformed domain $\Omega$.

Again, we assume

$$\boldsymbol{x} \longleftrightarrow \eta = (\eta^1, \eta^2, \eta^3) \tag{2.8}$$

to be a unique mapping between the material point of the deformed body and its coordinates. Therefore, with the parametrization (2.7) of $\Omega$, we can denote a co-variant and a contra-variant tensor basis again:

Let

$$\boldsymbol{g}_i = \frac{\partial}{\partial \eta^i} \boldsymbol{x}, \quad i = 1, \ldots, 3,$$

be the basis vectors belonging to the co-variant tensor basis in $\Omega$. Then, there exists a contra-variant tensor basis $\boldsymbol{g}^j, \; j = 1, \ldots, 3$, such that $\boldsymbol{g}_i \cdot \boldsymbol{g}^j = \delta_i^j, \; i, j = 1, \ldots, 3$.

The co-variant tensor basis of the deformed domain $\Omega$ is connected to the co-variant tensor basis of the initial domain $\Omega_0$ via the displacement vector field $\boldsymbol{U}$:

$$\boldsymbol{g}_i = \frac{\partial}{\partial \eta^i} \boldsymbol{x} = \frac{\partial}{\partial \eta^i}(\boldsymbol{X} + \boldsymbol{U}) = \boldsymbol{G}_i + \frac{\partial}{\partial \eta^i} \boldsymbol{U} = \boldsymbol{G}_i + \boldsymbol{U}_{,i}, \tag{2.9}$$

and the gradient operator in the deformed domain $\Omega$ is defined analogously to (2.5):

$$\text{grad} = \boldsymbol{g}^i \frac{\partial}{\partial \eta^i}.$$

Obviously a Taylor expansion of the isomorphism (2.6) is supposed to be such that

$$\omega(\boldsymbol{X} + \boldsymbol{V}) = \omega(\boldsymbol{X}) + \mathcal{F} \cdot \boldsymbol{V} + \mathcal{O}(\|\boldsymbol{V}\|^2)$$

with a linear operator $\mathcal{F}$ (a second-order tensor) applied to any (small) direction $\boldsymbol{V}$. Furthermore from definition (2.5) we have

$$\omega(\boldsymbol{X} + \boldsymbol{V}) = \omega(\boldsymbol{X}) + \boldsymbol{V} \cdot \text{Grad}(\omega) + \mathcal{O}(\|\boldsymbol{V}\|^2).$$

Hence,

$$\begin{aligned}
\mathcal{F} &= (\text{Grad } \omega)^\top = (\text{Grad}(\boldsymbol{X} + \boldsymbol{U}))^\top \\
&= [\boldsymbol{G}^i \boldsymbol{G}_i + \boldsymbol{G}^i \boldsymbol{U}_{,i}]^\top \\
&= \mathcal{I} + (\text{Grad}(\boldsymbol{U}))^\top
\end{aligned}$$

denotes the so called **deformation gradient**.
($\mathcal{I}$ is the identity map, the second-order identity tensor.)

With (2.9) we have

$$\begin{aligned}
\mathcal{F} \cdot \boldsymbol{G}_k &= \boldsymbol{G}_k + \boldsymbol{U}_{,i} \boldsymbol{G}^i \cdot \boldsymbol{G}_k \\
&= \boldsymbol{G}_k + \boldsymbol{U}_{,k} = \boldsymbol{g}_k \\
&= \boldsymbol{G}_k \cdot \mathcal{F}^\top.
\end{aligned} \tag{2.10}$$

Hence $\mathcal{F} = \boldsymbol{g}_i \boldsymbol{G}^i \Rightarrow \mathcal{F}^\top = \boldsymbol{G}^i \boldsymbol{g}_i$ and $\mathcal{F}^{-1} = \boldsymbol{G}_i \boldsymbol{g}^i$.
The right Cauchy-Green deformation tensor is defined as

$$\mathcal{C} = \mathcal{F}^\top \cdot \mathcal{F} = \mathcal{I} + \text{Grad}(\boldsymbol{U}) + \text{Grad}(\boldsymbol{U})^\top + \text{Grad}(\boldsymbol{U}) \cdot \text{Grad}(\boldsymbol{U})^\top \tag{2.11}$$

and the Lagrangian strain tensor as

$$\begin{aligned}
\mathcal{E} &= \frac{1}{2}(\mathcal{F}^\top \cdot \mathcal{F} - \mathcal{I}) \\
&= \frac{1}{2}\left(\text{Grad}(\boldsymbol{U}) + \text{Grad}(\boldsymbol{U})^\top + \text{Grad}(\boldsymbol{U}) \cdot \text{Grad}(\boldsymbol{U})^\top\right).
\end{aligned} \tag{2.12}$$

Note that both $\mathcal{C}$ and $\mathcal{E}$ are symmetric tensors.

**Remark 2.1** *From (2.10) we have*

$$\begin{aligned}
[\boldsymbol{g}_1, \boldsymbol{g}_2, \boldsymbol{g}_3] &= [\mathcal{F} \cdot \boldsymbol{G}_1, \mathcal{F} \cdot \boldsymbol{G}_2, \mathcal{F} \cdot \boldsymbol{G}_3] \\
&= \det \mathcal{F}[\boldsymbol{G}_1, \boldsymbol{G}_2, \boldsymbol{G}_3].
\end{aligned} \tag{2.13}$$

*On the strength of (2.2) and of (2.8), respectively, we have*

$$[\boldsymbol{G}_1, \boldsymbol{G}_2, \boldsymbol{G}_3] \neq 0$$

*and*

$$[\boldsymbol{g}_1, \boldsymbol{g}_2, \boldsymbol{g}_3] \neq 0.$$

*Hence, with the constants $\underline{c}$ and $\overline{c}$*

$$0 < \underline{c} \leq \det \mathcal{F} \leq \overline{c} \ \forall \ \eta \in \mathcal{P} \tag{2.14}$$

*is the main assumption on our deformation.*

**Remark 2.2** *We consider vector fields $\boldsymbol{V}(\eta)$ as functions over $\Omega_0$ as well as over $\Omega$. Such a vector field can be considered to be in both $(L_2(\Omega_0))^3$ and $(L_2(\Omega))^3$, respectively, due to (2.14) together with the volume elements*

$$d\Omega_0 = [\boldsymbol{G}_1, \boldsymbol{G}_2, \boldsymbol{G}_3] \, d\eta^1 d\eta^2 d\eta^3$$

*and*

$$d\Omega = [\boldsymbol{g}_1, \boldsymbol{g}_2, \boldsymbol{g}_3] \, d\eta^1 d\eta^2 d\eta^3.$$

*Obviously, with (2.13) the volume element of the deformed domain, $d\Omega$, can be represented by the product of the determinant of $\mathcal{F}$ with the volume element of the undeformed domain, $d\Omega_0$.*

*(1) Hence*

$$\boldsymbol{V}(\eta) \in \left(L_2(\Omega)\right)^3 \iff \boldsymbol{V}(\eta) \in \left(L_2(\Omega_0)\right)^3, \tag{2.15}$$

*because*

$$\int_\Omega \boldsymbol{V} \cdot \boldsymbol{V} \, d\Omega = \int_\Omega \boldsymbol{V} \cdot \boldsymbol{V} \, [\boldsymbol{g}_1, \boldsymbol{g}_2, \boldsymbol{g}_3] \, d\eta^1 d\eta^2 d\eta^3$$

$$= \int_{\Omega_0} \boldsymbol{V} \cdot \boldsymbol{V} \, \det \mathcal{F} \, [\boldsymbol{G}_1, \boldsymbol{G}_2, \boldsymbol{G}_3] \, d\eta^1 d\eta^2 d\eta^3.$$

*With (2.14) we have*

$$\|\boldsymbol{V}\|^2_{L_2(\Omega)} \sim \|\boldsymbol{V}\|^2_{L_2(\Omega_0)}$$

*and both function spaces have the same set of vector functions $\boldsymbol{V}(\eta)$.*

*(2) Furthermore the same is true for $\mathbb{H}^1$ vector fields:*

$$\boldsymbol{V}(\eta) \in \left(\mathbb{H}^1(\Omega_0)\right)^3 \iff \boldsymbol{V}(\eta) \in \left(\mathbb{H}^1(\Omega)\right)^3.$$

*For the half norm we have*

$$\int\limits_{\Omega} (\operatorname{grad} \boldsymbol{V})^\top : (\operatorname{grad} \boldsymbol{V})\, d\Omega$$

$$= \int\limits_{\Omega_0} (\mathcal{F}^{-\top} \cdot \operatorname{Grad} \boldsymbol{V})^\top : (\mathcal{F}^{-\top} \cdot \operatorname{Grad} \boldsymbol{V}) \det \mathcal{F}\, d\Omega_0$$

$$= \int\limits_{\Omega_0} \operatorname{tr}\left((\operatorname{Grad} \boldsymbol{V})^\top \cdot (\mathcal{F}^{-1} \cdot \mathcal{F}^{-\top}) \cdot (\operatorname{Grad} \boldsymbol{V})\right) \det \mathcal{F}\, d\Omega_0$$

$$= \int\limits_{\Omega_0} \operatorname{tr}\left((\operatorname{Grad} \boldsymbol{V})^\top \cdot \mathcal{C}^{-1} \cdot (\operatorname{Grad} \boldsymbol{V})\right) \det \mathcal{F}\, d\Omega_0.$$

*Due to equation (2.14), there exist two constants $0 < \underline{\gamma} < \overline{\gamma}$ such that in sense of positive definiteness*

$$\underline{\gamma}\mathcal{I} \leq \mathcal{F}^\top \cdot \mathcal{F} = \mathcal{C} \leq \overline{\gamma}\mathcal{I}$$

*and therefore*

$$\frac{1}{\overline{\gamma}}\mathcal{I} \leq \mathcal{F}^{-1} \cdot \mathcal{F}^{-\top} = \mathcal{C}^{-1} \leq \frac{1}{\underline{\gamma}}\mathcal{I}$$

*are true.*

*Hence, together with (2.15) we obtain*

$$\|\boldsymbol{V}\|^2_{\mathbb{H}^1(\Omega)} \sim \|\boldsymbol{V}\|^2_{\mathbb{H}^1(\Omega_0)}$$

*and both function spaces have the same set of vector functions $\boldsymbol{V}(\eta)$ again.*

## 2.2 Equilibrium of forces

We assume all force interactions being a result of the volume load and of the surface load. In the equilibrium of forces all these forces and moments compensate each other. Hence, after a deformation all forces and moments have to be balanced in the deformed domain $\Omega$ as well. Cauchy's theorem guarantees the existence of the so-called Cauchy stress tensor $\sigma$. The volume load is displayed by the volume force density $\rho p(\eta)$ in such a way that the equation

$$\operatorname{div} \sigma(\boldsymbol{x}) + \rho p(\boldsymbol{x}) = \boldsymbol{0} \ \forall \ \boldsymbol{x} \in \Omega \tag{2.16}$$

is true. Generally, the divergence operator $\operatorname{div} \sigma$ is defined as

$$\operatorname{div} \sigma = \boldsymbol{g}^i \cdot \frac{\partial}{\partial \eta^i} \sigma.$$

The proof of Cauchy's theorem and some more information can be found, for example, in [11].

To set up the weak formulation for the Finite Element Method (FEM) we have to multiply equation (2.16) with any vector function $\boldsymbol{V}$ and to integrate over the deformed domain $\Omega$.

Hence, for a special function space

$$\mathbb{H} := \left\{ \left( \mathbb{H}^1(\Omega_0) \right)^3 \text{ with additional boundary conditions} \right\}$$

we have to solve the integral equation

$$\int_\Omega \operatorname{div} \sigma \cdot \boldsymbol{V} + \rho p \cdot \boldsymbol{V} \; d\Omega = 0 \;\; \forall \, \boldsymbol{V}(\eta) \in \mathbb{H}.$$

Then integration by parts yields

$$\int_\Omega \sigma : \operatorname{grad} \boldsymbol{V}^\top \; d\Omega = \int_\Omega \rho p \cdot \boldsymbol{V} \; d\Omega + \int_{\partial\Omega} \boldsymbol{n} \cdot \sigma \cdot \boldsymbol{V} \; d\mathcal{S}. \tag{2.17}$$

Here $\partial\Omega$ describes the boundary of the deformed domain $\Omega$ and $d\mathcal{S}$ the surface element.

For the usual pullback into the initial configuration $\Omega_0$ we need one of both tensors, the first Piola-Kirchhoff stress tensor $\overset{1}{\mathcal{T}}$ or the second Piola-Kirchhoff stress tensor $\overset{2}{\mathcal{T}}$ with

$$(\det \mathcal{F})\sigma = \mathcal{F} \cdot \overset{1}{\mathcal{T}} = \mathcal{F} \cdot \overset{2}{\mathcal{T}} \cdot \mathcal{F}^\top.$$

While $\overset{1}{\mathcal{T}}$ is an unsymmetrical second-order tensor, the second-order tensor $\overset{2}{\mathcal{T}}$ is symmetric, which gives some advantages in the tensor analysis.

Let us now take a look at each of the three integrals in (2.17) separately, following the explanations in [19].

$$\int_\Omega \sigma : \operatorname{grad} \boldsymbol{V}^\top \; d\Omega = \int_{\Omega_0} J\sigma : \operatorname{grad} \boldsymbol{V}^\top \; d\Omega_0$$

$$= \int_{\Omega_0} (\mathcal{F} \cdot \overset{1}{\mathcal{T}}) : (\operatorname{Grad} \boldsymbol{V}^\top \cdot \mathcal{F}^{-1}) \; d\Omega_0$$

$$= \int_{\Omega_0} \overset{1}{\mathcal{T}} : \operatorname{Grad} \boldsymbol{V}^\top \; d\Omega_0 \tag{2.18}$$

$$= \int_{\Omega_0} \overset{2}{\mathcal{T}} : (\mathcal{F}^\top \cdot \operatorname{Grad} \boldsymbol{V}^\top) \; d\Omega_0$$

$$= \int_{\Omega_0} \overset{2}{\mathcal{T}} : (\mathcal{I} + \operatorname{Grad} \boldsymbol{U}) \cdot \operatorname{Grad} \boldsymbol{V}^\top \; d\Omega_0 \;\; \forall \, \boldsymbol{V}(\eta) \in \mathbb{H}.$$

Because of the symmetry of $\overset{2}{\mathcal{T}}$ and from equation (2.18) we have

$$\int_{\Omega_0} \overset{2}{\mathcal{T}} : (\mathcal{I} + \operatorname{Grad} \boldsymbol{U}) \cdot \operatorname{Grad} \boldsymbol{V}^\top \, d\Omega_0$$

$$= \int_{\Omega_0} \overset{2}{\mathcal{T}} : [(\mathcal{I} + \operatorname{Grad} \boldsymbol{U}) \cdot \operatorname{Grad} \boldsymbol{V}^\top]^\top \, d\Omega_0 \qquad (2.19)$$

$$= \int_{\Omega_0} \overset{2}{\mathcal{T}} : \mathcal{E}'(\boldsymbol{U}; \boldsymbol{V}) \, d\Omega_0 \ \forall \, \boldsymbol{V}(\eta) \in \mathbb{H}.$$

Obviously $\mathcal{E}'(\boldsymbol{U}; \boldsymbol{V})$ is the Fréchet derivative of $\mathcal{E}(\boldsymbol{U})$ applied to $\boldsymbol{V}$:

$$2\mathcal{E}(\boldsymbol{U}) = \mathcal{F}^\top \cdot \mathcal{F} - \mathcal{I} = (\mathcal{I} + \operatorname{Grad} \boldsymbol{U})^\top \cdot (\mathcal{I} + \operatorname{Grad} \boldsymbol{U}) - \mathcal{I}.$$

Therefore,

$$2\mathcal{E}(\boldsymbol{U} + \boldsymbol{V}) = 2\mathcal{E}(\boldsymbol{U}) + \operatorname{Grad} \boldsymbol{V} + \operatorname{Grad} \boldsymbol{V}^\top + \operatorname{Grad} \boldsymbol{U} \cdot \operatorname{Grad} \boldsymbol{V}^\top +$$
$$+ \operatorname{Grad} \boldsymbol{V} \cdot \operatorname{Grad} \boldsymbol{U}^\top + \operatorname{Grad} \boldsymbol{V} \cdot \operatorname{Grad} \boldsymbol{V}^\top$$
$$= 2\mathcal{E}(\boldsymbol{U}) + 2\mathcal{E}'(\boldsymbol{U}; \boldsymbol{V}) + \mathcal{O}(\|\boldsymbol{V}\|^2)$$

with

$$2\mathcal{E}'(\boldsymbol{U}; \boldsymbol{V}) = \operatorname{Grad} \boldsymbol{V} + \operatorname{Grad} \boldsymbol{V}^\top + \operatorname{Grad} \boldsymbol{U} \cdot \operatorname{Grad} \boldsymbol{V}^\top +$$
$$+ \operatorname{Grad} \boldsymbol{V} \cdot \operatorname{Grad} \boldsymbol{U}^\top \ \forall \, \boldsymbol{V}(\eta) \in \mathbb{H}. \qquad (2.20)$$

For the first integral of the right-hand side of (2.17) we obtain

$$\int_{\Omega} \rho p \cdot \boldsymbol{V} \, d\Omega = \int_{\Omega_0} (\det \mathcal{F}) \rho p \cdot \boldsymbol{V} \, d\Omega_0$$

$$= \int_{\Omega_0} \rho_0 p \cdot \boldsymbol{V} \, d\Omega_0 \ \forall \, \boldsymbol{V}(\eta) \in \mathbb{H}. \qquad (2.21)$$

Due to the mass conservation in $\Omega_0$ and $\Omega$, the equation $(\det \mathcal{F})\rho = \rho_0$ holds, where $\rho_0$ is the density in $\Omega_0$.

**Remark 2.3** *Usually the outer acceleration field $p$ is considered to be constant. Therefore the right-hand side of equation (2.17) is a linear functional over $\boldsymbol{V}$.*

*In case that $p$ depends on the position $\boldsymbol{x} = \boldsymbol{X} + \boldsymbol{U}$ we get an additional non-linearity in the right-hand side. To avoid this extra non-linearity, in the following, we only use a constant acceleration field.*

For the second integral of the right-hand side we have to consider the boundary conditions.

Let

$$\partial\Omega_0 = \Gamma_{0,N} \cup \Gamma_D$$

and

$$\partial\Omega = \Gamma_N \cup \Gamma_D$$

with $\boldsymbol{U}(\boldsymbol{X}) = \boldsymbol{0} \ \forall \ \boldsymbol{X} \in \Gamma_D$. Hence $\boldsymbol{x}$ and $\boldsymbol{X}$ coincide on $\Gamma_D$ (fixed boundary). In that way, we define

$$\mathbb{H} = \left\{ \boldsymbol{V} \in \left(\mathbb{H}^1(\Omega_0)\right)^3 : \boldsymbol{V} = \boldsymbol{0} \text{ on } \Gamma_D \right\}.$$

Then

$$\int_{\partial\Omega} \boldsymbol{n} \cdot \sigma \cdot \boldsymbol{V} \, d\mathcal{S} = \int_{\Gamma_N} \boldsymbol{n} \cdot \sigma \cdot \boldsymbol{V} \, d\mathcal{S} \ \forall \, \boldsymbol{V}(\eta) \in \mathbb{H}.$$

By fixing one of the coordinates, for instance, $\eta^3 = c$, we obtain (at least a part of) the boundary $\Gamma_N$ or $\Gamma_{0,N}$, respectively, with

$$\Gamma_N = \left\{ \boldsymbol{x}(\eta^1, \eta^2, c) : (\eta^1, \eta^2) \in \mathcal{P}_N \right\}.$$

Here, the vectors $\boldsymbol{g}_1$ and $\boldsymbol{g}_2$ of the appropriate co-variant tensor basis act as tangential vectors of this surface and with

$$d\mathcal{S} = \|\boldsymbol{g}_1 \times \boldsymbol{g}_2\| \ d\eta^1 d\eta^2$$

we obtain the surface element. In that way, the normal vector of the deformed mid surface is given by

$$\boldsymbol{n} = \frac{\boldsymbol{g}_1 \times \boldsymbol{g}_2}{\|\boldsymbol{g}_1 \times \boldsymbol{g}_2\|}.$$

Therefore

$$\int_{\Gamma_N} \boldsymbol{n} \cdot \sigma \cdot \boldsymbol{V} \, d\mathcal{S} = \int_{\mathcal{P}_N} \frac{[\boldsymbol{g}_1, \boldsymbol{g}_2, \sigma \cdot \boldsymbol{V}]}{\|\boldsymbol{g}_1 \times \boldsymbol{g}_2\|} \|\boldsymbol{g}_1 \times \boldsymbol{g}_2\| \ d\eta^1 d\eta^2$$

$$= \int_{\mathcal{P}_N} [\boldsymbol{g}_1, \boldsymbol{g}_2, \sigma \cdot \boldsymbol{V}] \, d\eta^1 d\eta^2$$

$$= \int_{\mathcal{P}_N} \frac{1}{\det \mathcal{F}} [\mathcal{F} \cdot \boldsymbol{G}_1, \mathcal{F} \cdot \boldsymbol{G}_2, \mathcal{F} \cdot \overset{1}{\mathcal{T}} \cdot \boldsymbol{V}] \, d\eta^1 d\eta^2 \tag{2.22}$$

$$= \int_{\mathcal{P}_N} [\boldsymbol{G}_1, \boldsymbol{G}_2, \overset{1}{\mathcal{T}} \cdot \boldsymbol{V}] \, d\eta^1 d\eta^2$$

$$= \int_{\Gamma_{0,N}} \boldsymbol{\mathcal{N}} \cdot \overset{1}{\mathcal{T}} \cdot \boldsymbol{V} \, d\mathcal{S}_0$$

13

with $d\mathcal{S}_0 = \|\boldsymbol{G}_1 \times \boldsymbol{G}_2\| \, d\eta_1 d\eta_2$ being the appropriate surface element and $\boldsymbol{\mathcal{N}} = \frac{\boldsymbol{G}_1 \times \boldsymbol{G}_2}{\|\boldsymbol{G}_1 \times \boldsymbol{G}_2\|}$ the external normal vector in the original domain $\Omega_0$ at all points $\boldsymbol{X} \in \Gamma_{0,N}$.

Now we can deduce the weak formulation from equations (2.17), (2.19), (2.21) and (2.22) as follows:

For a vector function $\boldsymbol{U}$ with $\boldsymbol{U} = \boldsymbol{0}$ on $\Gamma_D$ solve

$$\int_{\Omega_0} \overset{2}{\mathcal{T}} : \mathcal{E}'(\boldsymbol{U}; \boldsymbol{V}) \, d\Omega_0 = \int_{\Omega_0} \rho_0 p \cdot \boldsymbol{V} \, d\Omega_0 + \int_{\Gamma_{0,N}} \vec{g} \cdot \boldsymbol{V} \, d\mathcal{S}_0 \ \forall \ \boldsymbol{V} \in \mathbb{H}, \qquad (2.23)$$

where $\vec{g} = \boldsymbol{\mathcal{N}} \cdot \overset{1}{\mathcal{T}}$ are the given traction on $\Gamma_{0,N}$.

We are still not able to solve this non-linear equation system in (2.23), due to the fact that, until yet, the Piola-Kirchhoff stress tensor $\overset{2}{\mathcal{T}}$ is unknown. In literature these equations are called not to be closed. By consideration of the material laws this closure is done in the next section.

## 2.3 Material laws

In this thesis only those material laws are considered that map strains $\mathcal{E}(\boldsymbol{U})$ onto stresses $\overset{2}{\mathcal{T}}$. For convenience, we utilize non-linear elastic material behaviour, where $\overset{2}{\mathcal{T}}$ is a function of $\mathcal{E}$ (or of $\mathcal{C}$). Hence, material laws for devices with plastic behaviour are excluded, because for them only the change of stresses depends on the change of strain.

In order to get the weak formulation, we define the energy functional

$$\varphi(\boldsymbol{U}) = \int_{\Omega_0} \psi(\mathcal{C}(\boldsymbol{U})) d\Omega_0 - f(\boldsymbol{U}). \qquad (2.24)$$

Herein $\psi(\mathcal{C}(\boldsymbol{U}))$ denotes the energy density depending on the invariants of $\mathcal{C}$. These invariants we get from the characteristic polynomial

$$\det(\mathcal{C} - \lambda \mathcal{I}) = -\lambda^3 + I_{\mathcal{C}} \lambda^2 - II_{\mathcal{C}} \lambda + III_{\mathcal{C}}.$$

Here $I_{\mathcal{C}}, II_{\mathcal{C}}, III_{\mathcal{C}}$ are called the principal invariants of $\mathcal{C}$ and if $\lambda_1, \lambda_2, \lambda_3$ are the three eigenvalues of the tensor $\mathcal{C}$, these invariants can be worked out as

$$I_{\mathcal{C}} = tr(\mathcal{C}) = \lambda_1 + \lambda_2 + \lambda_3,$$
$$II_{\mathcal{C}} = \frac{1}{2}\left[(tr\mathcal{C})^2 - tr(\mathcal{C}^2)\right] = \lambda_1 \lambda_2 + \lambda_2 \lambda_3 + \lambda_3 \lambda_1,$$
$$III_{\mathcal{C}} = \det \mathcal{C} = \lambda_1 \lambda_2 \lambda_3.$$

For convenience, we introduce the functions

$$a_k = \frac{1}{k} tr(\mathcal{C}^k) \ (k = 1, \ldots, 3) \qquad (2.25)$$

and use these $a_k$ instead of the principal invariants of $\mathcal{C}$ to express material laws, i.e.

$$
\begin{aligned}
I_{\mathcal{C}} &= a_1, \\
II_{\mathcal{C}} &= \frac{1}{2}(a_1)^2 - a_2, \\
III_{\mathcal{C}} &= (a_1^3 - 6a_1 a_2 + 6a_3)/6.
\end{aligned}
\tag{2.26}
$$

Minimizing the energy functional (2.24) leads to

$$
\varphi'(\boldsymbol{U}; \boldsymbol{V}) = 0 \ \forall \ \boldsymbol{V} \in \mathbb{H}.
\tag{2.27}
$$

We can calculate (2.27) by the derivation of $\varphi$:

$$
\varphi(\boldsymbol{U} + \boldsymbol{V}) = \varphi(\boldsymbol{U}) + \varphi'(\boldsymbol{U}; \boldsymbol{V}) + \mathcal{O}(\|\boldsymbol{V}\|^2) \ \forall \ \boldsymbol{V} \in \mathbb{H}.
\tag{2.28}
$$

Furthermore,

$$
\psi(\mathcal{C}(\boldsymbol{U} + \boldsymbol{V})) = \psi\left(\mathcal{C}(\boldsymbol{U}) + \mathcal{C}'(\boldsymbol{U}; \boldsymbol{V}) + \mathcal{O}(\|\mathcal{C}\|^2)\right) \ \forall \ \boldsymbol{V} \in \mathbb{H}.
\tag{2.29}
$$

Because the strain tensor $\mathcal{E}$ is calculated by the Cauchy-Green deformation tensor $\mathcal{C}$ from the equations (2.11) and (2.12), we get

$$
\mathcal{C} = 2\mathcal{E} + \mathcal{I},
\tag{2.30}
$$

where $\mathcal{I}$ is the unity gain tensor in the first-order tensor space.

Let us now study

$$
\mathcal{C}(\boldsymbol{U} + \boldsymbol{V}) = \mathcal{C}(\boldsymbol{U}) + \mathcal{C}'(\boldsymbol{U}; \boldsymbol{V}) + \mathcal{O}(\|\boldsymbol{V}\|^2) \ \forall \ \boldsymbol{V} \in \mathbb{H}.
$$

With (2.30) we obviously have

$$
\mathcal{C}'(\boldsymbol{U}; \boldsymbol{V}) = 2\mathcal{E}'(\boldsymbol{U}; \boldsymbol{V}) \ \forall \ \boldsymbol{V} \in \mathbb{H}.
$$

Hence, for the energy density in (2.29) we get

$$
\begin{aligned}
\psi(\mathcal{C}(\boldsymbol{U} + \boldsymbol{V})) &= \psi(\mathcal{C}(\boldsymbol{U})) + \psi'(\mathcal{C}(\boldsymbol{U}); 2\mathcal{E}'(\boldsymbol{U}; \boldsymbol{V})) + \mathcal{O}(\|\mathcal{E}\|^2) \\
&= \psi(\mathcal{C}(\boldsymbol{U})) + \overset{2}{\mathcal{L}} : 2\mathcal{E}'(\boldsymbol{U}; \boldsymbol{V}) \ \forall \ \boldsymbol{V} \in \mathbb{H}.
\end{aligned}
\tag{2.31}
$$

In mechanical literature the second-order tensor $\overset{2}{\mathcal{L}}$ is usually written as

$$
\overset{2}{\mathcal{L}} = \frac{\partial \psi}{\partial \mathcal{C}}.
$$

Because of (2.25) and (2.26) we can write this tensor as follows:

$$
\overset{2}{\mathcal{L}} = \sum_{i=1}^{3} \frac{\partial \psi}{\partial a_i} \frac{\partial a_i}{\partial \mathcal{C}} = \sum_{i=1}^{3} \frac{\partial \psi}{\partial a_i} \mathcal{C}^{i-1}.
$$

With the equations (2.28) and (2.31) we get

$$\varphi'(\boldsymbol{U};\boldsymbol{V}) = \int_{\Omega_0} \left(2\sum_{i=1}^{3} \frac{\partial\psi}{\partial a_i} \mathcal{C}^{i-1}\right) : \mathcal{E}'(\boldsymbol{U};\boldsymbol{V})\, d\Omega_0 - f(\boldsymbol{V}) \ \forall\, \boldsymbol{V} \in \mathbb{H}. \quad (2.32)$$

Together with (2.23) the second Piola-Kirchhoff stress tensor is identified as

$$\overset{2}{\mathcal{T}} = 2\sum_{i=1}^{3} \frac{\partial\psi}{\partial a_i} \mathcal{C}^{i-1} \quad (2.33)$$

and, therefore, it can be calculated for $\boldsymbol{X} \in \Omega_0$ (which is needed for the calculation at the integration points of a FE-discretization, later on).

The materials with linear elastic behaviour represent a special case. For these materials we assume that there exists a linear map between the Right-Cauchy-Green deformation tensor and the second Piola-Kirchhoff stress tensor. So the density function can be calculated separately by (2.33). From Hook's law we have

$$\overset{2}{\mathcal{T}} = 2\mu\mathcal{E} + \lambda tr(\mathcal{E})\mathcal{I}$$

with the Lamé coefficients $\mu$ and $\lambda$. Using (2.30) we get

$$\overset{2}{\mathcal{T}} = \mu\mathcal{C}^1 + \mathcal{C}^0(-\mu + \frac{1}{2}\lambda a_1 - \frac{3}{2}\lambda) \overset{!}{=} 2\sum_{i=1}^{3} \frac{\partial\psi}{\partial a_i}\mathcal{C}^{i-1}.$$

Integration by parts leads to

$$\psi(a_1, a_2, a_3) = -a_1(\frac{1}{2}\mu + \frac{3}{4}\lambda) + \frac{1}{8}\lambda a_1^2 + \frac{1}{2}\mu a_2 + c$$

with a certain constant $c$.

If we claim zero energy for zero strain (e.g. $\mathcal{C} = \mathcal{I}$), the constant $c$ is fixed and

$$\psi(a_1, a_2, a_3) = \frac{1}{8}\lambda a_1^2 - \left(\frac{1}{2}\mu + \frac{3}{4}\lambda\right)a_1 + \frac{1}{2}\mu a_2 + \frac{3}{8}(2\mu + 3\lambda)$$

follows.

As mentioned in the introduction, we want to consider non-linear elastic materials, but as we have seen, this theory includes linear elastic behaviour as well.

However, there are many non-linear elastic material laws discussed in mechanical literature, i.e. the Neo-Hook material and some of its generalizations. For the Neo-Hooke material the density function is specified by

$$\psi(a_1, a_2, a_3) = c_{10}(a_1 - \ln(III_{\mathcal{C}}) - 3) + D_2\ln^2(III_{\mathcal{C}}), \quad (2.34)$$

where $c_{10}$ and $D_2$ are constants depending on the material itself.

Overall, the material law consists of the definition of a energy density function $\psi(a_1, a_2, a_3)$, which leads to the second Piola-Kirchhoff stress tensor $\overset{2}{\mathcal{T}}$ (2.33) depending on $\mathcal{C}$ (or $\mathcal{E}$).

## 2.4 The weak formulation

In the sections before we have seen that with the equilibrium of forces a energy functional (2.24) and its derivative (2.32) can be calculated by defining an energy density and therefore defining the second Piola-Kirchhoff stress tensor (2.33).

Then, with the abbreviations

$$a(\boldsymbol{U}; \boldsymbol{V}) = \int_{\Omega_0} \overset{2}{\mathcal{T}} : \mathcal{E}'(\boldsymbol{U}; \boldsymbol{V}) \, d\Omega_0$$

and

$$f(\boldsymbol{V}) = \int_{\Omega_0} \rho_0 p \cdot \boldsymbol{V} \, d\Omega_0 + \int_{\Gamma_{0,N}} \vec{g} \cdot \boldsymbol{V} \, d\mathcal{S}_0 \ \ \forall \, \boldsymbol{V}(\eta) \in \mathbb{H} \tag{2.35}$$

we can write the well-known weak formulation as:

Find the vector function $\boldsymbol{U}$ with $\boldsymbol{U} = \boldsymbol{0} \ \ \forall \, \boldsymbol{X} \in \Gamma_D$ with

$$a(\boldsymbol{U}; \boldsymbol{V}) = f(\boldsymbol{V}) \ \ \forall \, \boldsymbol{V} \in \mathbb{H}. \tag{2.36}$$

Obviously, equation (2.36) coincides with (2.23) and

$$\varphi'(\boldsymbol{U}; \boldsymbol{V}) = \boldsymbol{a}(\boldsymbol{U}; \boldsymbol{V}) - f(\boldsymbol{V}) \ \ \forall \, \boldsymbol{V} \in \mathbb{H} \tag{2.37}$$

holds.

# 3 Newton's method

The purpose of this chapter is to solve the non-linear equation system (2.36) using Newton's method. Therefore, the second derivative of the energy functional and the first derivative of the second Piola Kirchhoff stress tensor are needed. Due to the fact that Newton's method converges in a small ball around the unknown exact solution only, it is essential to choose a sufficiently well starting approximation. For small deformations $\boldsymbol{U} = \boldsymbol{0}$ as the initial approximation was adequate, but in the case of large deformations the displacement vector differs very much from zero. Hence, for Newton's method the well known incrementation of the forces $f(\boldsymbol{U})$ is used. In that way, we get a series of Newton iterations with an incremental increase of the outer forces $f(\boldsymbol{U})$. The proof of convergence for an incremental solving of equation systems and some more information about are given in, for example, [11].

## 3.1 The modified Newton algorithm

Newton's algorithm is about an iteration procedure solving non-linear equations or non-linear equation systems. Hence, computing the solution of the equation system

$$D(\boldsymbol{U}) = 0$$

where $D$ displays an operator, depending on the vector $\boldsymbol{U}$, means choosing a start vector $\boldsymbol{U}^{(0)}$ and using repeatedly the iteration code

$$\boldsymbol{\delta U} = \Big(D'(\boldsymbol{U}^{(k)})\Big)^{-1}\Big(-D(\boldsymbol{U}^{(k)})\Big)$$
$$\boldsymbol{U}^{(k+1)} = \boldsymbol{U}^{(k)} + \boldsymbol{\delta U}$$
$$k := k + 1.$$

Here, $D'$ is the Fréchet derivative of $D$.

Practically, we do not calculate the inverse $\Big(D'(\boldsymbol{U}^{(k)})\Big)^{-1}$ but consider the linearization of the operator equation

$$D'(\boldsymbol{U}; \boldsymbol{\delta U}) = -D(\boldsymbol{U})$$

in every Newton step.

Generally, the iteration ends if the stopping criterion

$$\frac{\|\boldsymbol{\delta U}\|}{\|\boldsymbol{U}\|} < \varepsilon$$

is fulfilled.

Applying Newton's method to the problem (2.36) means solving (2.37). Then, in every Newton step we have to calculate $\boldsymbol{\delta U}$ from

$$\varphi''(\boldsymbol{U}; \boldsymbol{\delta U}, \boldsymbol{V}) = -\varphi'(\boldsymbol{U}; \boldsymbol{V}) \ \forall \boldsymbol{V} \in \mathbb{H}.$$

Herein, with $\varphi''(\boldsymbol{U}; \boldsymbol{\delta U}, \boldsymbol{V})$ we depict the second linearization of the energy functional $\varphi(\boldsymbol{U})$ as linearization of $\varphi'(\boldsymbol{U}; \boldsymbol{V})$:

$$\varphi'(\boldsymbol{U} + \boldsymbol{\delta U}, \boldsymbol{V}) = \varphi'(\boldsymbol{U}; \boldsymbol{V}) + \varphi''(\boldsymbol{U}; \boldsymbol{\delta U}, \boldsymbol{V}) + \mathcal{O}(\|\boldsymbol{\delta U}\|^2).$$

Newton's method converges quadratically, only in the neighbourhood of the root. Hence, for ensuring a well-suited starting vector we have implemented an incremental algorithm, whereby a multiplier $t \in [0, 1]$ is applied to the force vector $f(\boldsymbol{U})$. This multiplier has to be increased appropriately.

**Algorithm 3.1** (Incremental Newton solution process)

*(1) Start: $\boldsymbol{U} = \boldsymbol{0}$, $t := \Delta t$*

*(2) for $\boldsymbol{\delta U}$ solve $\varphi''(\boldsymbol{U}; \boldsymbol{\delta U}, \boldsymbol{V}) = t f(\boldsymbol{V}) - a(\boldsymbol{U}; \boldsymbol{V}) \ \forall \boldsymbol{V} \in \mathbb{H}$*

*(3) update $\boldsymbol{U} := \boldsymbol{U} + \boldsymbol{\delta U}$*

*(4) if $(\|\boldsymbol{\delta U}\| / \|\boldsymbol{U}\| < \varepsilon)$: $t := t + \Delta t$ until $t = 1$*

*(5) goto (2).*

With the algorithm above, a series of Newton methods is applied, due to the incrementation of the force vector via $\Delta t$.

## 3.2 Second linearization of the energy functional

We achieve the second derivative of the energy functional by applying the chain rule to its derivative $\varphi'(\boldsymbol{U}; \boldsymbol{V})$ from (2.32):

$$\varphi''(\boldsymbol{U}; \boldsymbol{\delta U}, \boldsymbol{V}) = \int_{\Omega_0} \overset{2}{\mathcal{T}}{}' : \mathcal{E}'(\boldsymbol{U}; \boldsymbol{V}) \, d\Omega_0 + \int_{\Omega_0} \overset{2}{\mathcal{T}} : \mathcal{E}''(\boldsymbol{U}; \boldsymbol{\delta U}, \boldsymbol{V}) \, d\Omega_0.$$

For computing the derivative $\overset{2}{\mathcal{T}}{}'$ we have to linearize the second Piola-Kirchhoff stress tensor itself:

$$\overset{2}{\mathcal{T}}(\mathcal{C} + \delta\mathcal{C}) = \overset{2}{\mathcal{T}}(\mathcal{C}) + \mathfrak{C} : \delta\mathcal{C} + \mathcal{O}(\|\delta\mathcal{C}\|^2) \tag{3.1}$$

with a fourth-order tensor $\mathfrak{C}$.

Furthermore, we consider

$$\overset{2}{\mathcal{T}}\big(\mathcal{C}(\boldsymbol{U}+\boldsymbol{\delta U})\big) = \overset{2}{\mathcal{T}}\big(\mathcal{C}(\boldsymbol{U}) + 2\mathcal{E}'(\boldsymbol{U};\boldsymbol{\delta U}) + \mathcal{O}(\|\boldsymbol{\delta U}\|^2)\big).$$

Therefore, (3.1) in conjunction with (2.33) yields

$$\overset{2}{\mathcal{T}}\big(\mathcal{C}(\boldsymbol{U}+\boldsymbol{\delta U})\big) = \overset{2}{\mathcal{T}}\big(\mathcal{C}(\boldsymbol{U})\big) + \mathfrak{C}(\boldsymbol{U}) : \mathcal{E}'(\boldsymbol{U};\boldsymbol{\delta U}) + \mathcal{O}(\|\mathcal{C}\|^2).$$

Obviously, we achieve

$$\overset{2}{\mathcal{T}}{}' = \mathfrak{C}(\boldsymbol{U}) : \mathcal{E}'(\boldsymbol{U};\boldsymbol{\delta U}).$$

Thereby, the fourth-order tensor $\mathfrak{C}$ arises from the equations (2.33, 3.1) as

$$\mathfrak{C}(\boldsymbol{U}) = 4\sum_{i=1}^{3}\sum_{j=1}^{3}\frac{\partial^2\psi}{\partial a_i\partial a_j}\left[\mathcal{C}^{i-1}\ \mathcal{C}^{j-1}\right] + 4\frac{\partial\psi}{\partial a_2}\mathfrak{J} + 4\frac{\partial\psi}{\partial a_3}\widehat{\mathfrak{C}} \tag{3.2}$$

with the fourth-order unity tensor $\mathfrak{J}$, mapping any second order tensor to itself, and the fourth-order tensor $\widehat{\mathfrak{C}}$ with the property

$$\widehat{\mathfrak{C}} : \mathcal{X} = \mathcal{C} \cdot \mathcal{X} + \mathcal{X} \cdot \mathcal{C}$$

for all symmetric second-order tensors $\mathcal{X}$. $\widehat{\mathfrak{C}}$ emerges from the expansion of the square of the right Cauchy Green deformation tensor $\mathcal{C}^2(\boldsymbol{U})$.

The second derivative of the Lagrangian strain tensor is easily obtained by the linearization of its first derivative (2.20):

$$2\mathcal{E}''(\boldsymbol{U};\boldsymbol{\delta U},\boldsymbol{V}) = \mathrm{Grad}\ \boldsymbol{\delta U} \cdot \mathrm{Grad}\ \boldsymbol{V}^\top + \mathrm{Grad}\ \boldsymbol{V} \cdot \mathrm{Grad}\ \boldsymbol{\delta U}^\top \ \forall\ \boldsymbol{V}(\eta) \in \mathbb{H}. \tag{3.3}$$

To sum up, due to the symmetry of the fourth-order tensor $\mathfrak{C}$ and of the second-order tensor $\mathcal{E}'(\boldsymbol{U};\boldsymbol{\delta U})$, the second derivative of the energy functional can be written as

$$\varphi''(\boldsymbol{U};\boldsymbol{\delta U},\boldsymbol{V}) = \int_{\Omega_0} \mathcal{E}'(\boldsymbol{U};\boldsymbol{\delta U}) : \mathfrak{C} : \mathcal{E}'(\boldsymbol{U};\boldsymbol{V})\,d\Omega_0 + \int_{\Omega_0} \overset{2}{\mathcal{T}} : \mathcal{E}''(\boldsymbol{U};\boldsymbol{\delta U},\boldsymbol{V})\,d\Omega_0. \tag{3.4}$$

In the literature of mechanics the tensor $\mathfrak{C}(\boldsymbol{U})$ is called the material tangent. With (3.4) now the Algorithm 3.1 is complete.

# 4 Differential geometry of shells

In the geometrical characterization of shells we go along with the majority of mechanical literature. Therein, an initial shell $\Omega_0$ is characterized as a static, isotropic three-dimensional object. One regards a mid surface $\Omega_0^m \subset \mathbb{R}^3$ of the undeformed shell and a thickness $h \lll diam(\Omega_0^m)$. Now the deformation of the shell is approximated by a deformation of the mid surface.

This chapter begins with the differential geometry of shells in general. Later on, we consider the initial configuration as a plane shell, called plate. At the end of this chapter the Kirchhoff assumption is introduced and than combined with the theory for the plane shell.

In what follows all indices now run between 1 and 2. The content of this chapter refers to the explanations in [21] and [24].

## 4.1 The initial mid surface

In this paragraph we illustrate the basic theory of the differential geometry in the undeformed shell, the initial domain. In the initial configuration all vectors and matrices, mainly the co- and contra-variant basis vectors and the matrices of the first and the second fundamental forms, are typed in capital letters.

We denote

$$\Omega_0^m := \{\boldsymbol{Y}(\eta^1, \eta^2) : (\eta^1, \eta^2) \in \mathcal{P}_2 \subset \mathbb{R}^2\} \subset \mathbb{R}^3 \tag{4.1}$$

as mid surface of the undeformed shell. Here, the points of the surface in the three-dimensional space are denoted by $\boldsymbol{Y}$ and the coordinates $(\eta^1, \eta^2)$ run throughout the parameter domain $\mathcal{P}_2$. Therewith the tangential vectors are defined by

$$\boldsymbol{A}_i = \frac{\partial}{\partial \eta^i} \boldsymbol{Y}, \ \ i = 1, 2,$$

and the surface normal vector is described by

$$\boldsymbol{A}_3 = \boldsymbol{A}^3 = \frac{\boldsymbol{A}_1 \times \boldsymbol{A}_2}{|\boldsymbol{A}_1 \times \boldsymbol{A}_2|}. \tag{4.2}$$

The two tangential vectors together with the surface normal vector establish a co-variant tensor basis in $\mathbb{R}^3$.

The first fundamental forms $\underline{A}$ and the second fundamental forms $\underline{B}$ are written as $(2 \times 2)$-matrices:

$$\underline{A} = (A_{ij})_{i,j=1}^2, \ \ A_{ij} = \boldsymbol{A}_i \cdot \boldsymbol{A}_j,$$

and the second fundamental forms

$$\underline{B} = (B_{ij})^2_{i,j=1}, \quad B_{ij} = \left(\frac{\partial^2}{\partial \eta^i \partial \eta^j} \boldsymbol{Y}\right) \cdot \boldsymbol{A}_3 = \boldsymbol{A}_{i,j} \cdot \boldsymbol{A}_3 = -\boldsymbol{A}_i \cdot \boldsymbol{A}_{3,j},$$

respectively. We define the corresponding contra-variant tensor basis from

$$\boldsymbol{A}^j = A^{jk} \boldsymbol{A}_k \ \text{ with } \ \boldsymbol{A}^j \cdot \boldsymbol{A}_k = \delta^j_k, \ \text{ where } A^{jk} \text{ are the entries of } \underline{A}^{-1}.$$

The surface element is defined by

$$d\mathcal{S} = |\boldsymbol{A}_1 \times \boldsymbol{A}_2| \ d\eta^1 d\eta^2 = (\det \underline{A})^{\frac{1}{2}} \ d\eta^1 d\eta^2.$$

Therefore, the gradient operator on the tangential space, the surface gradient, is specified as

$$\text{Grad}_S = \boldsymbol{A}^i \frac{\partial}{\partial \eta^i}.$$

## 4.2 The initial shell

We understand the initial shell as a three-dimensional manifold

$$\Omega_0 := \left\{ \boldsymbol{X}(\eta^1, \eta^2, \tau = \eta^3) = \boldsymbol{Y}(\eta^1, \eta^2) + h\tau \boldsymbol{A}_3, \ (\eta^1, \eta^2) \in \mathcal{P}_2, |\tau| < \frac{1}{2} \right\}$$

with constant thickness $h$ and $\boldsymbol{A}_3$ from (4.2). Without loss of generality, we use $\tau = \eta^3$ as a synonym for the thickness coordinate and consider the coordinates $\eta^i, \ i = 1, 2$, providing the length of dimension in the corresponding direction. Then the basis vectors $\boldsymbol{A}_i$ and $\boldsymbol{A}^i, \ i = 1, 2$ have to be dimensionless, consistently, but $\boldsymbol{A}_3 = \boldsymbol{A}^3$ has no dimension, anyway. The co-variant tensor basis (2.3) from chapter 2 can now be calculated as

$$\boldsymbol{G}_i = \frac{\partial}{\partial \eta^i} \boldsymbol{X} = \boldsymbol{A}_i + h\tau \boldsymbol{A}_{3,i} \ i = 1, 2 \tag{4.3}$$

and

$$\boldsymbol{G}_3 = h \boldsymbol{A}_3.$$

Therefore the contra-variant tensor basis $\boldsymbol{G}^i, \ i = 1, 2$ as well as $\boldsymbol{G}^3 = h^{-1} \boldsymbol{A}^3 = h^{-1} \boldsymbol{A}_3$ and, moreover, the matrix of the metric coefficients (2.4) can be calculated. Obviously,

$$\det(\underline{G}) = h^2 \det(\widehat{\underline{G}})$$

with the $(2 \times 2)$-matrix

$$\begin{aligned}
\widehat{\underline{G}} = (G_{ij})^2_{i,j=1}, \ G_{ij} &= \boldsymbol{G}_i \cdot \boldsymbol{G}_j \\
&= \underline{A}(\underline{I} - h\tau \underline{A}^{-1} \underline{B})^2 \\
&= \underline{A} \left( \underline{I} - 2h\tau \underline{A}^{-1} \underline{B} + h^2 \tau^2 (\underline{A}^{-1} \underline{B})(\underline{A}^{-1} \underline{B}) \right) \\
&= \underline{A} - 2h\tau \underline{B} + h^2 \tau^2 \underline{B} \underline{A}^{-1} \underline{B} \\
&= (\underline{A} - h\tau \underline{B}) \underline{A}^{-1} (\underline{A} - h\tau \underline{B}).
\end{aligned} \tag{4.4}$$

Hence, the volume element of the shell can be restated as

$$dV = [\boldsymbol{G}_1, \boldsymbol{G}_2, \boldsymbol{G}_3] \ d\eta^1 d\eta^2 d\tau = h \det(\widehat{\underline{G}})^{\frac{1}{2}} \ d\eta^1 d\eta^2 d\tau.$$

## 4.3 The plate as an exception of a shell

As written before, we think of a plate as a shell which is initially plain. After applying some forces to the plate, which do not cause rigid body motions only, a shell arises.

Due to the plane initial state of a plate, we get some simplifications. So on the initial mid surface $\Omega_0^m$ in (4.1) the physical points $\boldsymbol{Y}$ are in the $\boldsymbol{e}_1$-$\boldsymbol{e}_2$-plane, for instance

$$\boldsymbol{Y}(\eta^1, \eta^2) = \boldsymbol{e}_1 \cdot \eta^1 + \boldsymbol{e}_2 \cdot \eta^2, \tag{4.5}$$

where the coordinates $\eta^i, \ i = 1, 2$, feature the length of the dimension in direction of each unit vector $\boldsymbol{e}_i, \ i = 1, 2$. With (4.2) this simplification yields

$$\boldsymbol{A}_3 = \boldsymbol{e}_3$$

for the normal vector of the undeformed mid surface independent of $(\eta^1, \eta^2)$. Together with the definition of the co-variant tensor basis (4.3) of the initial shell we get the co-variant tensor basis with the normal vector for the initial plate as

$$\boldsymbol{G}_i = \boldsymbol{G}^i = \boldsymbol{e}_i, \ i = 1, 2, \ \boldsymbol{G}_3 = h\boldsymbol{e}_3, \ \boldsymbol{G}^3 = \frac{1}{h}\boldsymbol{e}_3. \tag{4.6}$$

Because of the independence of the normal vector from the coordinates $(\eta^1, \eta^2)$, the second fundamental forms at the mid surface of the initial plate vanish:

$$\underline{B} = \mathbb{O}.$$

For simplicity, in the following we restrict ourselves to the plate.

## 4.4 Kirchhoff assumption and the deformed shell

### 4.4.1 Differential geometry of the deformed shell

The following assumption is one possibility to reduce the space dimension. The idea is to describe the deformed shell by its mid surface only. With the Kirchhoff hypothesis no change in thickness of the shell is allowed and the shell is assumed to be shear rigid. This means that a certain straight fibre of points

$$\left\{ \boldsymbol{Y}(\eta^1, \eta^2) + h\tau \boldsymbol{A}_3(\eta^1, \eta^2) : |\tau| \le \frac{1}{2} \right\}$$

which is perpendicular to the undeformed mid surface $\Omega_0^m$ (4.1) has to be straight and perpendicular to the deformed mid surface

$$\Omega_t^m = \left\{ \boldsymbol{y}(\eta_1, \eta_2) = \boldsymbol{Y}(\eta^1, \eta^2) + \boldsymbol{U}(\eta^1, \eta^2) : (\eta^1, \eta^2) \in \mathcal{P}_2 \right\}, \tag{4.7}$$

after deformation as well. Here, $\boldsymbol{U}$ is the unknown displacement vector of the mid surface, which is a function of $(\eta^1, \eta^2)$ as well as of $\boldsymbol{Y}$.

The Kirchhoff assumption defines the deformed shell as

$$\Omega_t = \left\{ \boldsymbol{x}(\eta^1, \eta^2, \tau) = \boldsymbol{y}(\eta^1, \eta^2) + h\tau \boldsymbol{a}_3 \right\}, \tag{4.8}$$

where $\boldsymbol{a}_3$ is the new surface normal vector of the deformed mid surface $\Omega_t^m$ following its differential geometry: With

$$\boldsymbol{a}_i = \frac{\partial}{\partial \eta^i} \boldsymbol{y} = \boldsymbol{A}_i + \boldsymbol{U}_{,i}, \quad i = 1, 2,$$

the tangential vectors of the mid surface after deformation, the surface normal vector of the deformed mid surface $\Omega_t^m$ can be calculated as

$$\boldsymbol{a}_3 = \frac{\boldsymbol{a}_1 \times \boldsymbol{a}_2}{|\boldsymbol{a}_1 \times \boldsymbol{a}_2|}. \tag{4.9}$$

Consequently, we get

$$\underline{a} = (a_{ij})_{i,j=1}^2 \quad \text{with} \quad a_{ij} = \boldsymbol{a}_i \cdot \boldsymbol{a}_j, \tag{4.10}$$

$$\underline{b} = (b_{ij})_{i,j=1}^2 \quad \text{with} \quad b_{ij} = \boldsymbol{a}_{i,j} \cdot \boldsymbol{a}_3, \tag{4.11}$$

the first and second fundamental forms in the deformed state.

Now the 3D co-variant basis is

$$\boldsymbol{g}_i = \frac{\partial}{\partial \eta^i} \boldsymbol{x} = \boldsymbol{a}_i + h\tau \boldsymbol{a}_{3,i} = \boldsymbol{A}_i + \boldsymbol{U}_{,i} + h\tau \boldsymbol{a}_{3,i}, \quad i = 1, 2 \tag{4.12}$$

$$\boldsymbol{g}_3 = h\boldsymbol{a}_3.$$

Analogously to $\widehat{G}$ in (4.4), we can define the $(2 \times 2)$-matrix $\widehat{g} = (g_{ij})_{i,j=1}^2$ with $g_{ij} = \boldsymbol{g}_i \cdot \boldsymbol{g}_j$, yielding

$$\widehat{g} = \underline{a}(\underline{I} - h\tau \underline{a}^{-1}\underline{b})^2 = (\underline{a} - h\tau \underline{b})\underline{a}^{-1}(\underline{a} - h\tau \underline{b}).$$

Hence, mathematically the Kirchhoff assumption means

$$\begin{aligned}
\boldsymbol{x}(\eta^1, \eta^2, \tau) :&= \boldsymbol{y}(\eta^1, \eta^2) + h\tau \boldsymbol{a}_3(\eta^1, \eta^2) \\
&= \boldsymbol{Y}(\eta^1, \eta^2) + \boldsymbol{U}(\eta^1, \eta^2) + h\tau \boldsymbol{a}_3 \left( \boldsymbol{U}(\eta^1, \eta^2) \right) \\
&= \begin{pmatrix} \eta^1 \\ \eta^2 \\ h\tau \end{pmatrix} + \boldsymbol{U}(\eta^1, \eta^2) + h\tau (\boldsymbol{a}_3 \left( \boldsymbol{U}(\eta^1, \eta^2) \right) - \boldsymbol{e}_3) \\
&= \boldsymbol{X}(\eta) + \boldsymbol{U}(\eta^1, \eta^2) + h\tau (\boldsymbol{a}_3 \left( \boldsymbol{U}(\eta^1, \eta^2) \right) - \boldsymbol{e}_3).
\end{aligned} \tag{4.13}$$

Accordingly, the new 3D displacement vector is

$$\boldsymbol{U}^{\mathrm{KH}}(\eta^1, \eta^2, \tau) = \boldsymbol{U} + h\tau(\boldsymbol{a}_3(\boldsymbol{U}) - \boldsymbol{e}_3), \tag{4.14}$$

with the vector field $\boldsymbol{U}$ depending on $(\eta^1, \eta^2)$ only.

## 4.4.2 The Lagrangian strain tensor of the deformed plate

We deduce the 3D-deformation gradient from (4.3) and (4.12) in connection with (4.6) as

$$\begin{aligned} \widehat{\mathcal{F}} &= \boldsymbol{g}_i \boldsymbol{G}^i + \boldsymbol{a}_3 \boldsymbol{A}^3 \\ &= (\boldsymbol{a}_1 + h\tau \boldsymbol{a}_{3,1})\boldsymbol{e}_1 + (\boldsymbol{a}_2 + h\tau \boldsymbol{a}_{3,2})\boldsymbol{e}_2 + \boldsymbol{a}_3 \boldsymbol{e}_3. \end{aligned}$$

Then, the coefficients of the right Cauchy-Green deformation tensor (2.11) are given by

$$\widehat{\mathcal{C}} = \widehat{\mathcal{F}}^\tau \cdot \widehat{\mathcal{F}} = c_{ij}\boldsymbol{e}_i\boldsymbol{e}_j + \boldsymbol{e}_3\boldsymbol{e}_3 \tag{4.15}$$

with

$$\begin{aligned} c_{ij} &= \boldsymbol{g}_i \cdot \boldsymbol{g}_j = g_{ij} \\ &= (\boldsymbol{a}_i + h\tau \boldsymbol{a}_{3,i}) \cdot (\boldsymbol{a}_j + h\tau \boldsymbol{a}_{3,j}), \quad i, j = 1, 2. \end{aligned} \tag{4.16}$$

In this way, the right Cauchy-Green deformation tensor is calculable as

$$\begin{aligned} \widehat{\mathcal{C}} &= g_{ij}\boldsymbol{e}_i\boldsymbol{e}_j + \boldsymbol{e}_3\boldsymbol{e}_3 \tag{4.17} \\ &= \big[(\boldsymbol{a}_i + \tau h \boldsymbol{a}_{3,i}) \cdot (\boldsymbol{a}_j + \tau h \boldsymbol{a}_{3,j})\big]\boldsymbol{e}_i\boldsymbol{e}_j + \boldsymbol{e}_3\boldsymbol{e}_3 \\ &= \big[(\boldsymbol{e}_i + \boldsymbol{U}_{,i} + \tau h \boldsymbol{a}_{3,i}) \cdot (\boldsymbol{e}_j + \boldsymbol{U}_{,j} + \tau h \boldsymbol{a}_{3,j})\big]\boldsymbol{e}_i\boldsymbol{e}_j + \boldsymbol{e}_3\boldsymbol{e}_3 \\ &= \delta_{ij}\boldsymbol{e}_i\boldsymbol{e}_j + \boldsymbol{e}_3\boldsymbol{e}_3 + \big[(\boldsymbol{U}_{,i} + \tau h \boldsymbol{a}_{3,i}) \cdot \boldsymbol{e}_j + \boldsymbol{e}_i \cdot (\boldsymbol{U}_{,j} + \tau h \boldsymbol{a}_{3,j}) \\ &\quad + (\boldsymbol{U}_{,i} + \tau h \boldsymbol{a}_{3,i}) \cdot (\boldsymbol{U}_{,j} + \tau h \boldsymbol{a}_{3,j})\big]\boldsymbol{e}_i\boldsymbol{e}_j \\ &= \mathcal{I} + \big[(\boldsymbol{U}_{,i} + \tau h \boldsymbol{a}_{3,i}) \cdot \boldsymbol{e}_j + \boldsymbol{e}_i \cdot (\boldsymbol{U}_{,j} + \tau h \boldsymbol{a}_{3,j}) \\ &\quad + (\boldsymbol{U}_{,i} + \tau h \boldsymbol{a}_{3,i}) \cdot (\boldsymbol{U}_{,j} + \tau h \boldsymbol{a}_{3,j})\big]\boldsymbol{e}_i\boldsymbol{e}_j. \end{aligned}$$

Thus, with (2.12) we can calculate the Lagrangian strain tensor of the plate as

$$\widehat{\mathcal{E}} = \varepsilon_{ij}\boldsymbol{e}_i\boldsymbol{e}_j \tag{4.18}$$

with

$$2\varepsilon_{ij} = g_{ij} - \delta_{ij} = (\boldsymbol{a}_i + h\tau \boldsymbol{a}_{3,i}) \cdot (\boldsymbol{a}_j + h\tau \boldsymbol{a}_{3,j}) - \delta_{ij}, \quad i, j = 1, 2.$$

Accordingly with (4.17) we can compute the Lagrangian strain tensor as

$$
\begin{aligned}
2\widehat{\mathcal{E}}(\boldsymbol{U}) &= \Big[(\boldsymbol{U}_{,i} + \tau h \boldsymbol{a}_{3,i}) \cdot \boldsymbol{e}_j + \boldsymbol{e}_i \cdot (\boldsymbol{U}_{,j} + \tau h \boldsymbol{a}_{3,j}) \\
&\quad + (\boldsymbol{U}_{,i} + \tau h \boldsymbol{a}_{3,i}) \cdot (\boldsymbol{U}_{,j} + \tau h \boldsymbol{a}_{3,j})\Big] \boldsymbol{e}_i \boldsymbol{e}_j \\
&= \boldsymbol{e}_i [(\boldsymbol{U}_{,i} + \tau h \boldsymbol{a}_{3,i}) \cdot \boldsymbol{e}_j] \boldsymbol{e}_j + \boldsymbol{e}_i [\boldsymbol{e}_i \cdot (\boldsymbol{U}_{,j} + \tau h \boldsymbol{a}_{3,j})] \boldsymbol{e}_j \\
&\quad + \boldsymbol{e}_i [(\boldsymbol{U}_{,i} + \tau h \boldsymbol{a}_{3,i}) \cdot (\boldsymbol{U}_{,j} + \tau h \boldsymbol{a}_{3,j})] \boldsymbol{e}_j \\
&= \mathrm{Grad}_{\mathcal{S}} \, (\boldsymbol{U} + \tau h \boldsymbol{a}_3) \cdot \boldsymbol{e}_j \boldsymbol{e}_j + \boldsymbol{e}_i \boldsymbol{e}_i \cdot \mathrm{Grad}_{\mathcal{S}} \, (\boldsymbol{U} + \tau h \boldsymbol{a}_3)^\top \\
&\quad + \mathrm{Grad}_{\mathcal{S}} \, (\boldsymbol{U} + \tau h \boldsymbol{a}_3) \cdot \mathrm{Grad}_{\mathcal{S}} \, (\boldsymbol{U} + \tau h \boldsymbol{a}_3)^\top.
\end{aligned}
$$

In that,

$$
\mathrm{Grad}_{\mathcal{S}} := \boldsymbol{G}^i \frac{\partial}{\partial \eta^i}, \quad i = 1, 2
$$

defines the surface gradient operator. Then, with the orthoprojector into the tangential space $\mathcal{A} = \boldsymbol{e}_i \boldsymbol{e}_i$ the Lagrangian strain tensor is written as

$$
\begin{aligned}
2\widehat{\mathcal{E}}(\boldsymbol{U}) &= \mathrm{Grad}_{\mathcal{S}} \, (\boldsymbol{U} + \tau h \boldsymbol{a}_3) \cdot \mathcal{A} + \mathcal{A} \cdot \mathrm{Grad}_{\mathcal{S}} \, (\boldsymbol{U} + \tau h \boldsymbol{a}_3)^\top \\
&\quad + \mathrm{Grad}_{\mathcal{S}} \, (\boldsymbol{U} + \tau h \boldsymbol{a}_3) \cdot \mathrm{Grad}_{\mathcal{S}} \, (\boldsymbol{U} + \tau h \boldsymbol{a}_3)^\top.
\end{aligned}
\tag{4.19}
$$

For using matrix syntax we define the matrices containing the coefficients of the associated tensors in the chosen tensor basis.

In case of the right Cauchy-Green deformation tensor $\widehat{\mathcal{C}}$ given in (4.15) and (4.16), the appropriate matrix is

$$
\begin{aligned}
\underline{c} &= (c_{ij})^2_{i,j=1} \\
&= [(\boldsymbol{a}_i + h\tau \boldsymbol{a}_{3,i}) \cdot (\boldsymbol{a}_j + h\tau \boldsymbol{a}_{3,j})]^2_{i,j=1} \\
&= \underline{a} + h\tau \, [\boldsymbol{a}_i \cdot \boldsymbol{a}_{3,j} + \boldsymbol{a}_{3,i} \cdot \boldsymbol{a}_j]^2_{i,j=1} + (h\tau)^2 \, [\boldsymbol{a}_{3,i} \cdot \boldsymbol{a}_{3,j}]^2_{i,j=1}.
\end{aligned}
\tag{4.20}
$$

From the definition (4.9) we have

$$
\boldsymbol{y}_{,i} \cdot \boldsymbol{a}_3 = \boldsymbol{a}_i \cdot \boldsymbol{a}_3 \equiv 0, \quad \forall i = 1, 2.
$$

Consequently,

$$
(\boldsymbol{a}_i \cdot \boldsymbol{a}_3)_{,j} \equiv 0 \quad \forall i = 1, 2
$$

is also true.

Hence, by using the product rule and the equation (4.11) we can deduce

$$
0 = (\boldsymbol{a}_i \cdot \boldsymbol{a}_3)_{,j} = \boldsymbol{a}_{i,j} \cdot \boldsymbol{a}_3 + \boldsymbol{a}_i \cdot \boldsymbol{a}_{3,j} = b_{ij} + \boldsymbol{a}_i \cdot \boldsymbol{a}_{3,j}.
$$

In this way, we get

$$
\boldsymbol{a}_i \cdot \boldsymbol{a}_{3,j} = -b_{ij} = -b_{ji} = \boldsymbol{a}_j \cdot \boldsymbol{a}_{3,i} = \boldsymbol{a}_{3,i} \cdot \boldsymbol{a}_j, \quad \forall i = 1, 2.
\tag{4.21}
$$

With (4.21) the following equation is true:

$$\boldsymbol{a}_{3,i} \cdot \boldsymbol{a}_j = -b_{ij} \quad \forall i = 1, 2.$$

Therefore

$$\begin{aligned}
\boldsymbol{a}_{3,i} &= -b_{ij} \cdot \boldsymbol{a}^j \\
&= -b_{ij} \cdot \boldsymbol{a}^j \cdot (\boldsymbol{a}^k \cdot \boldsymbol{a}_k) \\
&= -b_{ij} \cdot (\boldsymbol{a}^j \cdot \boldsymbol{a}^k) \cdot \boldsymbol{a}_k \\
&= -b_{ij} \cdot a^{jk} \cdot \boldsymbol{a}_k.
\end{aligned}$$

Consequently, we achieve

$$\begin{aligned}
\boldsymbol{a}_{3,i} \cdot \boldsymbol{a}_{3,j} &= (-b_{ik} \cdot a^{kl} \cdot \boldsymbol{a}_l) \cdot (-b_{jm} \cdot a^{mn} \cdot \boldsymbol{a}_n) \\
&= b_{ik} \cdot a^{kl} \cdot (\boldsymbol{a}_l \cdot \boldsymbol{a}_n) \cdot a^{nm} \cdot b_{mj} \\
&= b_{ik} \cdot a^{kl} \cdot a_{ln} \cdot a^{nm} \cdot b_{mj} \\
&= \delta_n^k \cdot b_{ik} \cdot a^{nm} \cdot b_{mj} \\
&= b_{in} \cdot a^{nm} \cdot b_{mj} \quad \forall i, j, k, m, n = 1, 2.
\end{aligned}$$

Obviously

$$(\boldsymbol{a}_{3,i} \cdot \boldsymbol{a}_{3,j})_{ij=1}^2 = \underline{b} \cdot \underline{a}^{-1} \cdot \underline{b} \tag{4.22}$$

and with (4.20), (4.21) and (4.22) the matrix of the right-Cauchy-Green deformation tensor can be calculated:

$$\begin{aligned}
\underline{c} &= \underline{a} - 2h\tau\underline{b} + (h\tau)^2\underline{b}\underline{a}^{-1}\underline{b} \\
&= (\underline{a} - h\tau\underline{b})\underline{a}^{-1}(\underline{a} - h\tau\underline{b}).
\end{aligned}$$

Analogously, the matrix with the coefficients of the strain tensor (4.18) is

$$\underline{e} = (\varepsilon_{ij})_{i,j=1}^2$$

with

$$2\underline{e} = (\underline{a} - h\tau\underline{b})\underline{a}^{-1}(\underline{a} - h\tau\underline{b}) - I. \tag{4.23}$$

# 5 Shell energy and boundary conditions

In this chapter we combine the three-dimensional theory for large deformations, described in the sections 2.2 and 2.3, with the new displacement vector $\boldsymbol{U}^{\text{KH}}$ from (4.14) as a result out of the Kirchhoff hypothesis. Consequently, we achieve a new $a$-form used in the variational formulation.

## 5.1 The resulting Kirchhoff deformation energy

We consider the energy functional (2.24) but use the displacement vector $\boldsymbol{U}^{\text{KH}}$ from (4.14) achieved from the Kirchhoff hypothesis.

Then

$$\varphi(\boldsymbol{U}^{\text{KH}}) = \int_{\Omega_0} \psi(\boldsymbol{U}^{\text{KH}})\, dV - f(\boldsymbol{U}^{\text{KH}}) \ \text{ with } \boldsymbol{U}^{\text{KH}} \in \left(\mathbb{H}^1_0(\Omega_0)\right)^3, \qquad (5.1)$$

where $\mathbb{H}^1_0$ is the Sobolev function space with functions vanishing at the Dirichlet boundary $\Gamma_D$.

As seen in (2.35), in the right-hand side of this new energy functional (5.1), for the boundary forces $f(\boldsymbol{U}^{\text{KH}})$ we have to integrate over $\Omega_0$. Within, the integration over the thickness parameter $\tau$ leads to zero for the second part in $\boldsymbol{U}^{\text{KH}}$ (4.14). Consequently, for the right-hand side in (5.1) we obtain

$$f(\boldsymbol{U}^{\text{KH}}) = f(\boldsymbol{U}).$$

Obviously we get the new energy functional

$$
\begin{aligned}
\varphi(\boldsymbol{U}^{\text{KH}}) &= \varphi(\boldsymbol{U} + h\tau(\boldsymbol{a}_3(\boldsymbol{U}) - \boldsymbol{e}_3)) \\
&= \int_{\Omega_0} \psi(\boldsymbol{U} + h\tau(\boldsymbol{a}_3(\boldsymbol{U}) - \boldsymbol{e}_3))\, dV - f(\boldsymbol{U}) \\
&= \int_{\Omega_0} \widehat{\psi}(\boldsymbol{U})\, dV - f(\boldsymbol{U}) \\
&=: \widehat{\varphi}(\boldsymbol{U}).
\end{aligned}
\qquad (5.2)
$$

**Remark 5.1** *With the Kirchhoff hypothesis we achieve a three-dimensional displacement vector $\boldsymbol{U}^{KH}$. This is the analogue to the displacement vector $\boldsymbol{U}$ in the*

*common three-dimensional theory of large deformations given in chapter 2. In what follows we consider the displacement vector of the mid surface $\boldsymbol{U} = \boldsymbol{U}(\eta^1, \eta^2)$, not to be mistaken for the displacement vector in the common three-dimensional theory.*

**Remark 5.2** *With the displacement vector* (4.14) *from the Kirchhoff hypothesis and remark 5.1 we have to consider the function space for the displacement vector $\boldsymbol{U}$ of the mid surface and the arbitrary test functions $\boldsymbol{V}$, respectively.*

*Therefore we define $\boldsymbol{U} \in \widehat{\mathbb{H}}$ where*

$$\widehat{\mathbb{H}} := \left\{ \left( \mathbb{H}^2(\Omega_0^m) \right)^3 \text{ with appropriate boundary conditions} \right\} \tag{5.3}$$

*is a special function space, due to the Kirchhoff assumption.*

*Later on in this chapter we consider the reason for using the Sobolev function space $(\mathbb{H}^2)^3$ and the appropriate boundary conditions.*

Analogously to the 3D-displacement vector $\boldsymbol{U}$ in (2.7) out of the common three-dimensional theory that minimizes the energy functional (2.24), the new displacement vector $\boldsymbol{U}(\eta^1, \eta^2)$ here minimizes the energy functional $\widehat{\varphi}$ above in such a way that the deformation energy (2.24) gets minimized over a non-linear set (4.14). Hence, the first derivative $\widehat{\varphi}'(\boldsymbol{U}; \boldsymbol{V})$ of the energy functional should vanish for all virtual displacements $\boldsymbol{V} \in \widehat{\mathbb{H}}$:

$$\widehat{\varphi}'(\boldsymbol{U}; \boldsymbol{V}) \stackrel{!}{=} 0.$$

The derivative of this energy functional arises from the variation of $\widehat{\psi}$,

$$\widehat{\psi}(\boldsymbol{U} + \boldsymbol{V}) = \widehat{\psi}(\boldsymbol{U}) + \widehat{\psi}'(\boldsymbol{U}; \boldsymbol{V}) + \text{ h.o.t.}$$

Here, the second Piola-Kirchhoff stress tensor $\overset{2}{\mathcal{T}}(\boldsymbol{U}^{\mathrm{KH}})$ is double the derivative of $\psi(\boldsymbol{U}^{\mathrm{KH}})$ w.r.t. $\mathcal{C}$. Hence

$$\widehat{\psi}'(\boldsymbol{U}, \boldsymbol{V}) = \frac{\partial \psi(\boldsymbol{U}^{\mathrm{KH}})}{\partial \boldsymbol{U}(\eta^1, \eta^2)} \circ \boldsymbol{V}$$

$$= \left[ \sum_{k=1}^{3} \frac{\partial \psi}{\partial a_k} \left( \frac{\partial a_k}{\partial \mathcal{C}} \right) : \frac{\partial \mathcal{C}}{\partial \boldsymbol{U}^{\mathrm{KH}}} \right] \circ \frac{\partial \boldsymbol{U}^{\mathrm{KH}}}{\partial \boldsymbol{U}} \circ \boldsymbol{V}$$

$$= \overset{2}{\mathcal{T}}(\mathcal{C}) : \mathcal{E}' \left( \boldsymbol{U}^{\mathrm{KH}}; \mathcal{L}(\boldsymbol{V}) \right) \quad \forall \boldsymbol{V} \in \widehat{\mathbb{H}}$$

with

$$\mathcal{L}(\boldsymbol{V}) := \frac{\partial \boldsymbol{U}^{\mathrm{KH}}}{\partial \boldsymbol{U}} \circ \boldsymbol{V}.$$

The symbol "$\circ$" denotes the application of the second part of the chain rule to an arbitrary vector function $\boldsymbol{V}$ in the way that $\mathcal{L}(\boldsymbol{V})$ is a linear operator with respect to $\boldsymbol{V}$ arising from the variation of $\boldsymbol{U}^{\mathrm{KH}}$:

$$\boldsymbol{U}^{\mathrm{KH}}(\boldsymbol{U} + \boldsymbol{V}) = \boldsymbol{U}^{\mathrm{KH}}(\boldsymbol{U}) + \mathcal{L}(\boldsymbol{V}) + \text{ h.o.t.} \tag{5.4}$$

Obviously,

$$\mathcal{L}(\boldsymbol{V}) = \boldsymbol{V} + h\tau \boldsymbol{a}_3'(\boldsymbol{U}; \boldsymbol{V}) \ \forall \boldsymbol{V} \in \widehat{\mathbb{H}}.$$

Let us consider the set

$$\mathbb{K} = \left\{ \boldsymbol{V}^{\mathrm{KH}} : \boldsymbol{V}^{\mathrm{KH}} = \boldsymbol{V} + \tau h (\boldsymbol{a}_3(\boldsymbol{V}) - \boldsymbol{e}_3); \ \ \boldsymbol{V} \in \widehat{\mathbb{H}} \right\} \tag{5.5}$$

of vector functions being defined in the same way as the displacement vector (4.14), resulting from the Kirchhoff hypothesis. Hence, with (4.18) the strain tensor $\mathcal{E}(\boldsymbol{U})$ forall $\boldsymbol{U} \in \mathbb{K}$ is of lower rank ($rank = 2$) without components of $\boldsymbol{e}_i \boldsymbol{e}_3$ or $\boldsymbol{e}_3 \boldsymbol{e}_3$.

Now, (5.4) is written formally in a correct way but it seems to result in a tensor $\mathcal{E}'\left(\boldsymbol{U}^{\mathrm{KH}}, \mathcal{L}(\boldsymbol{V})\right)$, which is of rank greater than two. Apparently, the derivative $\mathcal{L}(\boldsymbol{V})$ of the vector function $\boldsymbol{U}^{\mathrm{KH}}(\boldsymbol{U})$ in direction of a vector $\boldsymbol{V}$ is no longer in $\mathbb{K}$ (5.5) and lest in the considered non-linear set (4.14), over which the energy functional (5.1) should be minimized.

Contrary, if we consider the first derivative of the energy functional (2.32) directly and insist on the vector functions to be from $\mathbb{K}$ (5.5), we first need the linearization of the strain tensor $\widehat{\mathcal{E}}(\boldsymbol{U})$ (4.19):

$$
\begin{aligned}
2\widehat{\mathcal{E}}(\boldsymbol{U} + \boldsymbol{V}) = &\ \mathrm{Grad}_\mathcal{S} \left( \boldsymbol{U} + \boldsymbol{V} + \tau h \boldsymbol{a}_3(\boldsymbol{U} + \boldsymbol{V}) \right) \cdot \mathcal{A} \\
&+ \mathcal{A} \cdot \mathrm{Grad}_\mathcal{S} \left( \boldsymbol{U} + \boldsymbol{V} + \tau h \boldsymbol{a}_3(\boldsymbol{U} + \boldsymbol{V}) \right)^\top \\
&+ \mathrm{Grad}_\mathcal{S} \left( \boldsymbol{U} + \boldsymbol{V} + \tau h \boldsymbol{a}_3(\boldsymbol{U} + \boldsymbol{V}) \right) \cdot \mathrm{Grad}_\mathcal{S} \left( \boldsymbol{U} + \boldsymbol{V} + \tau h \boldsymbol{a}_3(\boldsymbol{U} + \boldsymbol{V}) \right)^\top \\
= &\ \left[ \mathrm{Grad}_\mathcal{S} \left( \boldsymbol{U} + \tau h \boldsymbol{a}_3(\boldsymbol{U}) \right) + \mathrm{Grad}_\mathcal{S} \left( \boldsymbol{V} + \tau h \boldsymbol{a}_3'(\boldsymbol{U}; \boldsymbol{V}) \right) + \mathrm{h.o.t.} \right] \cdot \mathcal{A} \\
&+ \mathcal{A} \cdot \left[ \mathrm{Grad}_\mathcal{S} \left( \boldsymbol{U} + \tau h \boldsymbol{a}_3(\boldsymbol{U}) \right) + \mathrm{Grad}_\mathcal{S} \left( \boldsymbol{V} + \tau h \boldsymbol{a}_3'(\boldsymbol{U}; \boldsymbol{V}) \right) + \mathrm{h.o.t.} \right]^\top \\
&+ \left[ \mathrm{Grad}_\mathcal{S} \left( \boldsymbol{U} + \tau h \boldsymbol{a}_3(\boldsymbol{U}) \right) + \mathrm{Grad}_\mathcal{S} \left( \boldsymbol{V} + \tau h \boldsymbol{a}_3'(\boldsymbol{U}; \boldsymbol{V}) \right) + \mathrm{h.o.t.} \right] \\
&\cdot \left[ \mathrm{Grad}_\mathcal{S} \left( \boldsymbol{U} + \tau h \boldsymbol{a}_3(\boldsymbol{U}) \right) + \mathrm{Grad}_\mathcal{S} \left( \boldsymbol{V} + \tau h \boldsymbol{a}_3'(\boldsymbol{U}; \boldsymbol{V}) \right) + \mathrm{h.o.t.} \right]^\top \\
= &\ 2\widehat{\mathcal{E}}(\boldsymbol{U}) + \mathrm{Grad}_\mathcal{S} \left( \boldsymbol{V} + \tau h \boldsymbol{a}_3'(\boldsymbol{U}; \boldsymbol{V}) \right) \cdot \mathcal{A} + \mathcal{A} \cdot \mathrm{Grad}_\mathcal{S} \left( \boldsymbol{V} + \tau h \boldsymbol{a}_3'(\boldsymbol{U}; \boldsymbol{V}) \right)^\top \\
&+ \mathrm{Grad}_\mathcal{S} \left( \boldsymbol{U} + \tau h \boldsymbol{a}_3(\boldsymbol{U}) \right) \cdot \mathrm{Grad}_\mathcal{S} \left( \boldsymbol{V} + \tau h \boldsymbol{a}_3'(\boldsymbol{U}; \boldsymbol{V}) \right)^\top \\
&+ \mathrm{Grad}_\mathcal{S} \left( \boldsymbol{V} + \tau h \boldsymbol{a}_3'(\boldsymbol{U}; \boldsymbol{V}) \right) \cdot \mathrm{Grad}_\mathcal{S} \left( \boldsymbol{U} + \tau h \boldsymbol{a}_3(\boldsymbol{U}) \right)^\top + \mathrm{h.o.t.}
\end{aligned}
$$

Hence

$$
\begin{aligned}
2\widehat{\mathcal{E}}'(\boldsymbol{U}; \boldsymbol{V}) = &\ \mathrm{Grad}_\mathcal{S} \left( \boldsymbol{V} + \tau h \boldsymbol{a}_3'(\boldsymbol{U}; \boldsymbol{V}) \right) \cdot \mathcal{A} \\
&+ \mathcal{A} \cdot \mathrm{Grad}_\mathcal{S} \left( \boldsymbol{V} + \tau h \boldsymbol{a}_3'(\boldsymbol{U}; \boldsymbol{V}) \right)^\top \\
&+ \mathrm{Grad}_\mathcal{S} \left( \boldsymbol{U} + \tau h \boldsymbol{a}_3(\boldsymbol{U}) \right) \cdot \mathrm{Grad}_\mathcal{S} \left( \boldsymbol{V} + \tau h \boldsymbol{a}_3'(\boldsymbol{U}; \boldsymbol{V}) \right)^\top \\
&+ \mathrm{Grad}_\mathcal{S} \left( \boldsymbol{V} + \tau h \boldsymbol{a}_3'(\boldsymbol{U}; \boldsymbol{V}) \right) \cdot \mathrm{Grad}_\mathcal{S} \left( \boldsymbol{U} + \tau h \boldsymbol{a}_3(\boldsymbol{U}) \right)^\top.
\end{aligned} \tag{5.6}
$$

This linearization of the strain tensor (5.6) is a second-order tensor of rank two with $\boldsymbol{a}_3'(\boldsymbol{U}; \boldsymbol{V})$ being a differential operator, which can be retrieved from the variation of $\boldsymbol{a}_3$:

$$
\begin{aligned}
\boldsymbol{a}_3(\boldsymbol{U} + \boldsymbol{V}) &= \boldsymbol{a}_3(\boldsymbol{U}) + \boldsymbol{a}_3'(\boldsymbol{U}; \boldsymbol{V}) + \text{ h.o.t.} \\
&= \frac{\boldsymbol{a}_1(\boldsymbol{U} + \boldsymbol{V}) \times \boldsymbol{a}_2(\boldsymbol{U} + \boldsymbol{V})}{\|\boldsymbol{a}_1(\boldsymbol{U} + \boldsymbol{V}) \times \boldsymbol{a}_2(\boldsymbol{U} + \boldsymbol{V})\|} \\
&= \frac{[\boldsymbol{a}_1(\boldsymbol{U}) + \boldsymbol{V}_{,1}] \times [\boldsymbol{a}_2(\boldsymbol{U}) + \boldsymbol{V}_{,2}]}{\|[\boldsymbol{a}_1(\boldsymbol{U}) + \boldsymbol{V}_{,1}] \times [\boldsymbol{a}_2(\boldsymbol{U}) + \boldsymbol{V}_{,2}]\|} \\
&= \frac{\boldsymbol{a}_1 \times \boldsymbol{a}_2 + \boldsymbol{V}_{,1} \times \boldsymbol{a}_2 + \boldsymbol{a}_1 \times \boldsymbol{V}_{,2} + \text{h.o.t.}}{\|\boldsymbol{a}_1 \times \boldsymbol{a}_2 + \boldsymbol{V}_{,1} \times \boldsymbol{a}_2 + \boldsymbol{a}_1 \times \boldsymbol{V}_{,2} + \text{h.o.t.}\|}
\end{aligned}
$$

The abbreviations

$$
\begin{aligned}
\boldsymbol{b} &:= \boldsymbol{a}_1 \times \boldsymbol{a}_2 \\
\tilde{\boldsymbol{v}} &:= \boldsymbol{V}_{,1} \times \boldsymbol{a}_2 + \boldsymbol{a}_1 \times \boldsymbol{V}_{,2}
\end{aligned}
\tag{5.7}
$$

yield

$$
\boldsymbol{a}_3(\boldsymbol{U} + \boldsymbol{V}) = \frac{\boldsymbol{b} + \tilde{\boldsymbol{v}} + \text{h.o.t.}}{\|\boldsymbol{b} + \tilde{\boldsymbol{v}} + \text{h.o.t.}\|}.
$$

The Taylor expansion for $\|\boldsymbol{b} + \tilde{\boldsymbol{v}}\|$ is calculated by

$$
\begin{aligned}
\|\boldsymbol{b} + \tilde{\boldsymbol{v}}\| = \sqrt{\|\boldsymbol{b} + \tilde{\boldsymbol{v}}\|^2} &\leq \sqrt{\|\boldsymbol{b}\|^2 + 2\boldsymbol{b} \cdot \tilde{\boldsymbol{v}} + \text{h.o.t}} \\
&\approx \|\boldsymbol{b}\| \left(1 + \frac{\boldsymbol{b} \cdot \tilde{\boldsymbol{v}}}{\|\boldsymbol{b}\|^2}\right)
\end{aligned}
$$

and in this way

$$
\|\boldsymbol{b} + \tilde{\boldsymbol{v}}\|^{-1} \approx \frac{1}{\|\boldsymbol{b}\|} \left(1 - \frac{\boldsymbol{b} \cdot \tilde{\boldsymbol{v}}}{\|\boldsymbol{b}\|^2}\right).
$$

Therefore, we can estimate

$$
\begin{aligned}
\boldsymbol{a}_3(\boldsymbol{U} + \boldsymbol{V}) &\approx (\boldsymbol{b} + \tilde{\boldsymbol{v}} + \text{h.o.t.}) \cdot \frac{1}{\|\boldsymbol{b}\|} \left(1 - \frac{\boldsymbol{b} \cdot \tilde{\boldsymbol{v}}}{\|\boldsymbol{b}\|^2}\right) \\
&= \frac{\boldsymbol{b}}{\|\boldsymbol{b}\|} + \frac{\tilde{\boldsymbol{v}}}{\|\boldsymbol{b}\|} - \frac{\boldsymbol{b}(\tilde{\boldsymbol{v}} \cdot \boldsymbol{b})}{\|\boldsymbol{b}\|^3} + \text{h.o.t.}
\end{aligned}
$$

Consequently

$$
\boldsymbol{a}_3'(\boldsymbol{U}; \boldsymbol{V}) = \frac{1}{\|\boldsymbol{b}\|} \left(\mathcal{I} - \frac{\boldsymbol{b}\boldsymbol{b}}{\|\boldsymbol{b}\|^2}\right) \cdot \tilde{\boldsymbol{v}} = \frac{1}{\|\boldsymbol{a}_1 \times \boldsymbol{a}_2\|} (\mathcal{I} - \boldsymbol{a}_3\boldsymbol{a}_3) \cdot \tilde{\boldsymbol{v}}
\tag{5.8}
$$

with $(\mathcal{I} - \boldsymbol{a}_3\boldsymbol{a}_3)$ being the orthoprojector onto the tangential space of the deformed mid surface. In mechanical literature this projector is also called the metric tensor of the deformed mid surface.

Concluding, we can write the first derivative of the new energy functional as

$$\widehat{\varphi}'(\boldsymbol{U};\boldsymbol{V}) = \int\limits_{\Omega_0} \overset{2}{\mathcal{T}}(\mathcal{C}) : \widehat{\mathcal{E}}'(\boldsymbol{U};\boldsymbol{V})d\Omega_0 - \int\limits_{\Omega_0} \rho_0 p \cdot \boldsymbol{V} \; d\Omega_0 + \int\limits_{\Gamma_{0,N}} \vec{g} \cdot \boldsymbol{V} \; d\mathcal{S}_0. \quad (5.9)$$

Until now, we have not considered any boundary conditions of the function space $\widehat{\mathbb{H}}$. Therefore we take a closer look onto this space in the following paragraph.

## 5.2 Boundary conditions

As one can see in (4.14), $\boldsymbol{U}^{\mathrm{KH}}$ contains the normal of the deformed mid surface, $\boldsymbol{a}_3$, which is a non-linear differential operator, applied to $\boldsymbol{U}$. In (5.9) differential operators are applied to $\boldsymbol{U}^{\mathrm{KH}}$ and accordingly to $\boldsymbol{a}_3$ as well. Hence, we need the second partial derivatives in $\boldsymbol{U}$. Therefore, the Sobolev function space $(\mathbb{H}_0^2(\Omega_0^m))^3$ is used in (5.3).

We consider the normal $\boldsymbol{a}_3$ in (4.9) at the boundary of the shell. Hence, one of the coordinates $(\eta^1, \eta^2)$ has to be constant. Without loss of generality we consider $\eta^1 = c$ with a fixed constant $c$, defining a boundary part (for all $\eta^2$ and for all $\tau \in \left[-\frac{1}{2}, \frac{1}{2}\right]$). If this boundary part is classified as hard clamped with homogeneous boundary conditions, then $\boldsymbol{U} = \boldsymbol{0}$ and $\boldsymbol{a}_3 = \boldsymbol{e}_3$ as can be easily seen in the equation for the undeformed mid surface of a plate (4.5) combined with the mid surface of the deformed shell (4.7) and the definition of the deformed shell (4.8) in conjunction with the definition of the normal vector (4.9). Generalized inhomogeneous boundary conditions mean that $\boldsymbol{U}$ and $\boldsymbol{a}_3$ are appropriately given. Now we evolute the contained cross product, omitting higher order parts of $\boldsymbol{U}$:

$$\boldsymbol{a}_3 = \frac{\boldsymbol{a}_1 \times \boldsymbol{a}_2}{\|\boldsymbol{a}_1 \times \boldsymbol{a}_2\|} = \frac{(\boldsymbol{e}_1 + \boldsymbol{U}_{,1}) \times (\boldsymbol{e}_2 + \boldsymbol{U}_{,2})}{\|(\boldsymbol{e}_1 + \boldsymbol{U}_{,1}) \times (\boldsymbol{e}_2 + \boldsymbol{U}_{,2})\|}$$

$$\Longleftrightarrow \quad (\boldsymbol{e}_1 + \boldsymbol{U}_{,1}) \times (\boldsymbol{e}_2 + \boldsymbol{U}_{,2}) = \boldsymbol{a}_3 \, \|(\boldsymbol{e}_1 + \boldsymbol{U}_{,1}) \times (\boldsymbol{e}_2 + \boldsymbol{U}_{,2})\|$$

$$\Longleftrightarrow \quad \boldsymbol{e}_3 + (\boldsymbol{e}_1 \times \boldsymbol{U}_{,2}) + (\boldsymbol{U}_{,1} \times \boldsymbol{e}_2) = \boldsymbol{a}_3 \, \|\boldsymbol{e}_3 + (\boldsymbol{e}_1 \times \boldsymbol{U}_{,2}) + (\boldsymbol{U}_{,1} \times \boldsymbol{e}_2)\|$$

$$\Longleftrightarrow \quad \boldsymbol{e}_3 + (\boldsymbol{e}_1 \times \boldsymbol{U}_{,2}) - (\boldsymbol{e}_2 \times \boldsymbol{U}_{,1}) = \boldsymbol{a}_3 \, \|\boldsymbol{e}_3 + (\boldsymbol{e}_1 \times \boldsymbol{U}_{,2}) - (\boldsymbol{e}_2 \times \boldsymbol{U}_{,1})\|.$$

For a hard clamped boundary part the condition $\boldsymbol{a}_3 = \boldsymbol{e}_3$ means

$$\begin{pmatrix} -U_{,1}^{(3)} \\ -U_{,2}^{(3)} \\ 1 + U_{,2}^{(2)} + U_{,1}^{(1)} \end{pmatrix} = \left\| \begin{pmatrix} -U_{,1}^{(3)} \\ -U_{,2}^{(3)} \\ 1 + U_{,2}^{(2)} + U_{,1}^{(1)} \end{pmatrix} \right\| \begin{pmatrix} 0 \\ 0 \\ 1 \end{pmatrix}.$$

Hence,

$$U^{(3)}_{,1} = U^{(3)}_{,2} = 0$$

and therefore

$$U^{(3)}_{,12} = 0$$

are the resulting boundary conditions for the displacement vector.

Consistently, the displacement vector has to be chosen out of the appropriate function space

$$\widehat{\mathbb{H}} = \left\{ \left( \mathbb{H}^2(\Omega_0) \right)^3 : U^{(3)}_{,1} = U^{(3)}_{,2} = U^{(3)}_{,12} = 0, \forall X \in \Gamma_D,\, j = 1, 2 \right\}.$$

In case of considering a soft clamped boundary part, one out of the two partial derivatives $U^{(3)}_{,i}$, $i = 1, 2$, is free.

## 5.3 The resulting weak formulation

We have seen that in comparison with the deformation energy in 2.24 from the common three-dimensional theory we have to accomplish a further operator $\mathcal{L}$, linear applied to $\boldsymbol{V}$, due to the Kirchhoff assumption. This operator $\mathcal{L}$ includes a differential operator $\boldsymbol{a}'_3(\boldsymbol{U}; \boldsymbol{V}) = \left( \frac{\partial \boldsymbol{a}_3}{\partial \boldsymbol{U}} \right) \circ \boldsymbol{V}$ (5.8), applied to virtual displacements $\boldsymbol{V} \in \widehat{\mathbb{H}}$.

In this way

$$\widehat{a}(\boldsymbol{U}; \boldsymbol{V}) = \int_{\Omega_0} \overset{2}{\mathcal{T}}(\mathcal{C}) : \widehat{\mathcal{E}}'(\boldsymbol{U}; \boldsymbol{V})\, dV, \ \ \forall \boldsymbol{V} \in \widehat{\mathbb{H}} \tag{5.10}$$

and

$$f(\boldsymbol{V}) = \int_{\Omega_0} \rho_0 p \cdot \boldsymbol{V}\, d\Omega_0 + \int_{\Gamma_{0,N}} \vec{g} \cdot \boldsymbol{V}\, d\mathcal{S}_0 \ \forall\, \boldsymbol{V} \in \widehat{\mathbb{H}}. \tag{5.11}$$

Hence, we can establish the new weak formulation:

Find the solution $\boldsymbol{U}$ in the appropriate function space $\widehat{\mathbb{H}}$ such that

$$\widehat{a}(\boldsymbol{U}; \boldsymbol{V}) = f(\boldsymbol{V}) \text{ for all } \boldsymbol{V} \in \widehat{\mathbb{H}}. \tag{5.12}$$

Additionally, with both equations above, (5.10) and (5.11), for the first derivative of the energy functional (5.9)

$$\widehat{\varphi}'(\boldsymbol{U}; \boldsymbol{V}) = \widehat{a}(\boldsymbol{U}; \boldsymbol{V}) - f(\boldsymbol{V}) \tag{5.13}$$

is true. Therefore, solving (5.12) is equivalent to compute

$$\widehat{\varphi}'(\boldsymbol{U}; \boldsymbol{V}) = 0.$$

# 6 Newton's method and implementation

## 6.1 Newton algorithm

In the Chapter 3 we have introduced Newton's method and we have defined the incremental algorithm (3.1). Therein the displacement vector $\boldsymbol{U}$ of the three-dimensional theory is used. We have replaced this displacement vector by the appropriate $\boldsymbol{U}^{\mathrm{KH}}$ in (4.14), resulting from the Kirchhoff hypothesis (4.13). As a consequence, we get the new energy functional (5.2) after recalculating the right Cauchy-Green deformation tensor $\widehat{\mathcal{C}}$ from (4.15) and, therefore, the Lagrangian strain tensor $\widehat{\mathcal{E}}$ in (4.19). By reason of this recalculation it takes much more effort to obtain the first linearization $\widehat{\mathcal{E}}'(\boldsymbol{U}; \boldsymbol{V})$ ((5.6) in conjunction with (5.8)) with the vector $\boldsymbol{V}$ so, that $\boldsymbol{U}^{\mathrm{KH}}(\boldsymbol{U} + \boldsymbol{V})$ is from $\mathbb{K}$, defined in (5.5).

In that way, we obtain the incremental Newton algorithm for this problem as

**Algorithm 6.1** (Incremental Newton solution process)

*(1) Start: $\boldsymbol{U} = \boldsymbol{0}, \ t := \Delta t$*

*(2) for $\boldsymbol{\delta U}$ solve $\widehat{\varphi}''(\boldsymbol{U}; \boldsymbol{\delta U}, \boldsymbol{V}) = t f(\boldsymbol{V}) - \widehat{a}(\boldsymbol{U}; \boldsymbol{V})$*

*(3) update $\boldsymbol{U} := \boldsymbol{U} + \boldsymbol{\delta U}$*

*(4) if ($\| \boldsymbol{\delta U} \| / \| \boldsymbol{U} \| < \varepsilon$): $t := t + \Delta t$ until $t = 1$*

*(5) goto (2).*

Herein the second linearization of the energy functional $\widehat{\varphi}''(\boldsymbol{U}; \boldsymbol{\delta U}, \boldsymbol{V})$ is needed, which we obtain as the linearization of equation (5.13). The chain rule, used in equation (5.10), implies

$$\widehat{\varphi}''(\boldsymbol{U}; \boldsymbol{\delta U}, \boldsymbol{V}) = \int_{\Omega_0} \overset{2}{\widehat{\mathcal{T}}'}(\boldsymbol{U}; \boldsymbol{\delta U}) : \widehat{\mathcal{E}}'(\boldsymbol{U}; \boldsymbol{V}) + \overset{2}{\widehat{\mathcal{T}}}(\widehat{\mathcal{C}}) : \widehat{\mathcal{E}}''(\boldsymbol{U}; \boldsymbol{\delta U}, \boldsymbol{V}) \, dV. \quad (6.1)$$

Here

$$\overset{2}{\widehat{\mathcal{T}}'}(\boldsymbol{U}; \boldsymbol{\delta U}) : \widehat{\mathcal{E}}'(\boldsymbol{U}; \boldsymbol{V}) = \widehat{\mathcal{E}}'(\boldsymbol{U}; \boldsymbol{\delta U}) : \mathfrak{C}(\boldsymbol{U}) : \widehat{\mathcal{E}}'(\boldsymbol{U}; \boldsymbol{V}) \quad (6.2)$$

using $\widehat{\mathcal{C}}$ instead of $\mathcal{C}$ for the material tangent $\mathfrak{C}(\boldsymbol{U})$ (3.2).

Hence, for the calculation of the second linearization of the energy functional $\widehat{\varphi}''(\boldsymbol{U}; \boldsymbol{\delta U}, \boldsymbol{V})$ we have to compute the second linearization of the strain tensor $\widehat{\mathcal{E}}''(\boldsymbol{U}; \boldsymbol{\delta U}, \boldsymbol{V})$. Therefore, we have to linearize the first linearization of the strain tensor $\widehat{\mathcal{E}}'(\boldsymbol{U}; \boldsymbol{V})$ (5.6) in connection with (5.8). For this purpose we get

$$
\begin{aligned}
2\widehat{\mathcal{E}}'(\boldsymbol{U} + \boldsymbol{\delta U}; \boldsymbol{V}) &= \mathrm{Grad}_{\mathcal{S}}\left(\boldsymbol{V} + \tau h \boldsymbol{a}_3'(\boldsymbol{U} + \boldsymbol{\delta U}; \boldsymbol{V})\right) \cdot \mathcal{A} \\
&+ \mathcal{A} \cdot \left[\mathrm{Grad}_{\mathcal{S}}\left(\boldsymbol{V} + \tau h \boldsymbol{a}_3'(\boldsymbol{U} + \boldsymbol{\delta U}; \boldsymbol{V})\right)\right]^{\top} \\
&+ \mathrm{Grad}_{\mathcal{S}}\left(\boldsymbol{U} + \boldsymbol{\delta U} + \tau h \boldsymbol{a}_3(\boldsymbol{U} + \boldsymbol{\delta U})\right) \cdot \left[\mathrm{Grad}_{\mathcal{S}}\left(\boldsymbol{V} + \tau h \boldsymbol{a}_3'(\boldsymbol{U} + \boldsymbol{\delta U}; \boldsymbol{V})\right)\right]^{\top} \\
&+ \mathrm{Grad}_{\mathcal{S}}\left(\boldsymbol{V} + \tau h \boldsymbol{a}_3'(\boldsymbol{U} + \boldsymbol{\delta U}; \boldsymbol{V})\right) \cdot \left[\mathrm{Grad}_{\mathcal{S}}\left(\boldsymbol{U} + \boldsymbol{\delta U} + \tau h \boldsymbol{a}_3(\boldsymbol{U} + \boldsymbol{\delta U})\right)\right]^{\top} \\
&= \left[\mathrm{Grad}_{\mathcal{S}}\left(\boldsymbol{V} + \tau h \boldsymbol{a}_3'(\boldsymbol{U}; \boldsymbol{V})\right) + \mathrm{Grad}_{\mathcal{S}}\left(\tau h \boldsymbol{a}_3''(\boldsymbol{U}; \boldsymbol{\delta U}, \boldsymbol{V})\right) + \mathrm{h.o.t.}\right] \cdot \mathcal{A} \\
&+ \mathcal{A} \cdot \left[\mathrm{Grad}_{\mathcal{S}}\left(\boldsymbol{V} + \tau h \boldsymbol{a}_3'(\boldsymbol{U}; \boldsymbol{V})\right) + \mathrm{Grad}_{\mathcal{S}}\left(\tau h \boldsymbol{a}_3''(\boldsymbol{U}; \boldsymbol{\delta U}, \boldsymbol{V})\right) + \mathrm{h.o.t.}\right]^{\top} \\
&+ \left[\mathrm{Grad}_{\mathcal{S}}\left(\boldsymbol{U} + \tau h \boldsymbol{a}_3(\boldsymbol{U})\right) + \mathrm{Grad}_{\mathcal{S}}\left(\boldsymbol{\delta U} + \tau h \boldsymbol{a}_3'(\boldsymbol{U}; \boldsymbol{\delta U})\right) + \mathrm{h.o.t.}\right] \\
&\quad \cdot \left[\mathrm{Grad}_{\mathcal{S}}\left(\boldsymbol{V} + \tau h \boldsymbol{a}_3'(\boldsymbol{U}; \boldsymbol{V})\right) + \mathrm{Grad}_{\mathcal{S}}\left(\tau h \boldsymbol{a}_3''(\boldsymbol{U}; \boldsymbol{\delta U}, \boldsymbol{V})\right) + \mathrm{h.o.t.}\right]^{\top} \\
&+ \left[\mathrm{Grad}_{\mathcal{S}}\left(\boldsymbol{V} + \tau h \boldsymbol{a}_3'(\boldsymbol{U}; \boldsymbol{V})\right) + \mathrm{Grad}_{\mathcal{S}}\left(\tau h \boldsymbol{a}_3''(\boldsymbol{U}; \boldsymbol{\delta U}, \boldsymbol{V})\right) + \mathrm{h.o.t.}\right] \\
&\quad \cdot \left[\mathrm{Grad}_{\mathcal{S}}\left(\boldsymbol{U} + \tau h \boldsymbol{a}_3(\boldsymbol{U})\right) + \mathrm{Grad}_{\mathcal{S}}\left(\boldsymbol{\delta U} + \tau h \boldsymbol{a}_3'(\boldsymbol{U}; \boldsymbol{\delta U})\right) + \mathrm{h.o.t.}\right]^{\top} \\
&= 2\widehat{\mathcal{E}}'(\boldsymbol{U}; \boldsymbol{V}) + \mathrm{Grad}_{\mathcal{S}}\left(\tau h \boldsymbol{a}_3''(\boldsymbol{U}; \boldsymbol{\delta U}, \boldsymbol{V})\right) \cdot \mathcal{A} + \mathcal{A} \cdot \left[\mathrm{Grad}_{\mathcal{S}}\left(\tau h \boldsymbol{a}_3''(\boldsymbol{U}; \boldsymbol{\delta U}, \boldsymbol{V})\right)\right]^{\top} \\
&+ \mathrm{Grad}_{\mathcal{S}}\left(\boldsymbol{U} + \tau h \boldsymbol{a}_3(\boldsymbol{U})\right) \cdot \left[\mathrm{Grad}_{\mathcal{S}}\left(\tau h \boldsymbol{a}_3''(\boldsymbol{U}; \boldsymbol{\delta U}, \boldsymbol{V})\right)\right]^{\top} \\
&+ \mathrm{Grad}_{\mathcal{S}}\left(\tau h \boldsymbol{a}_3''(\boldsymbol{U}; \boldsymbol{\delta U}, \boldsymbol{V})\right) \cdot \left[\mathrm{Grad}_{\mathcal{S}}\left(\boldsymbol{U} + \tau h \boldsymbol{a}_3(\boldsymbol{U})\right)\right]^{\top} \\
&+ \mathrm{Grad}_{\mathcal{S}}\left(\boldsymbol{\delta U} + \tau h \boldsymbol{a}_3'(\boldsymbol{U}; \boldsymbol{\delta U})\right) \cdot \left[\mathrm{Grad}_{\mathcal{S}}\left(\boldsymbol{V} + \tau h \boldsymbol{a}_3'(\boldsymbol{U}; \boldsymbol{V})\right)\right]^{\top} \\
&+ \mathrm{Grad}_{\mathcal{S}}\left(\boldsymbol{V} + \tau h \boldsymbol{a}_3'(\boldsymbol{U}; \boldsymbol{V})\right) \cdot \left[\mathrm{Grad}_{\mathcal{S}}\left(\boldsymbol{\delta U} + \tau h \boldsymbol{a}_3'(\boldsymbol{U}; \boldsymbol{\delta U})\right)\right]^{\top} + \mathrm{h.o.t.}
\end{aligned}
$$

In that way

$$
\begin{aligned}
2\widehat{\mathcal{E}}'(\boldsymbol{U}; \boldsymbol{\delta U}, \boldsymbol{V}) &= \mathrm{Grad}_{\mathcal{S}}\left(\tau h \boldsymbol{a}_3''(\boldsymbol{U}; \boldsymbol{\delta U}, \boldsymbol{V})\right) \cdot \mathcal{A} \\
&+ \mathcal{A} \cdot \left[\mathrm{Grad}_{\mathcal{S}}\left(\tau h \boldsymbol{a}_3''(\boldsymbol{U}; \boldsymbol{\delta U}, \boldsymbol{V})\right)\right]^{\top} \\
&+ \mathrm{Grad}_{\mathcal{S}}\left(\boldsymbol{U} + \tau h \boldsymbol{a}_3(\boldsymbol{U})\right) \cdot \left[\mathrm{Grad}_{\mathcal{S}}\left(\tau h \boldsymbol{a}_3''(\boldsymbol{U}; \boldsymbol{\delta U}, \boldsymbol{V})\right)\right]^{\top}
\end{aligned}
$$

$$+ \operatorname{Grad}_{\mathcal{S}} \left( \tau h \boldsymbol{a}_3''(\boldsymbol{U}; \boldsymbol{\delta U}, \boldsymbol{V}) \right) \cdot \left[ \operatorname{Grad}_{\mathcal{S}} \left( \boldsymbol{U} + \tau h \boldsymbol{a}_3(\boldsymbol{U}) \right) \right]^\top$$

$$+ \operatorname{Grad}_{\mathcal{S}} \left( \boldsymbol{\delta U} + \tau h \boldsymbol{a}_3'(\boldsymbol{U}; \boldsymbol{\delta U}) \right) \cdot \left[ \operatorname{Grad}_{\mathcal{S}} \left( \boldsymbol{V} + \tau h \boldsymbol{a}_3'(\boldsymbol{U}; \boldsymbol{V}) \right) \right]^\top$$

$$+ \operatorname{Grad}_{\mathcal{S}} \left( \boldsymbol{V} + \tau h \boldsymbol{a}_3'(\boldsymbol{U}; \boldsymbol{V}) \right) \cdot \left[ \operatorname{Grad}_{\mathcal{S}} \left( \boldsymbol{\delta U} + \tau h \boldsymbol{a}_3'(\boldsymbol{U}; \boldsymbol{\delta U}) \right) \right]^\top .$$

Obviously, for the completion of the calculation of the second derivative of the energy functional $\widehat{\varphi}''(\boldsymbol{U}; \boldsymbol{\delta U}, \boldsymbol{V})$ the second linearization of the normal vector of the deformed mid surface $\boldsymbol{a}_3''(\boldsymbol{U}; \boldsymbol{\delta U}, \boldsymbol{V})$ has to be calculated.

In addition to the abbreviations (5.7) we define

$$\widetilde{\boldsymbol{\delta U}} := \boldsymbol{\delta U}_{,1} \times \boldsymbol{a}_2 + \boldsymbol{a}_1 \times \boldsymbol{\delta U}_{,2}.$$

Furthermore, the first derivative of the normal of the deformed mid surface is already given in (5.8). Then, the variation of the orthoprojector in (5.8) yields

$$\left( \mathcal{I} - \boldsymbol{a}_3(\boldsymbol{U} + \boldsymbol{\delta U}) \boldsymbol{a}_3(\boldsymbol{U} + \boldsymbol{\delta U}) \right)$$
$$= (\mathcal{I} - \boldsymbol{a}_3 \boldsymbol{a}_3) - \boldsymbol{a}_3(\boldsymbol{U}) \boldsymbol{a}_3'(\boldsymbol{U}; \boldsymbol{\delta U}) - \boldsymbol{a}_3'(\boldsymbol{U}; \boldsymbol{\delta U}) \boldsymbol{a}_3(\boldsymbol{U}) + \text{h.o.t.}$$

Hence, its linearization is

$$-\boldsymbol{a}_3(\boldsymbol{U}) \boldsymbol{a}_3'(\boldsymbol{U}; \boldsymbol{\delta U}) - \boldsymbol{a}_3'(\boldsymbol{U}; \boldsymbol{\delta U}) \boldsymbol{a}_3(\boldsymbol{U})$$
$$= -\frac{1}{\|\boldsymbol{b}\|} \boldsymbol{a}_3(\mathcal{I} - \boldsymbol{a}_3 \boldsymbol{a}_3) \cdot \widetilde{\boldsymbol{\delta U}} - \frac{1}{\|\boldsymbol{b}\|} (\mathcal{I} - \boldsymbol{a}_3 \boldsymbol{a}_3) \cdot \widetilde{\boldsymbol{\delta U}} \boldsymbol{a}_3$$
$$= -\frac{1}{\|\boldsymbol{b}\|} \left[ \boldsymbol{a}_3 \widetilde{\boldsymbol{\delta U}} + \widetilde{\boldsymbol{\delta U}} \boldsymbol{a}_3 - (\boldsymbol{a}_3 \cdot \widetilde{\boldsymbol{\delta U}}) \boldsymbol{a}_3 \boldsymbol{a}_3 - (\widetilde{\boldsymbol{\delta U}} \cdot \boldsymbol{a}_3) \boldsymbol{a}_3 \boldsymbol{a}_3 \right] \qquad (6.3)$$
$$= \frac{1}{\|\boldsymbol{b}\|} \left[ 2(\boldsymbol{a}_3 \cdot \widetilde{\boldsymbol{\delta U}}) \boldsymbol{a}_3 \boldsymbol{a}_3 - \boldsymbol{a}_3 \widetilde{\boldsymbol{\delta U}} - \widetilde{\boldsymbol{\delta U}} \boldsymbol{a}_3 \right] .$$

Therefore, the variation of the first derivative of the normal of the deformed mid surface $\boldsymbol{a}_3'(\boldsymbol{U}; \boldsymbol{V})$ is obtained as

$$\boldsymbol{a}_3'(\boldsymbol{U}+\boldsymbol{\delta U}; \boldsymbol{V}) = \frac{\mathcal{I} - \boldsymbol{a}_3(\boldsymbol{U} + \boldsymbol{\delta U}) \boldsymbol{a}_3(\boldsymbol{U} + \boldsymbol{\delta U})}{\|\boldsymbol{a}_1(\boldsymbol{U} + \boldsymbol{\delta U}) \times \boldsymbol{a}_2(\boldsymbol{U} + \boldsymbol{\delta U})\|}$$
$$\cdot (\boldsymbol{V}_{,1} \times \boldsymbol{a}_2(\boldsymbol{U} + \boldsymbol{\delta U}) + \boldsymbol{a}_1(\boldsymbol{U} + \boldsymbol{\delta U}) \times \boldsymbol{V}_{,2})$$
$$= \frac{1}{\left\| \boldsymbol{b} + \widetilde{\boldsymbol{\delta U}} + \text{h.o.t.} \right\|} \left( (\mathcal{I} - \boldsymbol{a}_3 \boldsymbol{a}_3) - \boldsymbol{a}_3(\boldsymbol{U}) \boldsymbol{a}_3'(\boldsymbol{U}; \boldsymbol{\delta U}) \right.$$
$$\left. - \boldsymbol{a}_3'(\boldsymbol{U}; \boldsymbol{\delta U}) \boldsymbol{a}_3(\boldsymbol{U}) + \text{h.o.t.} \right) \cdot (\widetilde{\boldsymbol{v}} + \boldsymbol{V}_{,1} \times \boldsymbol{\delta U}_{,2} + \boldsymbol{\delta U}_{,1} \times \boldsymbol{V}_{,2})$$
$$= \frac{1}{\|\boldsymbol{b}\|} \left( 1 - \frac{\widetilde{\boldsymbol{\delta U}} \cdot \boldsymbol{b}}{\|\boldsymbol{b}\|^2} \right) \left( (\mathcal{I} - \boldsymbol{a}_3 \boldsymbol{a}_3) - \boldsymbol{a}_3(\boldsymbol{U}) \boldsymbol{a}_3'(\boldsymbol{U}; \boldsymbol{\delta U}) \right.$$
$$\left. - \boldsymbol{a}_3'(\boldsymbol{U}; \boldsymbol{\delta U}) \boldsymbol{a}_3(\boldsymbol{U}) + \text{h.o.t.} \right) \cdot (\widetilde{\boldsymbol{v}} + \boldsymbol{V}_{,1} \times \boldsymbol{\delta U}_{,2} + \boldsymbol{\delta U}_{,1} \times \boldsymbol{V}_{,2})$$
$$= \left( \frac{1}{\|\boldsymbol{b}\|} (\mathcal{I} - \boldsymbol{a}_3 \boldsymbol{a}_3) \cdot \widetilde{\boldsymbol{v}} \right) + \frac{1}{\|\boldsymbol{b}\|} (\mathcal{I} - \boldsymbol{a}_3 \boldsymbol{a}_3)$$
$$\cdot (\boldsymbol{V}_{,1} \times \boldsymbol{\delta U}_{,2} + \boldsymbol{\delta U}_{,1} \times \boldsymbol{V}_{,2}) - \frac{1}{\|\boldsymbol{b}\|} \left( \boldsymbol{a}_3(\boldsymbol{U}) \boldsymbol{a}_3'(\boldsymbol{U}; \boldsymbol{\delta U}) \right.$$

$$+ \boldsymbol{a}_3'(\boldsymbol{U};\boldsymbol{\delta U})\boldsymbol{a}_3(\boldsymbol{U})\Big) \cdot \tilde{\boldsymbol{v}} - \frac{\widetilde{\boldsymbol{\delta U}} \cdot \boldsymbol{b}}{\|\boldsymbol{b}\|^3}(\mathcal{I} - \boldsymbol{a}_3\boldsymbol{a}_3) \cdot \tilde{\boldsymbol{v}} + \text{h.o.t.}$$

$$= \boldsymbol{a}_3'(\boldsymbol{U};\boldsymbol{V}) + \boldsymbol{a}_3''(\boldsymbol{U};\boldsymbol{\delta U},\boldsymbol{V}) + \text{h.o.t.}$$

In that way, the second linearization $\boldsymbol{a}_3''(\boldsymbol{U};\boldsymbol{\delta U},\boldsymbol{V})$ can be identified as

$$
\begin{aligned}
\boldsymbol{a}_3''(\boldsymbol{U};\boldsymbol{\delta U},\boldsymbol{V}) = {} & \frac{1}{\|\boldsymbol{b}\|}(\mathcal{I} - \boldsymbol{a}_3\boldsymbol{a}_3) \cdot (\boldsymbol{V}_{,1} \times \boldsymbol{\delta U}_{,2} + \boldsymbol{\delta U}_{,1} \times \boldsymbol{V}_{,2}) \\
& - \frac{1}{\|\boldsymbol{b}\|}\Big(\boldsymbol{a}_3(\boldsymbol{U})\boldsymbol{a}_3'(\boldsymbol{U};\boldsymbol{\delta U}) + \boldsymbol{a}_3'(\boldsymbol{U};\boldsymbol{\delta U})\boldsymbol{a}_3(\boldsymbol{U})\Big) \cdot \tilde{\boldsymbol{v}} \\
& - \frac{\widetilde{\boldsymbol{\delta U}} \cdot \boldsymbol{b}}{\|\boldsymbol{b}\|^3}(\mathcal{I} - \boldsymbol{a}_3\boldsymbol{a}_3) \cdot \tilde{\boldsymbol{v}} \\
= {} & \frac{1}{\|\boldsymbol{b}\|}(\boldsymbol{V}_{,1} \times \boldsymbol{\delta U}_{,2} + \boldsymbol{\delta U}_{,1} \times \boldsymbol{V}_{,2}) \\
& + \frac{1}{\|\boldsymbol{b}\|}\boldsymbol{a}_3\boldsymbol{a}_3 \cdot (\boldsymbol{\delta U}_{,2} \times \boldsymbol{V}_{,1} + \boldsymbol{V}_{,2} \times \boldsymbol{\delta U}_{,1}) \\
& + \frac{1}{\|\boldsymbol{b}\|^2}\Big[2(\boldsymbol{a}_3 \cdot \widetilde{\boldsymbol{\delta U}})\boldsymbol{a}_3\boldsymbol{a}_3 - \boldsymbol{a}_3\widetilde{\boldsymbol{\delta U}} - \widetilde{\boldsymbol{\delta U}}\boldsymbol{a}_3\Big] \cdot \tilde{\boldsymbol{v}} \\
& - \frac{1}{\|\boldsymbol{b}\|^2}(\widetilde{\boldsymbol{\delta U}} \cdot \boldsymbol{a}_3)\Big((\mathcal{I} - \boldsymbol{a}_3\boldsymbol{a}_3) \cdot \tilde{\boldsymbol{v}}\Big) \\
= {} & \frac{1}{\|\boldsymbol{b}\|}(\boldsymbol{V}_{,1} \times \boldsymbol{\delta U}_{,2} + \boldsymbol{\delta U}_{,1} \times \boldsymbol{V}_{,2}) \\
& + \frac{1}{\|\boldsymbol{b}\|}\Big([\boldsymbol{\delta U}_{,2}, \boldsymbol{V}_{,1}, \boldsymbol{a}_3] + [\boldsymbol{V}_{,2}, \boldsymbol{\delta U}_{,1}, \boldsymbol{a}_3]\Big)\boldsymbol{a}_3 \\
& + \frac{2}{\|\boldsymbol{b}\|^2}(\boldsymbol{a}_3 \cdot \widetilde{\boldsymbol{\delta U}})(\boldsymbol{a}_3 \cdot \tilde{\boldsymbol{v}})\boldsymbol{a}_3 - \frac{1}{\|\boldsymbol{b}\|^2}(\widetilde{\boldsymbol{\delta U}} \cdot \tilde{\boldsymbol{v}})\boldsymbol{a}_3 \\
& - \frac{1}{\|\boldsymbol{b}\|^2}(\tilde{\boldsymbol{v}} \cdot \boldsymbol{a}_3)\widetilde{\boldsymbol{\delta U}} - \frac{1}{\|\boldsymbol{b}\|^2}(\widetilde{\boldsymbol{\delta U}} \cdot \boldsymbol{a}_3)\tilde{\boldsymbol{v}} \\
& + \frac{1}{\|\boldsymbol{b}\|^2}(\boldsymbol{a}_3 \cdot \widetilde{\boldsymbol{\delta U}})(\boldsymbol{a}_3 \cdot \tilde{\boldsymbol{v}})\boldsymbol{a}_3 \\
= {} & \frac{1}{\|\boldsymbol{b}\|}(\boldsymbol{V}_{,1} \times \boldsymbol{\delta U}_{,2} + \boldsymbol{\delta U}_{,1} \times \boldsymbol{V}_{,2}) \\
& - \frac{1}{\|\boldsymbol{b}\|^2}(\tilde{\boldsymbol{v}} \cdot \boldsymbol{a}_3)\widetilde{\boldsymbol{\delta U}} - \frac{1}{\|\boldsymbol{b}\|^2}(\widetilde{\boldsymbol{\delta U}} \cdot \boldsymbol{a}_3)\tilde{\boldsymbol{v}} \\
& + \frac{1}{\|\boldsymbol{b}\|}\Big([\boldsymbol{\delta U}_{,2}, \boldsymbol{V}_{,1}, \boldsymbol{a}_3] + [\boldsymbol{V}_{,2}, \boldsymbol{\delta U}_{,1}, \boldsymbol{a}_3] \\
& + \frac{3}{\|\boldsymbol{b}\|}(\boldsymbol{a}_3 \cdot \widetilde{\boldsymbol{\delta U}})(\boldsymbol{a}_3 \cdot \tilde{\boldsymbol{v}}) - \frac{1}{\|\boldsymbol{b}\|}(\widetilde{\boldsymbol{\delta U}} \cdot \tilde{\boldsymbol{v}})\Big)\boldsymbol{a}_3.
\end{aligned}
$$

$$(6.3)$$

$$(6.4)$$

With the linear functional

$$\gamma_1(\boldsymbol{U}) = \frac{1}{\|\boldsymbol{b}\|^2}\boldsymbol{U} \cdot \boldsymbol{a}_3$$

and the bilinear functional

$$
\gamma_2(\boldsymbol{U}, \boldsymbol{V}) = \frac{1}{\|\boldsymbol{b}\|} \Big( [\boldsymbol{U}_{,2}, \boldsymbol{V}_{,1}, \boldsymbol{a}_3] + [\boldsymbol{V}_{,2}, \boldsymbol{U}_{,1}, \boldsymbol{a}_3]
$$
$$
+ \frac{3}{\|\boldsymbol{b}\|} (\boldsymbol{a}_3 \cdot \widetilde{\boldsymbol{\delta U}})(\boldsymbol{a}_3 \cdot \widetilde{\boldsymbol{v}}) - \frac{1}{\|\boldsymbol{b}\|}(\widetilde{\boldsymbol{\delta U}} \cdot \widetilde{\boldsymbol{v}}) \Big)
$$

equation (6.4) is transformed into

$$
\boldsymbol{a}_3''(\boldsymbol{U}; \boldsymbol{\delta U}, \boldsymbol{V}) = \frac{1}{\|\boldsymbol{b}\|}(\boldsymbol{V}_{,1} \times \boldsymbol{\delta U}_{,2} + \boldsymbol{\delta U}_{,1} \times \boldsymbol{V}_{,2})
$$
$$
- \gamma_1(\widetilde{\boldsymbol{\delta U}})\widetilde{\boldsymbol{V}} - \gamma_1(\widetilde{\boldsymbol{V}})\widetilde{\boldsymbol{\delta U}} + \gamma_2(\boldsymbol{\delta U}, \boldsymbol{V})\boldsymbol{a}_3.
$$

In that way, equation (6.1) in conjunction with (6.2) is now calculable as

$$
\widehat{\varphi}''(\boldsymbol{U}; \boldsymbol{\delta U}, \boldsymbol{V}) = \int_{\Omega_0} \widehat{\mathcal{E}}'(\boldsymbol{U}; \boldsymbol{\delta U}) : \mathfrak{C}(\boldsymbol{U}) : \widehat{\mathcal{E}}'(\boldsymbol{U}; \boldsymbol{V}) \, dV
$$
$$
+ \int_{\Omega_0} \overset{2}{\widehat{\mathcal{T}}}(\widehat{\mathcal{C}}) : \widehat{\mathcal{E}}''(\boldsymbol{U}; \boldsymbol{\delta U}, \boldsymbol{V}) \, dV. \tag{6.5}
$$

We have seen, that the calculation of the second derivative of the Lagrangian strain tensor $\widehat{\mathcal{E}}''(\boldsymbol{U}; \boldsymbol{\delta U}, \boldsymbol{V})$ is much more labour-intensive as for the appropriate derivative in the 3D theory (3.3).

## 6.2 Finite Element Method (FEM)

The incremental Newton's method is embedded into the Finite Element Method (FEM), that approximates the infinite dimensional problem (5.12) above with a finite dimensional sub-space $\mathbb{V}_h$ of piecewise low order polynomials $p_k$. Therefore, the solution of the weak formulation (5.12) is discretized by a finite dimensional solution $\boldsymbol{U}_h$ out of this sub-space. The ansatz functions $p_k$ are defined on a mesh $\mathbb{T}_h$ of non overlapping finite elements $T$. This mesh of elements completely covers the given domain,

$$
\Omega_0^m = \bigcup_{T \in \mathbb{T}_h} T, \ \ T_i \cap T_j = \emptyset \ \ \forall T_i, T_j \in \mathbb{T}_h, \ \ i \neq j.
$$

In general, finite elements are triangles or quadrilaterals for $\mathbb{R}^2$ and for example tetrahedrons or hexahedrons for $\mathbb{R}^3$, respectively.

A finite element mesh is called a conform mesh, if every side of a finite element $T_i \in \mathbb{T}_h$ is either part of the boundary $\partial \Omega$ or a side of another finite element $T_j \in \mathbb{T}_h$. We speak of isotropic finite elements $T$, if there exists a constant $c$ such that

$$
h_T \leq c \rho_T
$$

with the element diameter $h_T$ and $\rho_T$ the diameter of the inner element circle or of the inner element sphere, respectively. A finite element mesh is called shape regular, if it only consists of isotropic finite elements.

Now, with $h = \max_{T \in \mathbb{T}_h} h_T$ we consider the biggest element diameter of the mesh $\mathbb{T}_h$. Then, we call a mesh quasi uniform, if the constants $c_1$ and $c_2$ exist such that

$$c_1 h \leq h_T \leq c_2 h.$$

In that way, for example locally refined meshes are not quasi uniform.

FEM is used to approximate the solutions. Hence, we consider equation (6.5). In the first integral we have the first derivative of the strain tensor, depending linearly on $\boldsymbol{\delta U}$ and once again linearly on $\boldsymbol{V}$. The material tangent $\mathfrak{C}$ depends only on $\boldsymbol{U}$. In the second integral of (6.5) the second derivative of the strain tensor depends linearly on $\boldsymbol{\delta U}$ and $\boldsymbol{V}$ at once.

Therefore, we now consider the sub-space $\mathbb{V}_h$ with its ansatz functions $\boldsymbol{p}_i$, forming a basis of $\mathbb{V}_h$. Then the displacement vector $\boldsymbol{U}$ as well as the directions $\boldsymbol{V}$ and $\boldsymbol{\delta U}$ are displayed in $\mathbb{V}_h$ by

$$\boldsymbol{U}_h = \sum_{i=1}^{3N} \boldsymbol{p}_i \cdot u_i, \quad \boldsymbol{V}_h = \sum_{i=1}^{3N} \boldsymbol{p}_i \cdot v_i, \quad \boldsymbol{\delta U}_h = \sum_{i=1}^{3N} \boldsymbol{p}_i \cdot du_i. \tag{6.6}$$

Here, the entire number of degrees of freedom in the sub-space $\mathbb{V}_h$ is denoted by $3N$. Let $\underline{du} = (du_1, du_2, \ldots, du_{3N})^\top$ and $\underline{u} = (u_1, u_2, \ldots, u_{3N})^\top$. Then (5.12) is approximated in the finite dimensional sub-space $\mathbb{V}_h$ via Newton's method as

**Algorithm 6.2** (Discretized Newton solution process for one fixed increment t)

*(1)* $\underline{b} = \left[ t f(\boldsymbol{p}_i) - a(\boldsymbol{U}_h, \boldsymbol{p}_i) \right]_{i=1}^{3N}$,

*(2)* $\underline{K}(\boldsymbol{U}_h) = \left[ \int_{\Omega_0} \widehat{\mathcal{E}}'(\boldsymbol{U}_h; \boldsymbol{p}_j) : \mathfrak{C} : \widehat{\mathcal{E}}'(\boldsymbol{U}_h; \boldsymbol{p}_i) + \overset{2}{\mathcal{T}} : \widehat{\mathcal{E}}''(\boldsymbol{U}_h; \boldsymbol{p}_j, \boldsymbol{p}_i) \, d\Omega_0 \right]_{i,j=1}^{3N}$

*(3)* *solve* $\underline{K}(\boldsymbol{U}_h) \, \underline{du} = \underline{b}$

*(4)* *update* $\underline{u} := \underline{u} + \underline{du}$, *until* $\varepsilon = \|\underline{du}\| \, / \, \|\underline{u}\| \leq 10^{-8}$.

As written before, the ansatz functions $\boldsymbol{p}_i$ are piecewise polynomials in $\Omega_0^m$ w.r.t. $\mathbb{T}_h$. Obviously, the vector valued ansatz functions $\boldsymbol{p}_i$ are $p_j \boldsymbol{e}_1, p_j \boldsymbol{e}_2, p_j \boldsymbol{e}_3$, $(j = 1, \ldots, N)$ and the scalar functions $p_j$ are defined elementwise via the form functions $q_k$ on $T$

$$p_j|_T =: q_{k,T}.$$

With this form functions $q_{k,T}$ we can define the element stiffness matrix $K_T(\boldsymbol{U}_h)$ and the element right hand side $\underline{b}_T$ as

$$
\underline{K}_T(\boldsymbol{U}_h) = \left[ \int\limits_{-\frac{1}{2}}^{\frac{1}{2}} \int\limits_T \widehat{\mathcal{E}}'(\boldsymbol{U}_h; q_{j,T}\boldsymbol{e}_k) : \mathfrak{C} : \widehat{\mathcal{E}}'(\boldsymbol{U}_h; q_{i,T}\boldsymbol{e}_l) \right.
$$
$$
\left. + \overset{2}{\mathcal{T}} : \widehat{\mathcal{E}}''(\boldsymbol{U}_h; q_{j,T}\boldsymbol{e}_k, q_{i,T}\boldsymbol{e}_l) \, d\mathcal{S}_0 \, h d\tau \right]_{i,j=1 \ \ k,l=1}^{N_T \quad 3}, \tag{6.7}
$$
$$
\underline{b}_T = \left[ f(q_{i,T}\boldsymbol{e}_l) - a(\boldsymbol{U}_h, q_{i,T}\boldsymbol{e}_l) \right]_{i=1 \ \ l=1}^{N_T \quad 3}.
$$

$3N_T$ is the number of the local degrees of freedom in the element $T$. After calculating the element stiffness matrix and the element right hand side in every element $T \in \mathbb{T}_h$ the stiffness matrix $\underline{K}(\boldsymbol{U}_h)$ and the right hand side $\underline{b}$ are assembled in the common way.

After calculating the solution on the actual mesh, a mesh refinement may possibly improve the approximation. Then, the interpolated solution of the coarser mesh is the starting solution for the calculation on the refined triangulation.

Due to the problem (5.12) with functions in $\mathbb{H}^2$, the conformal FE-approach requires $C^1$-continuity of the ansatz functions $p_j$ as proved in [5].

For axis-parallel rectangular elements, the Bogner-Fox-Schmidt elements can be used and are considered. For a more general shape of the plate some generalizations using triangular meshes are known, such as the (reduced) Hsiegh-Clough-Tocher element or similar.

## 6.2.1 Bogner-Fox-Schmidt (BFS) elements

Using the FEM in the $(\eta^1, \eta^2)$-coordinate system, we apply BFS elements for our numerical experiments, in that the mid surface of the plate is a polygon with its boundaries parallel to the $\eta^1$- and to the $\eta^2$-axis. Due to quasi uniform mesh refinement, the boundaries of all finite elements in the FEM-mesh remain parallel to the axes, too.

One typical axis-parallel element $T$ should be represented by the four nodes

$$
x_1 = \begin{pmatrix} \eta_1^1 \\ \eta_1^2 \end{pmatrix}; \quad x_2 = \begin{pmatrix} \eta_2^1 \\ \eta_2^2 \end{pmatrix}; \quad x_3 = \begin{pmatrix} \eta_3^1 \\ \eta_3^2 \end{pmatrix}; \quad x_4 = \begin{pmatrix} \eta_4^1 \\ \eta_4^2 \end{pmatrix}.
$$

As written in the section above, we use ansatz functions with a local support. For that purpose, in the BFS-element $T$ 16 bi-cubic form functions $q_{k,T}^{ab}$, $k = 1, \ldots 4$, $a, b = 0, 1$ have to be defined. To avoid the definition of these form functions on every finite element we consider a reference element $\widehat{T} \in [-1, 1]^2 \subset \mathbb{R}^2$, also

called master element. We map $\widehat{T} = [-1, 1]^2$ to $T$ simply by

$$x = \begin{pmatrix} \eta^1 \\ \eta^2 \end{pmatrix} = \frac{1}{2} \begin{pmatrix} h_1 & 0 \\ 0 & h_2 \end{pmatrix} \widehat{x} + x_0, \tag{6.8}$$

with the master coordinates $\widehat{x} = (\xi^1, \xi^2)^\top$. Furthermore,

$$\begin{pmatrix} h_1 \\ 0 \end{pmatrix} := x_2 - x_1 = x_4 - x_3,$$

$$\begin{pmatrix} 0 \\ h_2 \end{pmatrix} := x_4 - x_1 = x_3 - x_2,$$

and

$$x_0 = \frac{1}{4}(x_1 + x_2 + x_3 + x_4)$$

is the element mid point.

As proved in [5], for a $C^1$-continuous FE-approach we need bi-cubic form functions in the master element $\widehat{T}$. For this purpose, we consider the four cubic functions $p_L^a$ and $p_R^a$ $(a = 0, 1)$, displayed in Figure 6.1.
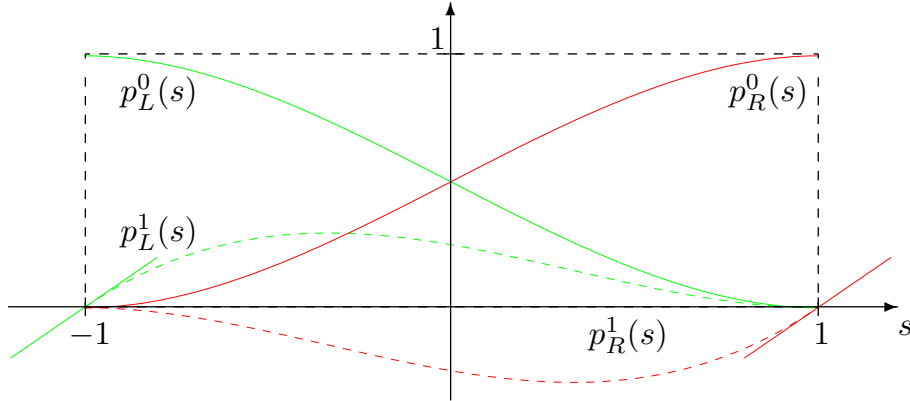


Figure 6.1: third-order polynomials.

These functions are given by

$$\begin{aligned}
p_L^0 &: [-1, 1] \mapsto \mathbb{R}; \; p_L^0(s) := \frac{1}{4}(1 - s)^2(2 + s), \\
p_L^1 &: [-1, 1] \mapsto \mathbb{R}; \; p_L^1(s) := \frac{1}{4}(1 - s)^2(1 + s), \\
p_R^0 &: [-1, 1] \mapsto \mathbb{R}; \; p_R^0(s) := p_L^0(-s), \\
p_R^1 &: [-1, 1] \mapsto \mathbb{R}; \; p_R^1(s) := -p_L^1(-s).
\end{aligned} \tag{6.9}$$

The derivatives of the cubic functions (6.9) are

$$\left(p_L^0\right)'(s) = \frac{3}{4}(s+1)(s-1),$$

$$\left(p_L^0\right)''(s) = \frac{3}{2}s,$$

$$\left(p_L^1\right)'(s) = \frac{1}{4}(3s+1)(s-1),$$

$$\left(p_L^1\right)''(s) = \frac{1}{2}(3s-1).$$

Note, that the values of these polynomials and their derivatives in $(\pm 1)$ are

$$p_L^0(-1) = 1, \qquad p_L^0(1) = 0, \qquad \left(p_L^0\right)'(\pm 1) = 0,$$

$$p_L^1(\pm 1) = 0, \qquad \left(p_L^1\right)'(-1) = 1, \qquad \left(p_L^1\right)'(1) = 0$$

Analogously, the values of $p_R^a(s)$, $(a = 0,1)$ at $s = (\pm 1)$ as well as the values of their derivatives at $s = (\pm 1)$ can be calculated.

Now, we define the bi-cubic form functions on the master element $\widehat{T}$ as

$$\begin{aligned}
\widehat{q}_1^{ab}(\xi^1, \xi^2) &:= p_L^a(\xi^1)p_L^b(\xi^2), \\
\widehat{q}_2^{ab}(\xi^1, \xi^2) &:= p_R^a(\xi^1)p_L^b(\xi^2), \\
\widehat{q}_3^{ab}(\xi^1, \xi^2) &:= p_L^a(\xi^1)p_R^b(\xi^2), \\
\widehat{q}_4^{ab}(\xi^1, \xi^2) &:= p_R^a(\xi^1)p_R^b(\xi^2).
\end{aligned} \tag{6.10}$$

Finally, with the mapping (6.8) we define the form functions for the element $T$ as

$$q_k^{ab}(\mathrm{x}) = \left(\frac{1}{2}h_1\right)^a \left(\frac{1}{2}h_2\right)^b \widehat{q}_k^{ab}(\widehat{\mathrm{x}}). \tag{6.11}$$

Herein, the factors are needed, due to the transformation of the derivatives

$$\partial_i = \frac{2}{h_i}\widehat{\partial}_i.$$

With (6.10) as well as the abbreviations

$$\partial_i := \frac{\partial}{\partial \eta^i}, \quad \nabla := (\partial_1, \partial_2)^\top \text{ and } \partial_i\partial_j := \frac{\partial^2}{\partial \eta^i \partial \eta^j} \tag{6.12}$$

for these form functions (6.11) the following properties are obtained:

$$\begin{aligned}
q_k^{00}(\mathrm{x}_i) &= \delta_i^k, & \nabla q_k^{00}(\mathrm{x}_i) &= (0,0)^\top, & \partial_1\partial_2 q_k^{00}(\mathrm{x}_i) &= 0, \\
q_k^{10}(\mathrm{x}_i) &= 0, & \nabla q_k^{10}(\mathrm{x}_i) &= (1,0)^\top \delta_{ik}, & \partial_1\partial_2 q_k^{10}(\mathrm{x}_i) &= 0, \\
q_k^{01}(\mathrm{x}_i) &= 0, & \nabla q_k^{01}(\mathrm{x}_i) &= (0,1)^\top \delta_{ik}, & \partial_1\partial_2 q_k^{01}(\mathrm{x}_i) &= 0, \\
q_k^{11}(\mathrm{x}_i) &= 0, & \nabla q_k^{11}(\mathrm{x}_i) &= (0,0)^\top, & \partial_1\partial_2 q_k^{11}(\mathrm{x}_i) &= \delta_{ik}.
\end{aligned}$$

Hence,

$$\partial_c \partial_d q_k^{ab}(\mathrm{x}_l) = \delta_{kl} \cdot \delta_{ca} \cdot \delta_{db}$$

for all $k, l = 1, \ldots, 4$ and for all $a, b, c, d = 1, 2$.

For the rearrangement of the expansion coefficients $\underline{u} = (u_1, u_2, \ldots, u_{3N})$ of $\boldsymbol{U}_h$ from (6.6), we define the $N = 4n$ vectors $\boldsymbol{u}_k^{ab} \in \mathbb{R}^3$ as

$$\boldsymbol{u}_k^{ab} = (\partial_1)^a (\partial_2)^b \ \boldsymbol{U}_h(\mathrm{x}_k), \quad k = 1, \ldots, n; \ \ a, b = 0, 1, \tag{6.13}$$

wherein $n$ denotes the total number of nodes in the actual triangulation.

Then, in every element the displacement vector is approximated by

$$\boldsymbol{U}_h(\mathrm{x})|_T = \sum_{k=1}^{4} \sum_{a,b=0}^{1} \boldsymbol{u}_k^{ab} q_k^{ab}(\mathrm{x}),$$

with $\boldsymbol{u}_1^{ab}, \boldsymbol{u}_2^{ab}, \boldsymbol{u}_3^{ab}$ and $\boldsymbol{u}_4^{ab}$ the nodal values of $T$ after resorting their indices. Hence, for the BFS-element we have 12 degrees of freedom per node and globally

$$3N = 3 \cdot 4 \cdot n = 12n.$$

Let us now consider the approximation of $\boldsymbol{\delta U}$. Then, with the same rearrangement (6.13) of the appropriate expansion coefficients $\underline{du} \in \mathbb{R}^{3N}$ on each element we have

$$\boldsymbol{\delta U}_h(\mathrm{x})|_T = \sum_{k=1}^{4} \sum_{a,b=0}^{1} \boldsymbol{du}_k^{ab} q_k^{ab}(\mathrm{x}).$$

## 6.2.2 Hsiegh-Clough-Tocher (HCT) elements

As written above, the BFS elements are used for example with edges, parallel to the axis. For all other plate examples, especially for plates with curved boundary, triangle elements are more suitable. An appropriate $C^1$-continuous triangle element is the HCT element. Here, we have three degrees of freedom at each node. These are the values of the finite element function $\boldsymbol{U}$ and its partial derivatives. Furthermore the normal derivative at the mid point of each edge of the element, which is a quadratic polynomial, is specified. For the reduced HCT element we insist on the normal derivative to be linear along the edges of the element. For our numerical experiments we have implemented the reduced HCT element.

The form functions are not polynomials (as usual) in the whole element $T$, but polynomial within three sub-triangles. Hence, we subdivide $T$ into three sub-triangles $T_k$. Therefore, an arbitrary internal point $\mathrm{x}_0 \in T$ has to be connected

with the vertices $x_j$, $(j = 1, \ldots, 3)$ of the element $T$. In the literature the center of gravity is preferred, due to the effect that the calculation of the Jacobian is simplified. Hence,

$$x_0 = \frac{1}{3} \sum_{j=1}^{3} x_j.$$

We define three form functions

$$q_i^a, \quad a = 0, 1, 2,$$

associated with the vertex $x_i$, which are cubic inside of each sub-triangles fulfilling the following properties:

- $q_i^a$ are $C^1$ continuous over $T$,

- $q_i^a(x_j) = \delta_{ij} \cdot \delta_{0a}$, $\quad \nabla q_i^a(x_j) = \delta_{ij} \cdot (\delta_{1a} \ \ \delta_{2a})^\top$,

- $\frac{\partial}{\partial \boldsymbol{n}} q_i^a$ is linear along each edge of $T$, with $\boldsymbol{n}$ the outer normal vector of the considered edge.

As result we get nine nodal base functions $q_i^a$. For further information we refer to [22].

## 6.3 Efficient solution of the linear systems of equation

It is well known that the arising tangential stiffness matrix $\underline{K}(\boldsymbol{U}_h)$ is very ill conditioned even in the linear elastic case (which can be understood as $\underline{K}(\boldsymbol{0})$ in the very first step of Newton's method). From the character of the bi-harmonic plate equation together with the local basic functions, a condition number proportional to $h^{-4}$ is expected.

Here, we solve these linear systems with a preconditioned conjugate gradient method, where the appropriate preconditioner is the key for obtaining an efficient procedure. It should be noted that we use a multilevel technique at least for the construction of the mesh, that is given as a coarse mesh of some relatively large rectangles, which are successively subdivided into 4 quarters from level to level. This hierarchical mesh generation procedure is successfully used for preconditioning the linear system by hierarchical techniques.

The ansatz functions of the BFS-elements as described above fulfil a refinement formula, such that the 4-tuple of functions belonging to one node $x_k$:

$$(p_k^{00}, p_k^{10}, p_k^{01}, p_k^{11})^{coarse}$$

for a fixed level $l$ of the mesh refinement, are linear combinations of the next finer functions

$$(p_i^{00}, p_i^{10}, p_i^{01}, p_i^{11})^{finer}$$

for nodes $\mathrm{x}_i$ around the coarse-mesh node $\mathrm{x}_k$ of the next level $(l+1)$.

Based on this refinement formula a BPX-preconditioner [6] has been investigated in [17],[27] and [28] for the case of a linear Koiter-shell equation. All the details of the refinement and the resulting base transformation are found in [27].

Here, we have used a slightly simpler approach, a hierarchical basis preconditioner due to [29], which is a simple matrix multiply $\underline{C}^{-1} = \underline{Q}\,\underline{J}\,\underline{Q}^{\top}$, where $\underline{Q}$ is three times the $(N \times N)$-matrix of basis transformation of the hierarchical basis of the finest FE-space into the given nodal basis. (This matrix multiplication is extremely cheep from using the refinement formula above.)

The diagonal matrix $\underline{J}$ contains important scaling factors, which are different for the 4 functions $p_k^{ab}$ $(a, b = 0, 1)$ on each node $\mathrm{x}_k$. These factors can be obtained during the mesh refinement from the diagonals of the actual stiffness matrices together with the nodal hierarchy used in the $\underline{Q}$-multiply.

So, these ingredients would remain valid when our uniform mesh refinement is replaced by an adaptive regime.

## 6.4 Implementation

In this section we want to give an overview of the ideas for the realization of the theoretical aspects from the last chapters. The basic principles of the implementation for computing the element stiffness matrix will follow.

For simplicity we restrict ourselves to BFS-elements. For the reduced HCT-element the implementation is nearly the same, but the number of form functions and the dimension of the element stiffness matrix differs. The mathematical procedures are equal.

For the implementation of the element stiffness matrix $\underline{K}_T$ from (6.7) the most interesting second-order tensors are $\widehat{\mathcal{E}}'(\boldsymbol{U}; \boldsymbol{V})$ in the first part and $\widehat{\mathcal{E}}(\boldsymbol{U}; \boldsymbol{\delta U}, \boldsymbol{V})$ in the second part of the integral. Note, that these tensors are of rank 2. Therefore, their Cartesian coefficients are displayed as the $(2 \times 2)$-matrices $\underline{e}'(\boldsymbol{U}, \boldsymbol{V})$ and $\underline{e}''(\boldsymbol{U}; \boldsymbol{\delta U}, \boldsymbol{V})$, respectively. These matrices are obtained by applying the chain rule to (4.23):

$$
\begin{aligned}
\underline{e}'(\boldsymbol{U}; \boldsymbol{V}) &= \left(\varepsilon_{ij}\right)_{i,j=1}^{2} \\
&= \left(\underline{a}'(\boldsymbol{U}; \boldsymbol{V}) - \tau\underline{b}'(\boldsymbol{U}; \boldsymbol{V})\right)\underline{a}^{-1}(\boldsymbol{U})\left(\underline{a}(\boldsymbol{U}) - h\tau\underline{b}(\boldsymbol{U})\right) & (I) \\
&\quad - \left(\underline{a}(\boldsymbol{U}) - h\tau\underline{b}(\boldsymbol{U})\right)\underline{a}^{-1}(\boldsymbol{U})\underline{a}'(\boldsymbol{U}; \boldsymbol{V})\underline{a}^{-1}(\boldsymbol{U})\left(\underline{a}(\boldsymbol{U}) - h\tau\underline{b}(\boldsymbol{U})\right) & (II) \\
&\quad + \left(\underline{a}(\boldsymbol{U}) - h\tau\underline{b}(\boldsymbol{U})\right)\underline{a}^{-1}(\boldsymbol{U})\left(\underline{a}'(\boldsymbol{U}; \boldsymbol{V}) - \tau\underline{b}'(\boldsymbol{U}; \boldsymbol{V})\right). & (III)
\end{aligned}
\tag{6.14}
$$

Obviously, the matrix of the first derivative of the strain tensor is a result of multiplications of the matrix of the first fundamental forms $\underline{a}(\boldsymbol{U})$ from (4.10), the matrix of the second fundamental forms $\underline{b}(\boldsymbol{U})$ from (4.11) as well as the matrix of their linearization $\underline{a}'(\boldsymbol{U};\boldsymbol{V})$ and $\underline{b}'(\boldsymbol{U};\boldsymbol{V})$, respectively. These linearizations are obtained by utilizing the chain rule to (4.10) and (4.11), respectively. For the first fundamental forms we achieve

$$\underline{a}'_{ij}(\boldsymbol{U};\boldsymbol{V}) = a_i(\boldsymbol{U}) \cdot \boldsymbol{V}_{,j} + a_j(\boldsymbol{U}) \cdot \boldsymbol{V}_{,i}, \;\; i,j = 1,2. \tag{6.15}$$

For the second fundamental forms $\underline{b}$ we define

$$D(\boldsymbol{U}) = \left( \det \underline{a} \right)^{-\frac{1}{2}}$$

and obtain

$$\underline{b}'_{ij}(\boldsymbol{U};\boldsymbol{V}) = D'(\boldsymbol{U};\boldsymbol{V})\widetilde{\underline{b}}_{ij}(\boldsymbol{U}) + D(\boldsymbol{U})\widetilde{\underline{b}}'_{ij}(\boldsymbol{U};\boldsymbol{V}) \;\; (i,j = 1,2) \tag{6.16}$$

with

$$\widetilde{\underline{b}}'_{ij}(\boldsymbol{U};\boldsymbol{V}) = [\boldsymbol{a}_1, \boldsymbol{V}_{,2}, \boldsymbol{U}_{,ij}] + [\boldsymbol{V}_{,1}, \boldsymbol{a}_2, \boldsymbol{U}_{,ij}] + [\boldsymbol{a}_1, \boldsymbol{a}_2, \boldsymbol{V}_{,ij}], \;\; i,j = 1,2$$

and $D'(\boldsymbol{U};\boldsymbol{V})$ a scalar function. With $[*,*,*]$ the scalar triple product is displayed.

For a simple implementation and due to the fact that we have symmetric $(2 \times 2)$-matrices only, we introduce Voigt's notation. With that a $(2 \times 2)$-matrix is written as a vector with three components. In that way, the vector notation of the matrix of the first derivative of the strain tensor (6.14) is

$$\mathrm{E}'(\boldsymbol{U};\boldsymbol{V}) = \left( \varepsilon_{11}(\boldsymbol{U};\boldsymbol{V}), \varepsilon_{22}(\boldsymbol{U};\boldsymbol{V}), 2\varepsilon_{12}(\boldsymbol{U};\boldsymbol{V}) \right)^{\top}.$$

Let us consider the $(3 \times 3)$-matrices

$$\underline{D}_A(\mathrm{z}) = \begin{pmatrix} 2\boldsymbol{e}_1^{\top} z_1 \\[1ex] 2\boldsymbol{e}_2^{\top} z_2 \\[1ex] \boldsymbol{e}_1^{\top} z_2 + \boldsymbol{e}_2^{\top} z_1 \end{pmatrix} \;\text{ and }\; \underline{D}_A(\boldsymbol{U}, z) = \begin{pmatrix} 2\boldsymbol{U}_{,1}^{\top} z_1 \\[1ex] 2\boldsymbol{U}_{,2}^{\top} z_2 \\[1ex] \boldsymbol{U}_{,1}^{\top} z_2 + \boldsymbol{U}_{,2}^{\top} z_1 \end{pmatrix}. \tag{6.17}$$

With these linear operators, applied to $\nabla$ from (6.12), the first derivative of the first fundamental forms can be computed in Voigt's notation by

$$\mathrm{A}'(\boldsymbol{U};\boldsymbol{V}) = \underline{D}_A(\nabla)\boldsymbol{V} + \underline{D}_A(\boldsymbol{U}, \nabla)\boldsymbol{V}.$$

Now, let us consider the operators

$$
\underline{D}_B(z) = \begin{pmatrix} (\boldsymbol{a}_1 \times \boldsymbol{a}_2)^\top z_1 z_1 \\[2mm] (\boldsymbol{a}_1 \times \boldsymbol{a}_2)^\top z_2 z_2 \\[2mm] (\boldsymbol{a}_1 \times \boldsymbol{a}_2)^\top z_1 z_2 \end{pmatrix} \quad \text{and} \quad \underline{D}_{B_a}(\boldsymbol{U}, z_b) = \begin{pmatrix} (\boldsymbol{U}_{,11} \times \boldsymbol{a}_a)^\top z_b \\[2mm] (\boldsymbol{U}_{,22} \times \boldsymbol{a}_a)^\top z_b \\[2mm] (\boldsymbol{U}_{,12} \times \boldsymbol{a}_a)^\top z_b \end{pmatrix}, \quad (6.18)
$$

which are $(3 \times 3)$-matrices, too. Then, using the abbreviations from (6.12), the vector notation of $\underline{\tilde{b}}'(\boldsymbol{U}; \boldsymbol{V})$ is computable as

$$
\widetilde{\mathrm{B}}'(\boldsymbol{U}; \boldsymbol{V}) = \underline{D}_B(\nabla)\boldsymbol{V} + \underline{D}_{B_1}(\boldsymbol{U}, \partial_2)\boldsymbol{V} - \underline{D}_{B_2}(\boldsymbol{U}, \partial_1)\boldsymbol{V}.
$$

Hence, the vector notation of the first derivative of the strain tensor $\mathrm{E}'(\boldsymbol{U}; \boldsymbol{V})$ is a linear combination of the components of the first derivative of the first fundamental forms in vector notation $\mathrm{A}'(\boldsymbol{U}; \boldsymbol{V})$ and the one of the second fundamental forms $\mathrm{B}'(\boldsymbol{U}; \boldsymbol{V})$, following the matrix multiplication rules, using $\mathrm{A}(\boldsymbol{U})$ as the vector notation of the first fundamental forms and $\mathrm{B}(\boldsymbol{U})$ the one of the second fundamental forms, respectively.

In that way, the first part of the integral in (6.7)

$$
\int_{\Omega_0} \widehat{\mathcal{E}}'(\boldsymbol{U}; \boldsymbol{V}_1) : \mathfrak{C}(\boldsymbol{U}) : \widehat{\mathcal{E}}(\boldsymbol{U}; \boldsymbol{V}_2)\, dV
$$

is the same as

$$
\int_{\Omega_0} \mathrm{E}'(\boldsymbol{U}; \boldsymbol{V}_1)^\top \underline{C}\, \mathrm{E}'(\boldsymbol{U}; \boldsymbol{V}_2)\, dV \tag{6.19}
$$

with the corresponding $(3 \times 3)$-matrix $\underline{C} = \underline{C}(\boldsymbol{U})$ of the material tangent $\mathfrak{C}$.

For the BFS element $T$ the directions $\boldsymbol{V}_i$ $(i = 1, 2)$ in (6.19) have to pass through the 48 form functions $q_k^{ab}(\mathrm{x})\boldsymbol{e}_i$, $k = 1, \ldots, 4$, $a, b = 0, 1$, $i = 1, \ldots, 3$, with $q_k^{ab}(\mathrm{x})$ from (6.11) and $\boldsymbol{e}_i$ the unity vectors in the Euclidean space. Let $Q$ be the row vector of the 16 values of the form functions $q_k^{ab}(\mathrm{x})$ and $\underline{I}$ the $(3 \times 3)$-unity matrix. Furthermore, with

$$
\underline{D}(\boldsymbol{U}, \nabla)\boldsymbol{V} = \mathrm{E}'(\boldsymbol{U}, \boldsymbol{V})
$$

the derivation operator $\underline{D}(\boldsymbol{U}, \nabla)$ defines all the linear combinations of the derivation operators (6.17) and (6.18) for calculating $\boldsymbol{E}'(\boldsymbol{U}, *)$, following the matrix calculus. Then, there exists the $(3 \times 48)$-matrix

$$
\underline{M} = \underline{D}(\boldsymbol{U}, \nabla)(\underline{Q} \otimes \underline{I})
$$

with $\otimes$ denoting the Kronecker product. With this matrix $\underline{M}$ above, the first part of the element stiffness matrix (6.19), written in Voigt's notation, yields

$$\int\limits_{\Omega_0} \underline{M}^\top \underline{C}(\boldsymbol{U}) \, \underline{M} \, dV.$$

As written before, for the second part of equation (6.7) for the element stiffness matrix $\underline{K}_T$ the matrix of the second linearization of the strain tensor is needed. The reapplication of the chain rule to (6.14) yields

$$\underline{e}''(\boldsymbol{U}; \boldsymbol{\delta U}, \boldsymbol{V}) = \left(\underline{a}''(\boldsymbol{U}; \boldsymbol{\delta U}, \boldsymbol{V}) - \tau \underline{b}''(\boldsymbol{U}; \boldsymbol{\delta U}, \boldsymbol{V})\right)\underline{a}^{-1}(\boldsymbol{U})\left(\underline{a}(\boldsymbol{U}) - h\tau\underline{b}(\boldsymbol{U})\right)$$
$$- \left(\underline{a}'(\boldsymbol{U}; \boldsymbol{V}) - \tau \underline{b}'(\boldsymbol{U}; \boldsymbol{V})\right)\underline{a}^{-1}(\boldsymbol{U})\underline{a}'(\boldsymbol{U}; \boldsymbol{\delta U})\underline{a}^{-1}(\boldsymbol{U})\left(\underline{a}(\boldsymbol{U}) - h\tau\underline{b}(\boldsymbol{U})\right) \qquad (I)$$
$$+ \left(\underline{a}'(\boldsymbol{U}; \boldsymbol{V}) - \tau \underline{b}'(\boldsymbol{U}; \boldsymbol{V})\right)\underline{a}^{-1}(\boldsymbol{U})\left(\underline{a}'(\boldsymbol{U}; \boldsymbol{\delta U}) - \tau \underline{b}'(\boldsymbol{U}; \boldsymbol{\delta U})\right)$$

$$- \left(\underline{a}'(\boldsymbol{U}; \boldsymbol{\delta U}) - \tau \underline{b}'(\boldsymbol{U}; \boldsymbol{\delta U})\right)\underline{a}^{-1}(\boldsymbol{U})\underline{a}'(\boldsymbol{U}; \boldsymbol{V})\underline{a}^{-1}(\boldsymbol{U})\left(\underline{a}(\boldsymbol{U}) - h\tau\underline{b}(\boldsymbol{U})\right)$$
$$+ \left(\underline{a}(\boldsymbol{U}) - h\tau\underline{b}(\boldsymbol{U})\right)\underline{a}^{-1}(\boldsymbol{U})\underline{a}'(\boldsymbol{U}; \boldsymbol{\delta U})\underline{a}^{-1}(\boldsymbol{U})\underline{a}'(\boldsymbol{U}; \boldsymbol{V})\underline{a}^{-1}(\boldsymbol{U})\left(\underline{a}(\boldsymbol{U}) - h\tau\underline{b}(\boldsymbol{U})\right)$$
$$- \left(\underline{a}(\boldsymbol{U}) - h\tau\underline{b}(\boldsymbol{U})\right)\underline{a}^{-1}(\boldsymbol{U})\underline{a}''(\boldsymbol{U}; \boldsymbol{\delta U}, \boldsymbol{V})\underline{a}^{-1}(\boldsymbol{U})\left(\underline{a}(\boldsymbol{U}) - h\tau\underline{b}(\boldsymbol{U})\right) \qquad (II)$$
$$+ \left(\underline{a}(\boldsymbol{U}) - h\tau\underline{b}(\boldsymbol{U})\right)\underline{a}^{-1}(\boldsymbol{U})\underline{a}'(\boldsymbol{U}; \boldsymbol{V})\underline{a}^{-1}(\boldsymbol{U})\underline{a}'(\boldsymbol{U}; \boldsymbol{\delta U})\underline{a}^{-1}(\boldsymbol{U})\left(\underline{a}(\boldsymbol{U}) - h\tau\underline{b}(\boldsymbol{U})\right)$$
$$- \left(\underline{a}(\boldsymbol{U}) - h\tau\underline{b}(\boldsymbol{U})\right)\underline{a}^{-1}(\boldsymbol{U})\underline{a}'(\boldsymbol{U}; \boldsymbol{V})\underline{a}^{-1}(\boldsymbol{U})\left(\underline{a}'(\boldsymbol{U}; \boldsymbol{\delta U}) - \tau \underline{b}'(\boldsymbol{U}; \boldsymbol{\delta U})\right)$$

$$+ \left(\underline{a}'(\boldsymbol{U}; \boldsymbol{\delta U}) - \tau \underline{b}'(\boldsymbol{U}; \boldsymbol{\delta U})\right)\underline{a}^{-1}(\boldsymbol{U})\left(\underline{a}'(\boldsymbol{U}; \boldsymbol{V}) - \tau \underline{b}'(\boldsymbol{U}; \boldsymbol{V})\right)$$
$$- \left(\underline{a}(\boldsymbol{U}) - h\tau\underline{b}(\boldsymbol{U})\right)\underline{a}^{-1}(\boldsymbol{U})\underline{a}'(\boldsymbol{U}; \boldsymbol{\delta U})\underline{a}^{-1}(\boldsymbol{U})\left(\underline{a}'(\boldsymbol{U}; \boldsymbol{V}) - \tau \underline{b}'(\boldsymbol{U}; \boldsymbol{V})\right) \qquad (III)$$
$$+ \left(\underline{a}(\boldsymbol{U}) - h\tau\underline{b}(\boldsymbol{U})\right)\underline{a}^{-1}(\boldsymbol{U})\left(\underline{a}''(\boldsymbol{U}; \boldsymbol{\delta U}, \boldsymbol{V}) - \tau \underline{b}''(\boldsymbol{U}; \boldsymbol{\delta U}, \boldsymbol{V})\right).$$

Obviously, the matrix of the second linearization of the strain tensor is a result of multiple matrix multiplications of the matrices of the first and second fundamental forms from (4.10) and (4.11), respectively, with their first linearizations from (6.15) and (6.16) as well as their second derivatives. These second derivatives we obtain by applying the chain rule to their first derivatives, respectively. Hence,

$$\underline{a}''_{ij}(\boldsymbol{U}; \boldsymbol{\delta U}, \boldsymbol{V}) = \boldsymbol{\delta U}_{,i} \cdot \boldsymbol{V}_{,j} + \boldsymbol{\delta U}_{,j} \cdot \boldsymbol{V}_{,i} \ \ (i, j = 1, 2)$$

and

$$\underline{b}''(\boldsymbol{U}; \boldsymbol{\delta U}, \boldsymbol{V}) = D''(\boldsymbol{U}; \boldsymbol{\delta U}, \boldsymbol{V})\widetilde{\underline{b}}(\boldsymbol{U}) + D'(\boldsymbol{U}; \boldsymbol{V})\widetilde{\underline{b}}'(\boldsymbol{U}; \boldsymbol{\delta U})$$
$$+ D'(\boldsymbol{U}; \boldsymbol{\delta U})\widetilde{\underline{b}}'(\boldsymbol{U}; \boldsymbol{V}) + D(\boldsymbol{U})\widetilde{\underline{b}}''(\boldsymbol{U}; \boldsymbol{\delta U}, \boldsymbol{V})$$

with

$$\widetilde{\underline{b}}''(\boldsymbol{U}; \boldsymbol{\delta U}, \boldsymbol{V}) = \left([\boldsymbol{V}_{,1}, \boldsymbol{\delta U}_{,2}, \boldsymbol{U}_{,ij}] - [\boldsymbol{V}_{,2}, \boldsymbol{\delta U}_{,1}, \boldsymbol{U}_{,ij}] + [\boldsymbol{V}_{,2}, \boldsymbol{\delta U}_{,ij}, \boldsymbol{a}_1]\right.$$

$$- [\boldsymbol{V}_{,ij}, \boldsymbol{\delta U}_{,2}, \boldsymbol{a}_1] + [\boldsymbol{V}_{,ij}, \boldsymbol{\delta U}_{,1}, \boldsymbol{a}_2] - [\boldsymbol{V}_{,1}, \boldsymbol{\delta U}_{,ij}, \boldsymbol{a}_2] \Big)_{i,j=1}^{2}.$$

$D''(\boldsymbol{U}; \boldsymbol{\delta U}, \boldsymbol{V})$ is a scalar function arising from the linearization of $D'(\boldsymbol{U}; \boldsymbol{V})$ in direction $\boldsymbol{\delta U}$.

Thus, with the second integral of the element stiffness matrix for two fixed directions $\boldsymbol{V}$ and $\boldsymbol{\delta U}$ we have to integrate over a matrix multiplication

$$\sum_{i,j=1}^{2} \overset{2}{\underline{\mathcal{T}}}_{ij}\, e''_{ji}(\boldsymbol{U}; \boldsymbol{\delta U}, \boldsymbol{V}),$$

with $\overset{2}{\underline{\mathcal{T}}} = \overset{2}{\underline{\mathcal{T}}}(\boldsymbol{U}) = \left(\overset{2}{\mathcal{T}}_{ij}\right)_{i,j=1}^{2}$ the coefficients of the second Piola-Kirchhoff stress tensor as well as $\underline{e}''(\boldsymbol{U}; \boldsymbol{\delta U}, \boldsymbol{V}) = \left(e''_{ij}(\boldsymbol{U}; \boldsymbol{\delta U}, \boldsymbol{V})\right)_{i,j=1}^{2}$.

For calculating the element stiffness matrix the vectors $\boldsymbol{V}$ and $\boldsymbol{\delta U}$ now pass through all 48 vector valued form functions of the BFS element. Therefore, every component $H_{ij} = \underline{e}''_{ij}(\boldsymbol{U}; Q \times \underline{I}, Q \times \underline{I})$ is understood as a $(48 \times 48)$-matrix, itself.

Hence, the element stiffness matrix (6.7) is

$$\underline{K}_T(\boldsymbol{U}) = \int_{\Omega_0} \underline{M}^\top\, \underline{C}(\boldsymbol{U})\, \underline{M}\, dV + \int_{\Omega_0} \sum_{i,j=1}^{2} \overset{2}{\underline{\mathcal{T}}}_{ij}\, \underline{H}_{ji}\, dV. \tag{6.20}$$

The integration over the undeformed plate $\Omega_0$ in (6.20) is realized in two steps. First, the integration over the undeformed mid surface $\Omega_0^m$ is accomplished by a Gaussian integration with $4 \times 4$ points and weights. For the integration over the thickness numerical experiments have shown that we achieve good results in a acceptable time for the Gaussian integration with 7 points and weights.

For each Gaussian point the matrix multiplications above, have to be done. Hence, in the realization of the theory we reduce the calculations to the Kronecker products, which are needed. After that, we multiply them with all scalars, which result from the matrix multiplications. In that way, the performing time for the assembly of the element stiffness matrices has been reduced to less than a fourth in contrast to apply the full matrix multiplications in (6.20).

## 6.5 Newton's method and mesh refinement

As mentioned before, the calculation of our plate deformations require Newton's Algorithm 6.2 for two reasons:

(1) As generally known, Newton's method converges only locally. Hence, for large deformations an incrementation of the forces (possibly of the inhomogeneous Dirichlet boundary conditions) is used in Algorithm 6.2, analogously to Algorithm 6.1. In the case that the algorithm diverges, the increment has to be decreased. For a well suited increment the method certainly converges. This issue is proved, for example, in [11].

(2) After the forces are fully applied to the considered device on a relatively coarse mesh, we may start mesh refinements to obtain an appropriate approximation of displacements, stresses or strains. Then, in every refinement stage we apply Newton's Algorithm 6.2 on the actual finite element mesh. Hence, on a mesh of level $l$ we achieve an approximated vector function $\boldsymbol{U}_h$. After the next refinement is performed, on the finer mesh with the level $(l+1)$ we need an initial vector function $\boldsymbol{U}_{h/2}(x)$ for the continuation of Newton's method. For that, the vector function $\boldsymbol{U}_h(x)$ is interpolated with the ansatz functions of the finer mesh and we claim pointwise

$$\boldsymbol{U}_{h/2}(x_i) \equiv \boldsymbol{U}_h(x_i) \tag{6.21}$$

at all nodes $x_i$ of the finer mesh. Now, on this finer mesh Newton's Algorithm 6.2 starts with the interpolated vector function $\boldsymbol{U}_{h/2}(x)$. Note, that the stiffness matrix $\underline{K}\big(\boldsymbol{U}_{h/2}(x)\big)$ now is of a higher dimension than it was on the coarser mesh of level $l$, due to the increased number of elements.

For BFS-elements we achieve nested function spaces for the ansatz functions,

$$\mathbb{V}^1 \subseteq \mathbb{V}^2 \subseteq \ldots \subseteq \mathbb{V}^l \subseteq \mathbb{V}^{(l+1)}.$$

Therefore, the ansatz functions in the mesh of level $l$ can be displayed as linear combinations of the ansatz functions of the next finer mesh. For that purpose the demand (6.21) is not only fulfilled pointwise at $x_i$, but the vector functions are obviously identical.

Unfortunately, the mesh refinement does not generate nested function spaces in the case of HCT-elements. That means

$$\mathbb{V}^l \nsubseteq \mathbb{V}^{(l+1)}. \tag{6.22}$$

Here, the vector function $\boldsymbol{U}_{h/2}(x)$ defined by (6.21) in the finer mesh differs from the vector function $\boldsymbol{U}_h(x)$ in the mesh of level $l$. Therefore, the interpolated vector function $\boldsymbol{U}_{h/2}(x)$ as a starting vector function in Algorithm 6.2 is not as good as in the case of BFS-elements. Consistently, Newton's method needs some more steps in the HCT-case.

Additionally from using shape regular triangles, the HCT-elements are more flexible and may be used for approximating curved boundaries. In this case, after the refinement the new boundary nodes are corrected to the true boundary position (another reason for (6.22) and for more complications with Newton's method).

There are some approaches in [13] or [26] for generalizing HCT-elements in a way that nested function spaces for the ansatz functions arise. But for these elements more degrees of freedom have to be regarded.

# 7 Numerical examples

In this chapter we present some numerical examples. For that, we consider plates in different forms and sizes. The goal of the theory, which was presented in the last chapters, is the calculation of large deformations for thin plates. Hence, for all devices a thickness is chosen, which is one eightieth of the half of the sum of its width and its length.

Furthermore, we use the Neo-Hooke material law for all plates. The density function of this material was already defined in (2.34).

The examples are grouped by their kind of plate deformation as membrane-dominated and bending-dominated examples. For the deflection of a plate we apply a volume force, perpendicular to the mid surface. The second group consists of examples with bending-dominated plate deformations, where one or more edges will follow a prescribed movement.

The procedure of the simulation in nearly all examples is the same. First of all the forces are applied to the plate incrementally. For each increment a Newton iteration has to be done. The incremental stage is followed by a number of mesh refinements to improve the approximation.

For all examples we present some pictures in different approximation stages of the plate's mid surface. With the exception of the pictures of the initial states, the surfaces are coloured by the Frobenius norm of the mid surface strain tensor or by one component of the displacement vector. The colour bar is adapted particularly to each example. For this postprocessing the open source software ParaView, version 3.98.0 nightly, was used.

**A word of caution on the graphical output: Note, that for the display of the deformed mid surface we have chosen the following simplification. Even though the obtained solutions are piecewise (bi)cubic functions, the figures only display their linear interpolation with the nodal values (additionally calculated nodal derivatives are ignored). Especially for coarser meshes the reader should keep in mind this simplification for the graphics only – the calculated functions are correctly $C^1$-continuous!**

## 7.1 Plate deflection

For this work the main focus of attention lies on the group of bending-dominated examples. Nevertheless, for the other group of examples approximating membrane-dominated deformations Newton's method converges very fast.

However, a further word of caution on the results of these deflection examples should be said. In addition to the error obtained by the FEM, which decreases due to the mesh refinement, the error resulting from the Kirchhoff hypothesis has a significant effect. Due to this assumption, the plate is assumed to be shear rigid in thickness direction and its thickness does not change during the deformation process. If you consider small deformations, it does not matter too much. But for large strain the displacements are not as large approximated as they would be in the reality. Hence, the plate is considered to be more inflexible then it truly would be. For the deflection examples this is a serious problem, because here the in-plane-stresses are much higher than they are for bending-dominated problems. Hence, the displacement vector is approximated too short. The true value of this work can be seen particularly in the application of the theory for bending-dominated examples.

However, we present one deflection example for each kind of finite elements to show the excellent convergence of the Algorithm 6.1.

### 7.1.1 Approximation with FEM using BFS-elements

In the first example we consider a quadratic plate with sides of length 4. The thickness is fixed to 0.05 over the full length of the plate. All four boundaries are hard clamped. Figure 7.1 displays the FE-mesh of the undeformed mid surface consisting of 16 uniform elements.
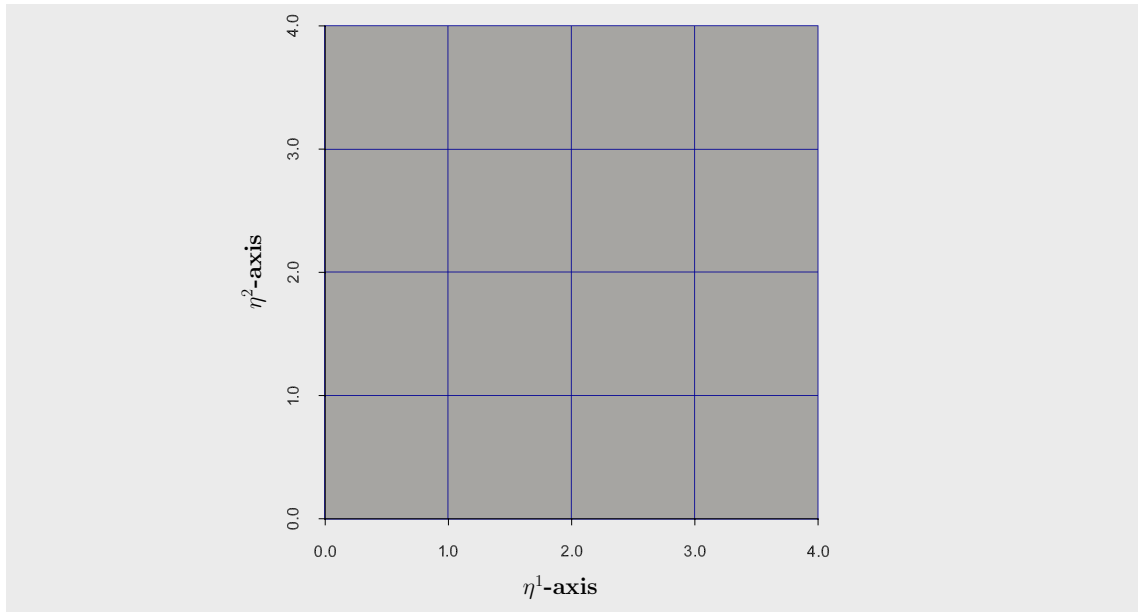


Figure 7.1: Undeformed mid surface, 16 elements.

We apply a volume force vector in normal direction $\boldsymbol{A}_3$ to the plate. As written before, this force vector is not applied at once but it is increased incrementally (ten increments for $\Delta t = \frac{1}{10}$ in Algorithm 6.1). The stopping criterion for each

Newton iteration is determined to $\varepsilon = 10^{-8}$. For this $\varepsilon$ the Newton iteration ends, if the calculated correction term $\boldsymbol{\delta U}$ is smaller than $10^{-8}$ of the actual computed displacement vector. Figure 7.2 shows the deformed mid surface after one Newton iteration in the first increment.
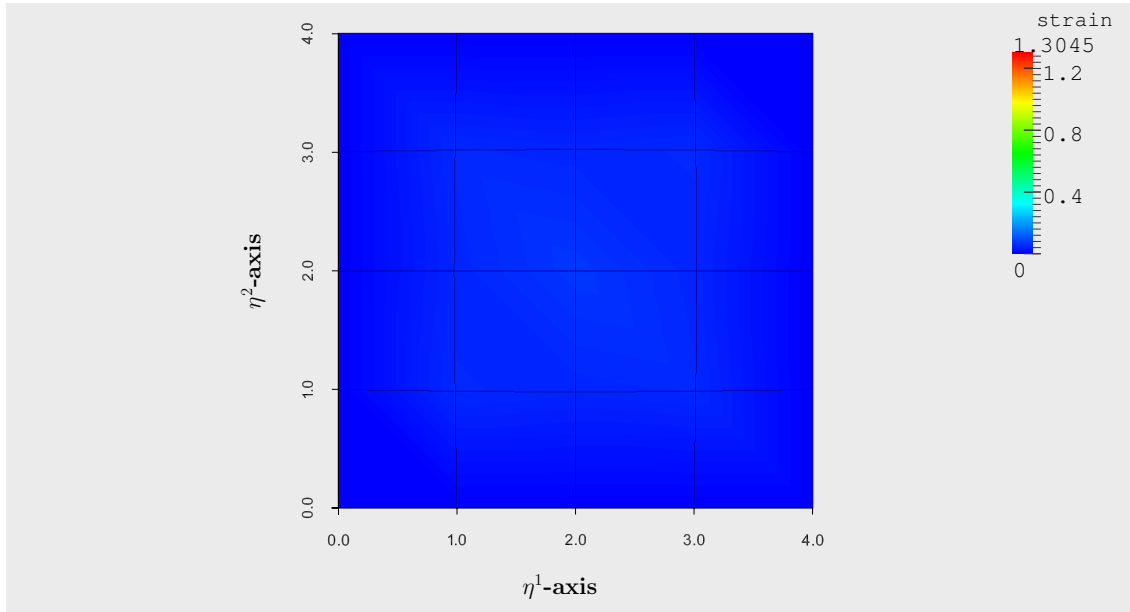


Figure 7.2: Deformed mid surface after applying the first increment, 16 elements.

Expectedly, the values in Figure 7.2 of each element are still small and do not differ very much over the different elements.
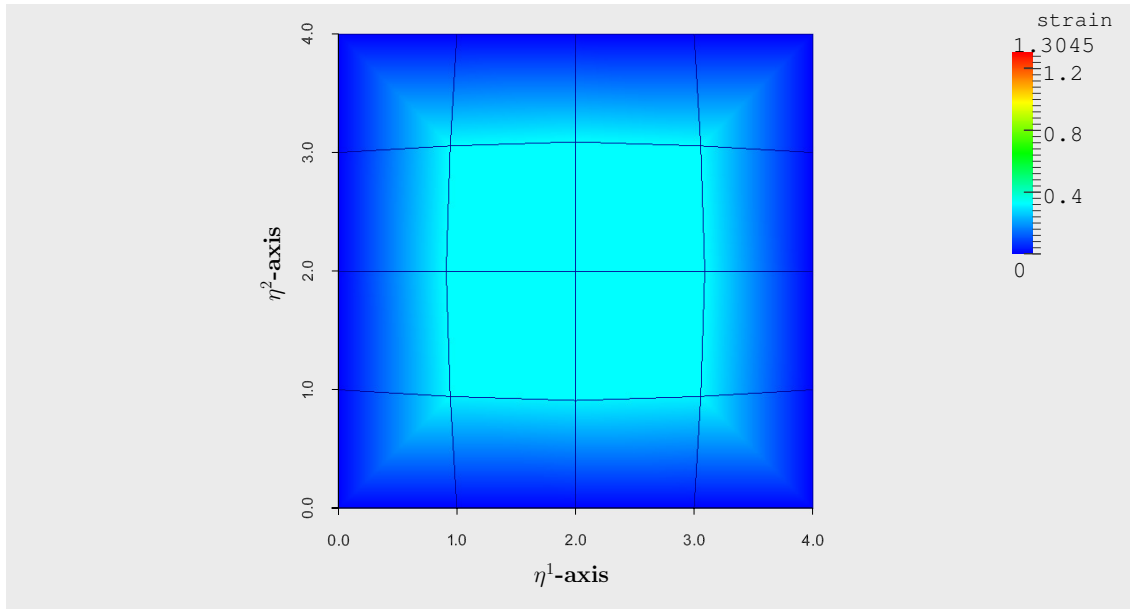


Figure 7.3: Deformed mid surface after applying the full force vector, 16 elements.

57

Note that for the graphical outputs a constant colour bar for the values of the norm of the strain tensor is defined to make the colouring for all pictures of one example comparable.

Following the algorithm, the increment would be increased until the full force vector is applied. The deformed mid surface, approximated in the coarse mesh, is illustrated in Figure 7.3. As can be seen, the interpolated value of the strain in the elements in the center of the surface increased a little bit but the resolution of the mid surface is far to coarse for a good approximation.

The proceeding before, was necessary to execute the full force to the plate. For the improvement of the approximation we adopt five mesh refinements. The following Table 7.1 shows the number of Newton steps per iteration in the single stages.

|  |  |
|---|---|
| 1st increment, 16 elements : | 15 |
| 2nd increment, 16 elements : | 4 |
| 3rd increment, 16 elements : | 4 |
| 4th increment, 16 elements : | 3 |
| . . . . . . . . . . . . . . . . . |  |
| 10th increment, 16 elements : | 3 |
| 1st refinement, 64 elements : | 5 |
| 2nd refinement, 256 elements : | 4 |
| 3rd refinement, 1.024 elements : | 4 |
| 4th refinement, 4.096 elements : | 3 |
| 5th refinement, 16.384 elements : | 3 |

Table 7.1: Example 7.1.1; number of Newton steps at the single periods.

The higher number of Newton steps in the first iteration is easily explained by the used starting vector $\boldsymbol{U}^0 = \boldsymbol{0}$. Obviously, it is not as close to the solution in the first increment as later the approximated values from the Newton iteration of the incremental step before, which are used as initial solution for the Newton iteration of the next increment. The number of Newton steps in the single refinement stages decreases, due to the fact, that the error for the approximation of the displacement vector in the finer mesh is smaller than in the coarser triangulation.

Note, that the number of Newton steps in each iteration is small, by reason of the fact that we get nested function spaces for BFS-elements.
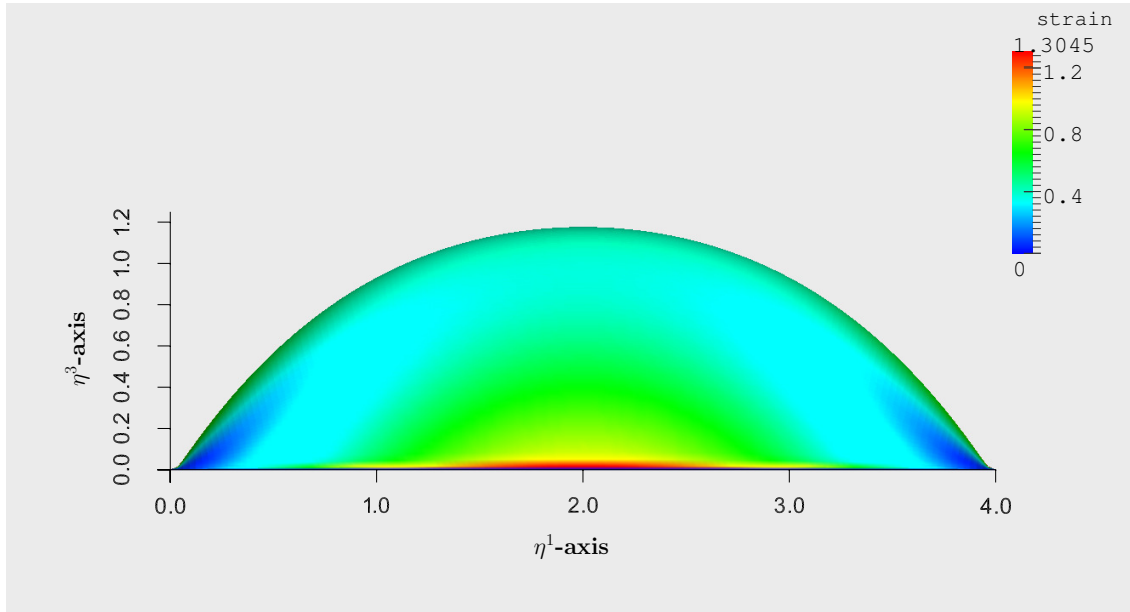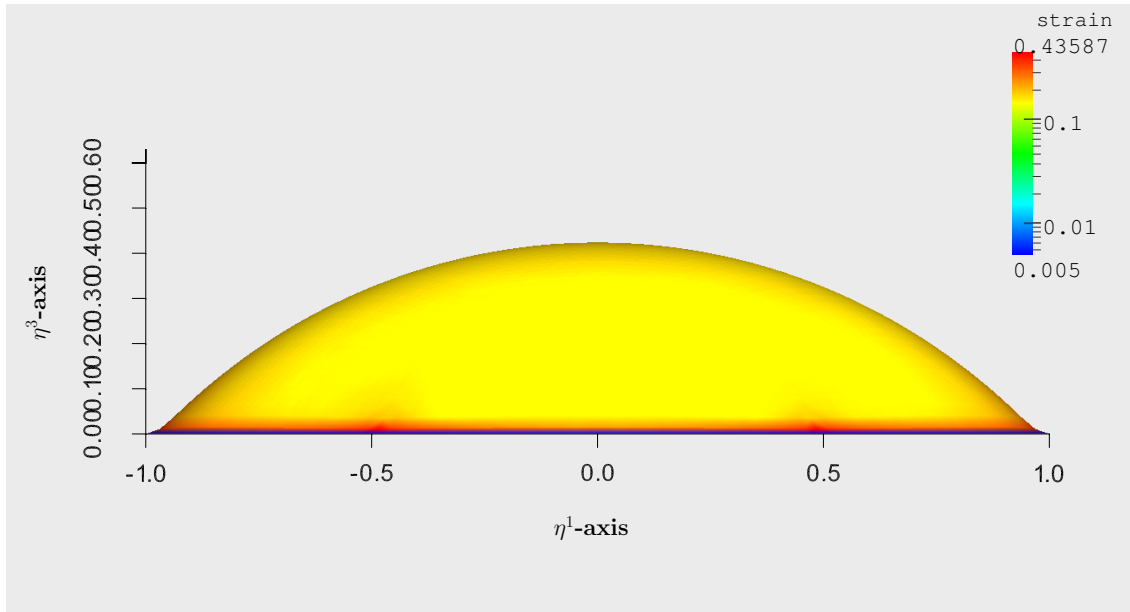


Figure 7.4: Deformed mid surface, 16.384 elements, full force applied.
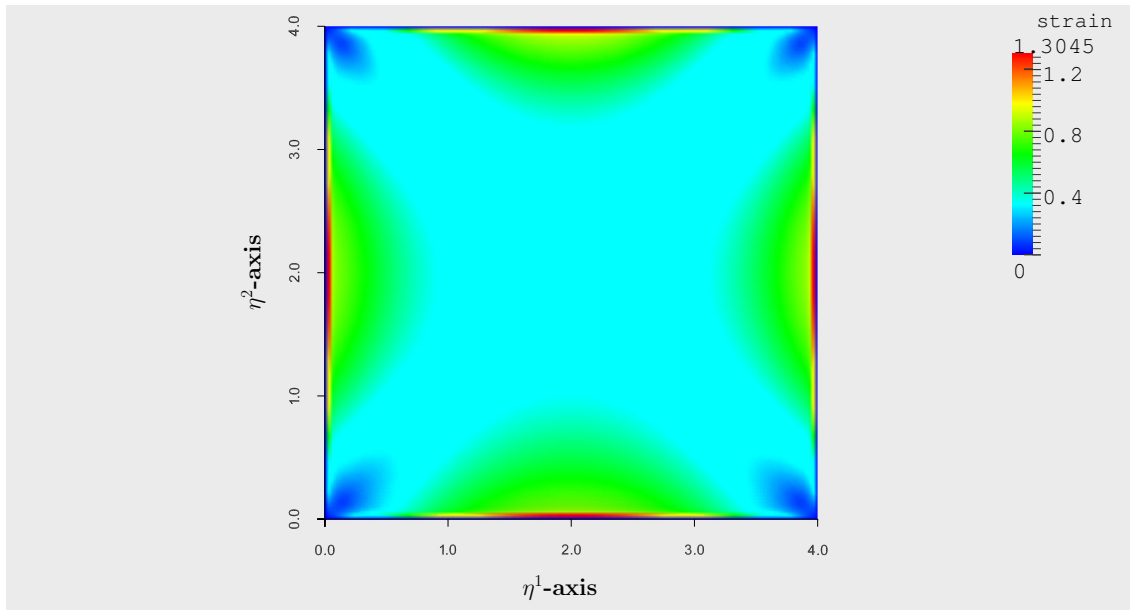


Figure 7.5: Deformed mid surface, 16.384 elements, full force applied, bird's eye view.

At this point, let us consider the deformed mid surface after five refinements, approximated by 16.384 elements. As seen in Figure 7.4 and Figure 7.5 the highest

strain occurs in the center of the surface boundaries. Due to the symmetry of the example, the side view in Figure 7.4 looks identically for all four sides.

Apart from the performance test of Newton's method, a second thought for considering this example above is the verification of our code. For that, we consider the third component of the displacement vector in Figure 7.6.
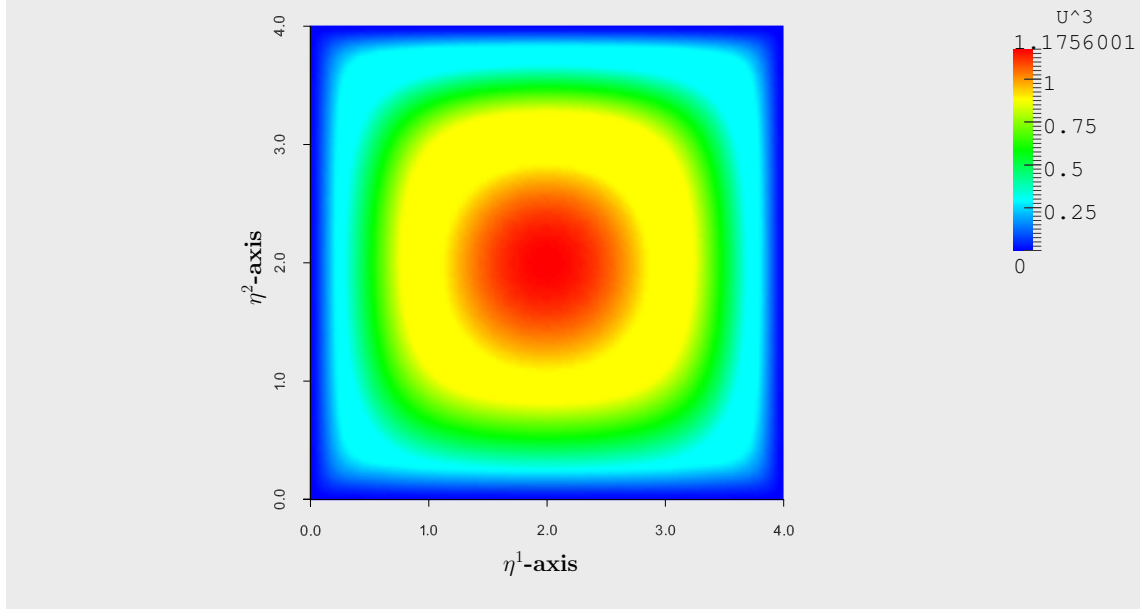


Figure 7.6: Deformed mid surface, 16.384 elements, third component of displacement vector $U^{(3)}$.

Here, a very small boundary layer is observable as it is typical for large deflection examples.

In contrast to that let us consider a small deformation example. For that purpose we apply a very small force vector to the plate. Due to that, we do not need to apply the forces incrementally. Figure 7.7 shows the resulting deformed mid surface after five refinements, which looks as similar as in the small deformation case.

As expected, in Figure 7.7 the values of the strain tensor as well as for the displacement vector are very small compared to the appliance of large deformations (Figure 7.4).

Another difference towards the results of large deformation are the boundary layers. So, in Figure 7.4 they have a steeper slope than in Figure 7.7. This fact is also seen directly in Figure 7.6 in comparison with Figure 7.8, which both display the third component of the displacement vector in the case of large and of small strain, respectively. In Figure 7.6 the coloured ranges get finer towards the boundary. On the contrary, in Figure 7.8 the coloured ranges are thicker at the boundary, in order to get finer in direction to the center of the plate, before they grow wider near this center again.
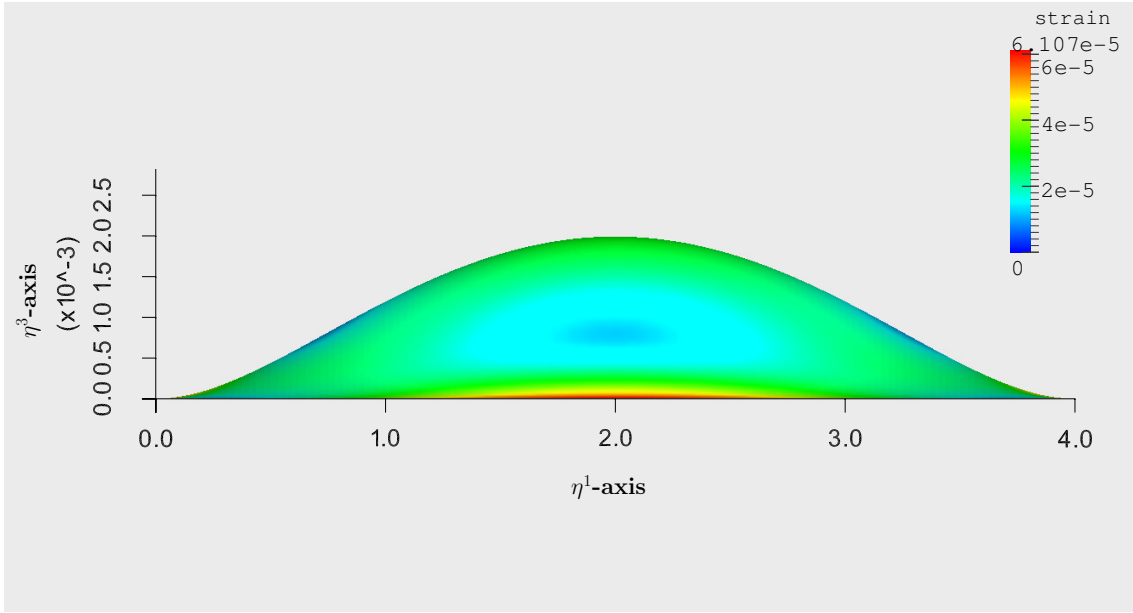
Figure 7.7: Deformed mid surface, 16.384 elements, small strain.
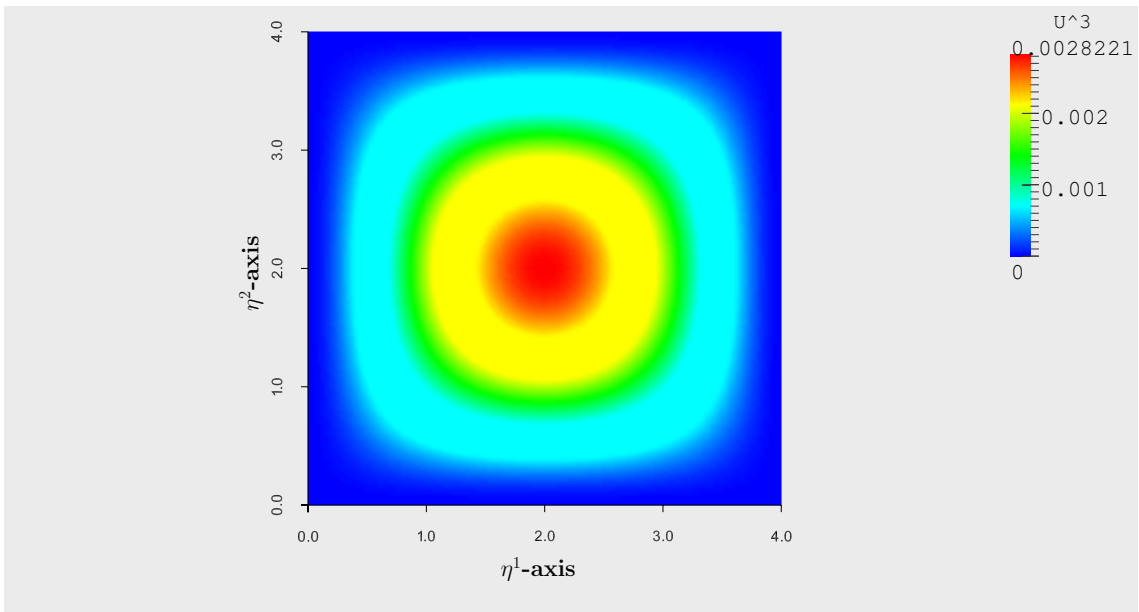


Figure 7.8: Deformed mid surface, 16.384 elements, small strain, third component of the displacement vector $U^{(3)}$.

Last, we consider the first and the second component of the displacement vector for small deformation, seen in Figure 7.9 and 7.10, respectively. In addition to the symmetry of the displacements in the corresponding direction $\eta^1$ or $\eta^2$, the values are very close to zero.

In contrast to this results $U^1$ and $U^2$ are obviously zero in the small strain theory.

With the use of our code, the first and the second component of the displacement vector differ from zero, because of the non-linear parts, which are not discarded as in the small deformation theory.
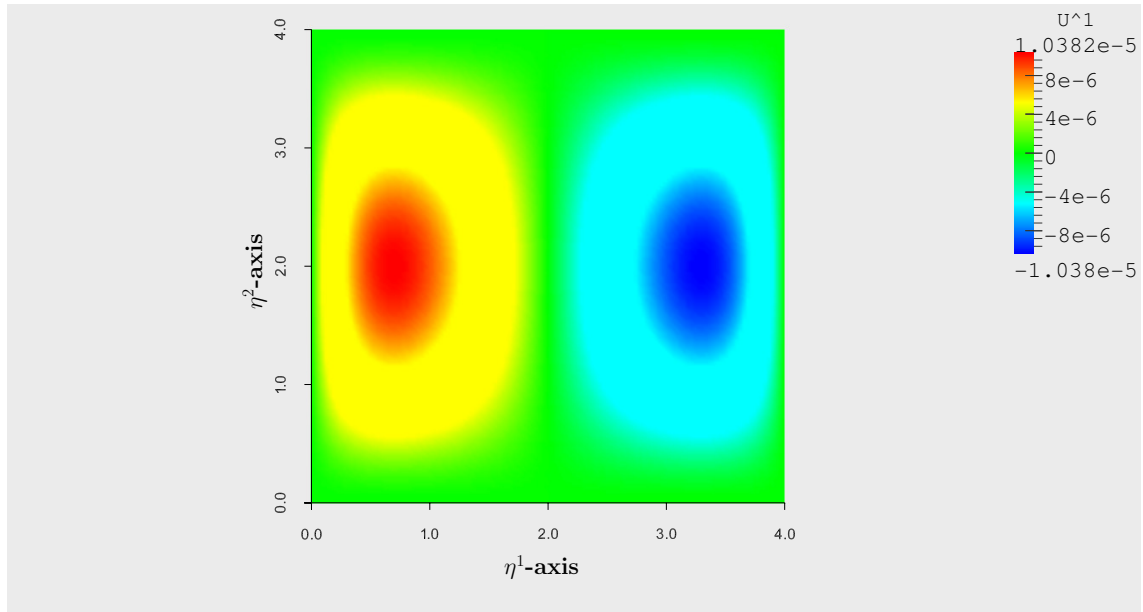


Figure 7.9: Deformed mid surface, 16.384 elements, small strain, first component of the displacement vector $U^{(1)}$.
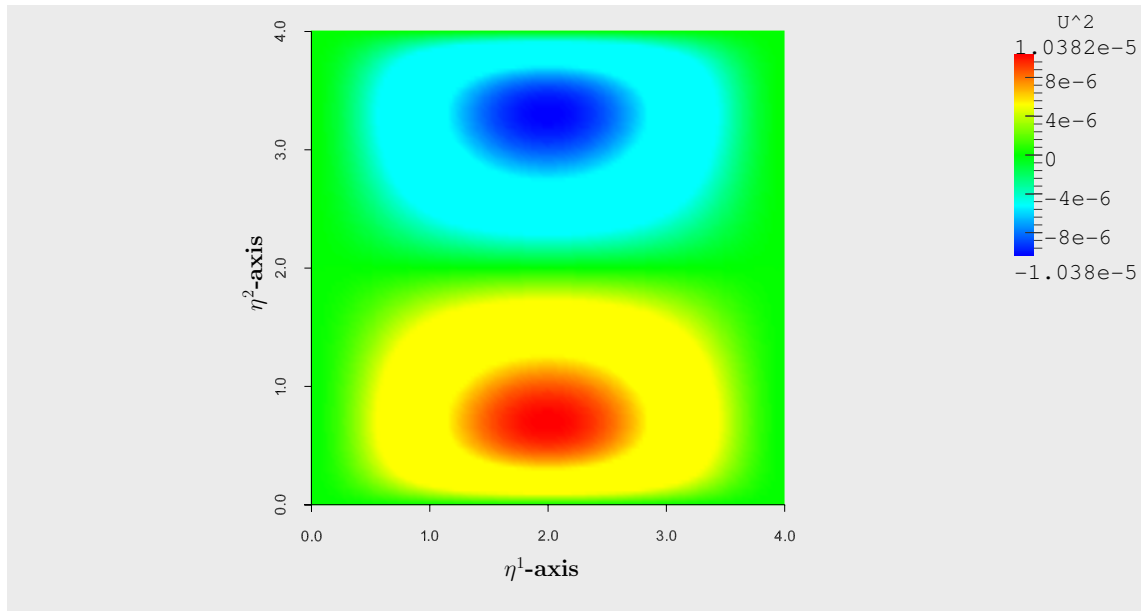


Figure 7.10: Deformed mid surface, 16.384 elements, small strain, second component of the displacement vector $U^{(2)}$.

## 7.1.2 Approximation with FEM using reduced HCT-elements

For approximating the deflection using reduced HCT-elements, we consider a circular slab with a diameter length of 2. The thickness of the plate is determined to 0.025 and we consider the boundary to be hard clamped. As in the example above, a volume force perpendicular to the mid surface is applied using ten increments.
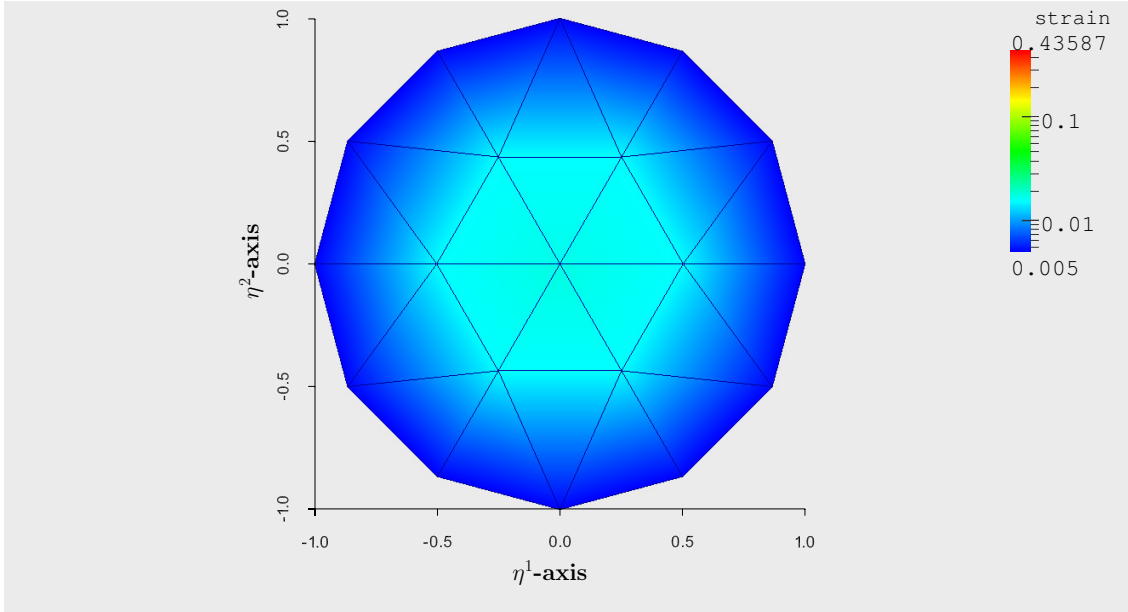


Figure 7.11: Deformed mid surface after applying first increment, 24 elements, bird's eye view.

The deformed mid surface after the first Newton iteration is shown in Figure 7.11, displayed with 24 elements. The values for the strain norm are very small. As before in the corresponding mesh of the quadrilateral plate, the mesh is much to coarse for a well suited approximation.

For comparison, Figure 7.12 depicts the view heading to the $(\eta^1, \eta^3)$ - plane of the deformed mid surface in the same mesh as seen in Figure 7.11. In that way, the third component of the displacement vector $U^{(3)}$ is shown at the same time.

Following the algorithm, at this point the increments are increased and for every increment a Newton iteration is computed. After 10 increments the full force vector is now applied and Figure 7.13 displays the deformed mid surface in this stage.

For approximating the displacement vector good enough, the mesh is refined four times, uniformly.
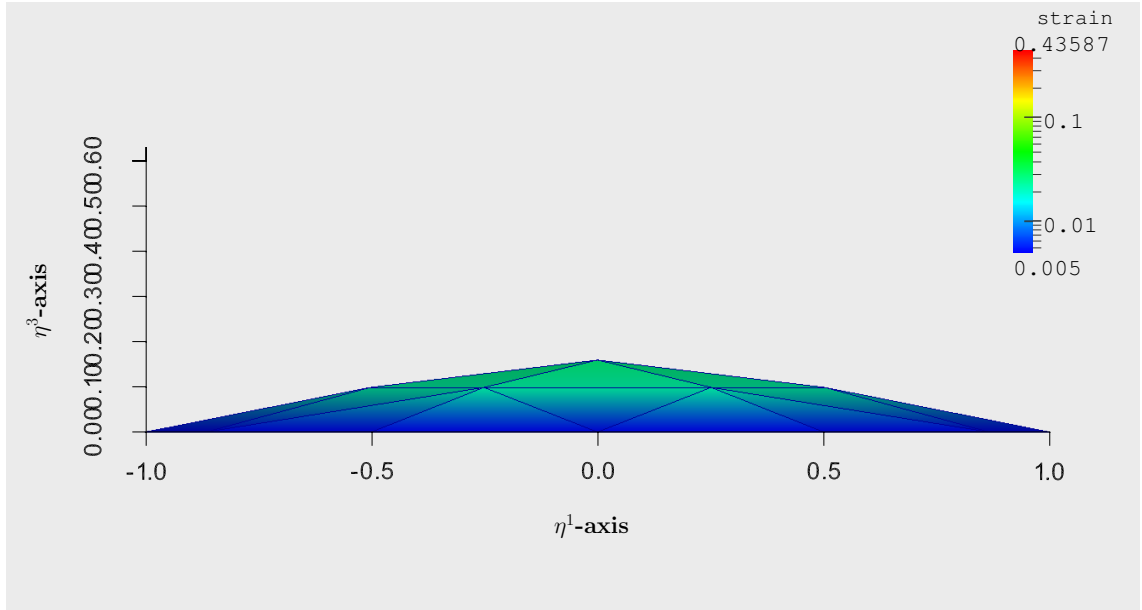
Figure 7.12: Deformed mid surface after applying the first increment, 24 elements.
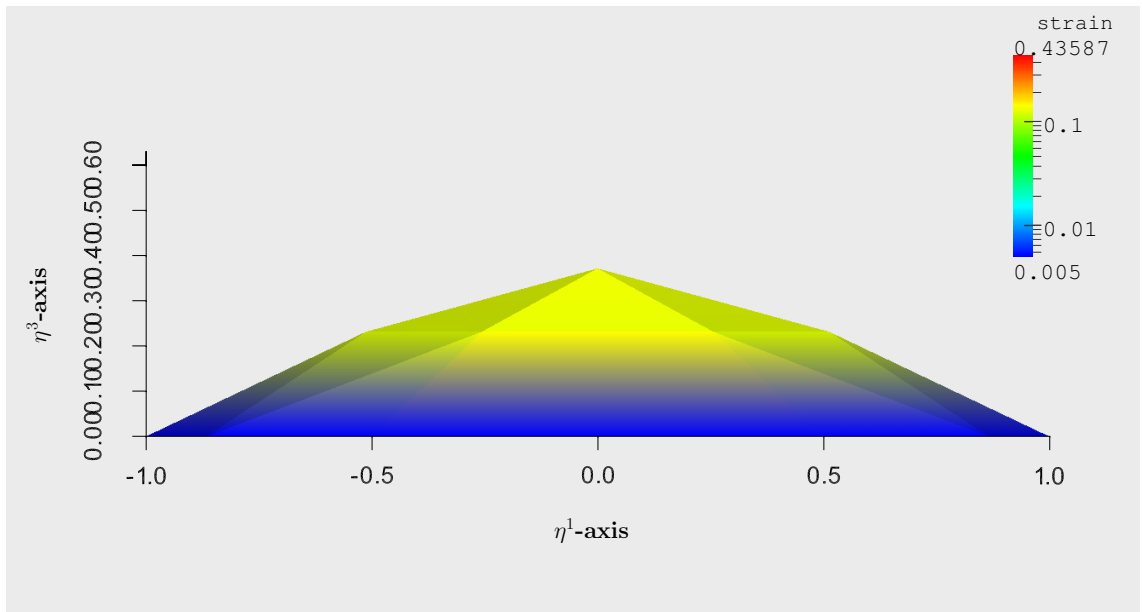


Figure 7.13: Deformed mid surface after applying the full force vector, 24 elements.

The deformed mid surface after all refinement steps is shown in Figure 7.14, above. It consists of 6.144 elements. Just like in the example for the BFS-elements the boundary layers are small, as it is typical for this kind of large deformations. Figure 7.15 displays the bird's eye view of the deformed mid surface in the finest triangulation. In both figures we can see that the maximum of the norm of the strain tensor is approximated near the boundary.

Figure 7.14:  Deformed mid surface, 6.144 elements, full force applied.
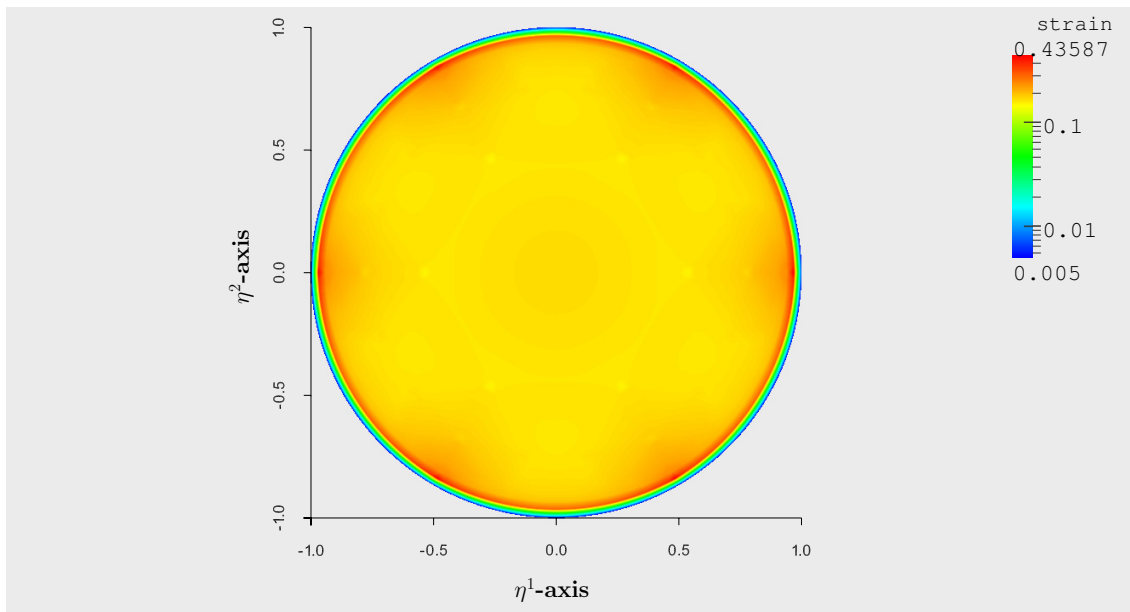


Figure 7.15:  Deformed mid surface, 6.144 elements, full force applied, bird's eye view.

In Table 7.2 the number of Newton steps per iteration is displayed in the respective situation.

| | |
|---|---|
| 1st increment, 24 elements : | 7 |
| 2nd increment, 24 elements : | 4 |
| 3rd increment, 24 elements : | 4 |
| 4th increment, 24 elements : | 3 |
| . . . . . . . . . . . . . . . . | |
| 10th increment, 24 elements : | 3 |
| 2nd refinement, 96 elements : | 5 |
| 3rd refinement, 384 elements : | 6 |
| 4th refinement, 1.536 elements : | 4 |
| 5th refinement, 6.144 elements : | 4 |

Table 7.2: Example 7.1.2; number of Newton steps at the single periods

The number of Newton steps per iteration in the single increment stages is similarly small as in the example before. However, we observe a slightly increase of the numbers in the individual refinement stages. This is due to the refinement technique of the HCT-elements. Furthermore, we have a curved boundary. Nevertheless, the algorithm converges, due to the fact that the boundary is hard clamped and only the lateral adjustment has to be put to the mid point of each outer edge.

## 7.2 Bending-dominated deformation

As written at the beginning of the last subsection, the main goal of this work is a fast approximation of large bending deformation problems. For this kind of problems the error emerging from the Kirchhoff hypothesis is considered to be small.

### 7.2.1 Approximation with FEM using BFS-elements

#### 7.2.1.1 1st example: Cylinder

For the first example for bending dominated problems we consider a plate with its mid surface $\Omega_0^m = [0, 1.5] \times [0, 1]$ and a thickness of 0.015625. The initial mesh consists of 8 elements, as can be seen in Figure 7.16.
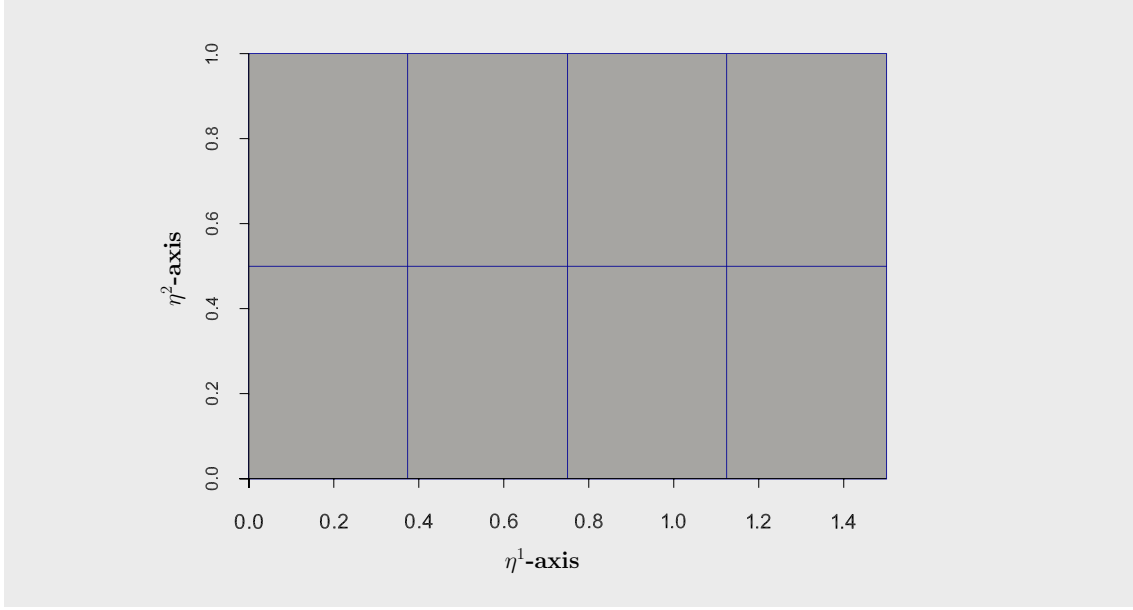
Figure 7.16: Undeformed mid surface, 8 elements.

As mentioned before, for this group of examples we do not apply any force vector to the plate but simulate an incremental transport of a part of the boundary.

Here, both boundaries in $\eta^2$-direction at $\eta^1 = 0$ and $\eta^1 = 1.5$, respectively, are hard clamped with inhomogeneous Dirichlet type boundary conditions. The remaining edges are left free ("do nothing condition").

For the left edge $(0, \eta^2, 0)^T$ we apply a prescribed displacement

$$\boldsymbol{U} = (0.75(1 - \cos t), 0, 0.75 \sin t)^T \tag{7.1}$$

and for the right edge $(1.5, \eta^2, 0)^T$

$$\boldsymbol{U} = (-0.75(1 - \cos t), 0, 0.75 \sin t)^T, \tag{7.2}$$

respectively, with $t \in \left[0, \frac{\pi}{2}\right]$. The outer normals of the edges will be rotated throughout their transport and are defined by

$$\boldsymbol{U}_{,1} = (\pm(1 - \cos 2t), 0, \pm \sin 2t)^T,$$

respectively.

The edge displacements are applied in 10 equidistant steps of $t$. The result of the first increment is displayed by Figure 7.17.

67
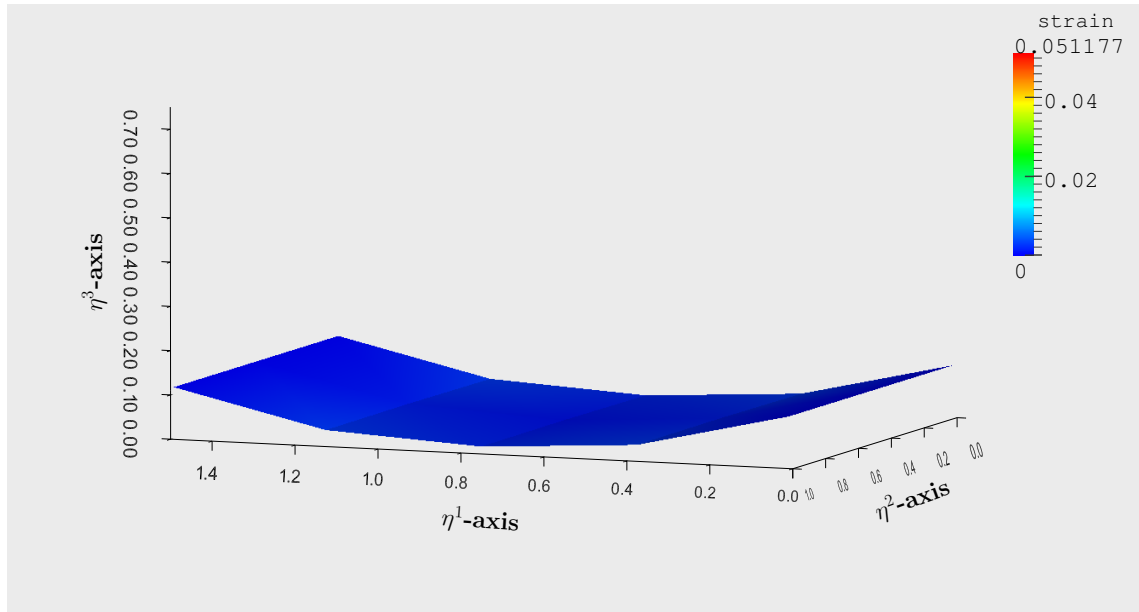
Figure 7.17: Deformed mid surface after applying the first increment, 8 elements.

Increasing the increments leads to a further bending, as we can see in Figure 7.18. Therein, the fully deformed mid surface, approximated with 8 elements is displayed.
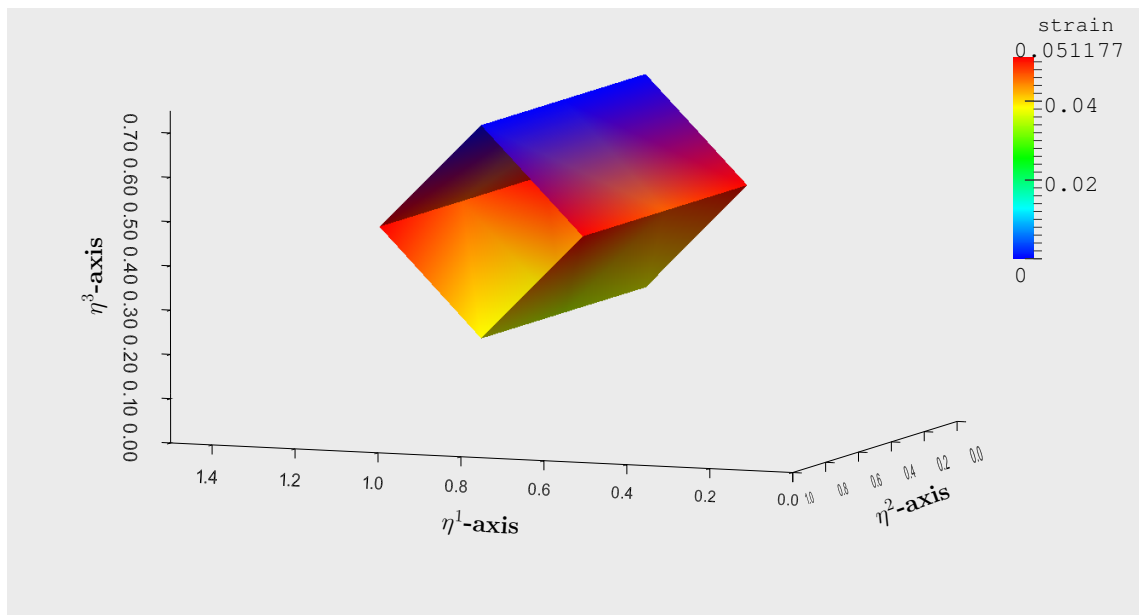


Figure 7.18: Deformed mid surface, 8 elements.

At that, as usual for the algorithm, we start the mesh refinement. After every refinement a Newton iteration is carried out.

For the full simulation progress the number of Newton steps per Newton iteration in every incremental stage and in the refinement states are displayed in Table 7.3.

| | |
|---|---|
| 1st increment, 8 elements : | 14 |
| 2nd increment, 8 elements : | 13 |
| 3rd increment, 8 elements : | 8 |
| 4th increment, 8 elements : | 8 |
| 5th increment, 8 elements : | 7 |
| 6th increment, 8 elements : | 6 |
| 7th increment, 8 elements : | 5 |
| 8th increment, 8 elements : | 4 |
| 9th increment, 8 elements : | 6 |
| 10th increment, 8 elements : | 5 |
| 1st refinement, 32 elements : | 3 |
| . . . . . . . . . . . . . . . . . | |
| 5th refinement, 8.192 elements : | 3 |
| 6th refinement, 32.768 elements : | 2 |

Table 7.3:  Example 7.2.1.1; number of Newton steps in the single periods.

Obviously, in contrast to the example in Section 7.1.1 the iteration numbers increases a little bit for each individual incremental stage. This may depend on the fact that for bending deformations the change of the displacement vector and of its partial derivatives from one to the next incremental state is much higher than in the deflection examples.

In the refinement stage the number of Newton steps per iteration are expectedly small, due to the nested function spaces of the ansatz functions for the refined triangulations.

As result of the six refinements we achieve a cylindrical shell. Its mid surface is shown in Figure 7.19, which consists of 32.768 elements. Furthermore, the strain is

much less than in the deflection examples.
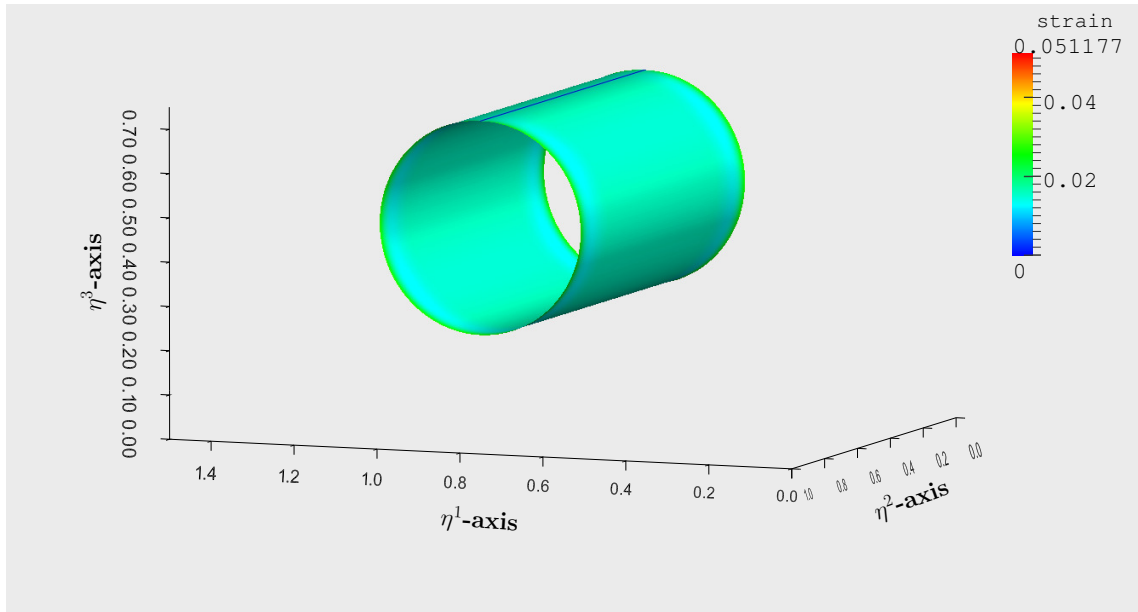


Figure 7.19: Deformed mid surface, 32.768 elements.

For a graphical depiction of the approximation process the graphical output for each incrementation and the one for the finest mesh is displayed in the following figure (Figure 7.20).
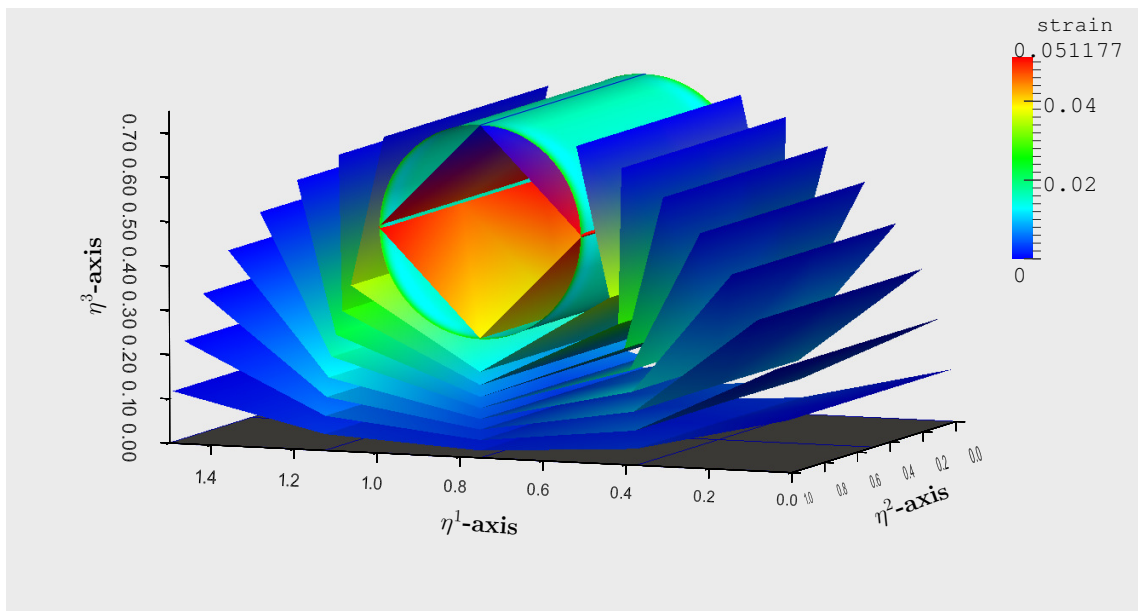


Figure 7.20: Cylinder, deformation progress.

### 7.2.1.2 2nd example: Cylinder with further rotated edge normals

In the second example we consider the same plate as in example 7.2.1.1, before, with equal boundary conditions. The transport of the two outer edges in $\eta^2$-direction follows the same prescribed path, as given in (7.1) and (7.2).

In contrast to example 7.2.1.1 we apply a further rotation of the outer normals of both edges, which now is defined by

$$\boldsymbol{U}_{,1} = (\mp(1 - \cos 3t), 0, \pm \sin 3t)^T,$$

respectively, with the increment $t \in [0, \frac{\pi}{2}]$.

We apply the transport of the edges and their simultaneous rotation in ten increments. In Figure 7.21 the deformed mid surface, approximated with eight elements, after the implementation of the first increment is seen.
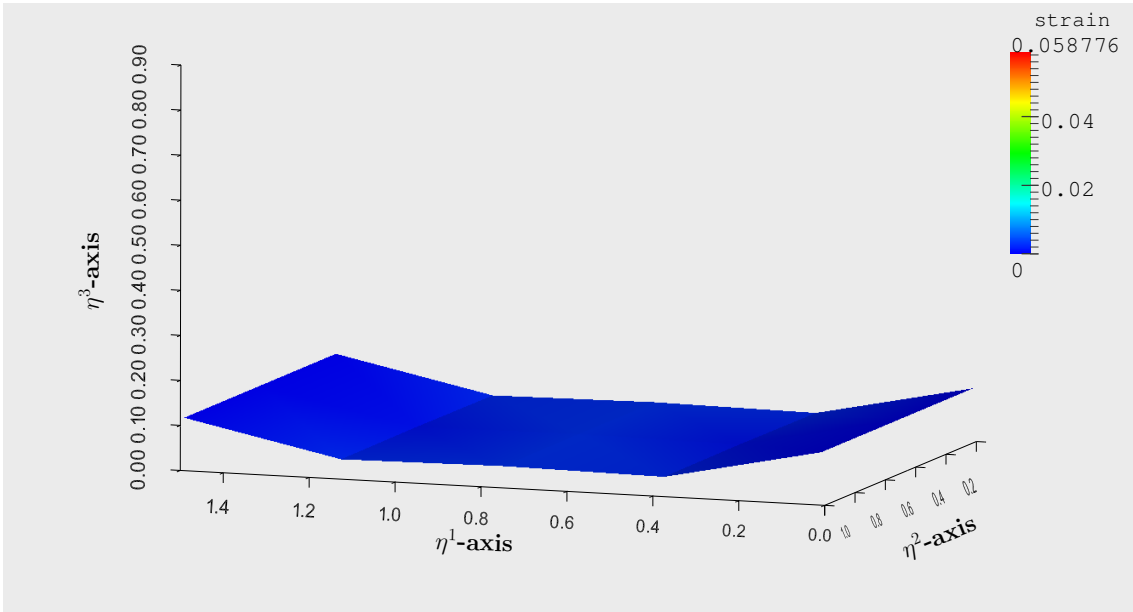


Figure 7.21: Deformed mid surface, 8 elements, first increment.

After applying further nine increments, the deformed mid surface looks like in Figure 7.22, displayed still with a mesh consisting of eight elements.
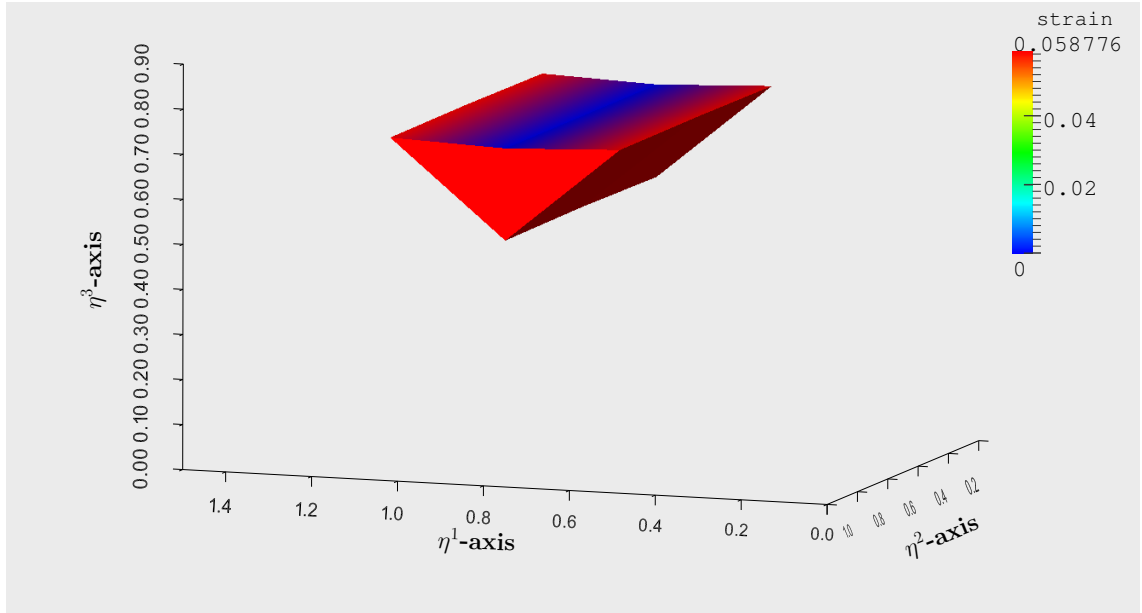
Figure 7.22: Deformed mid surface, 8 elements, full force applied.

At this point of the simulation, the complete edge transport and the full edge rotation is computed. For a useful approximation of the deformation the initial mesh for the mid surface has to be refined. As in the example before, six refinement steps are carried out. The graphical result can be seen beneath in Figure 7.23.
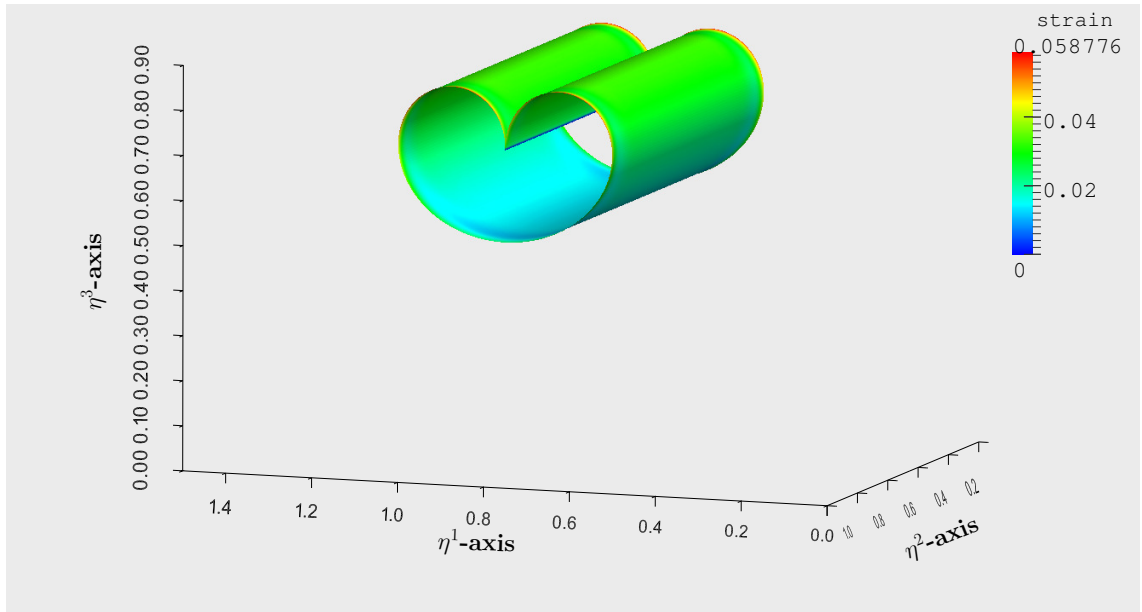


Figure 7.23: Deformed mid surface, 32.768 elements.

Here, we have plotted the mid surface with 32.768 elements. The mid-surface strain is slightly higher than in the example before, due to the further rotation

of the edge normals. But in contrast to the corresponding value in the deflection example 7.1.1 the coloured value here is much smaller.

In the following Table 7.4 the number of Newton steps per iteration are displayed.

| | |
|---|---|
| 1st increment, 8 elements : | 14 |
| 2nd increment, 8 elements : | 7 |
| 3rd increment, 8 elements : | 5 |
| 4th increment, 8 elements : | 7 |
| 5th increment, 8 elements : | 6 |
| 6th increment, 8 elements : | 5 |
| 7th increment, 8 elements : | 6 |
| 8th increment, 8 elements : | 7 |
| 9th increment, 8 elements : | 5 |
| 10th increment, 8 elements : | 5 |
| 1st refinement, 32 elements : | 11 |
| 2nd refinement, 128 elements : | 6 |
| 3rd refinement, 512 elements : | 3 |
| . . . . . . . . . . . . . . . . . | |
| 6th refinement, 32.768 elements : | 3 |

Table 7.4:  Example 7.2.1.2; number of Newton steps in the single periods.

The number of Newton steps in each single incremental situation does not differ very much from the corresponding number of steps in example 7.2.1.1. Obviously, the further edge rotation has only a small influence on the numbers of Newton steps for these stages. By comparison to the example before, the numbers in the refinement stages, respectively, increase a little bit, in particular for the first two refinement states. This shows that the approximation of the displacement vector and its partial derivatives in the coarser meshes is still far away from the approximations

in the finer triangulations.

### 7.2.1.3 3rd example: Möbiusstrip

For the next example we consider a new, longer plate with a mid surface $\Omega_0^m = [0, 64] \times [-2, 2]$ and a thickness of $0.425$. The boundary conditions are comparable to the one in Example 7.2.1.1 above. In contrast to that example, additionally to the boundary edge transport and the boundary edge normal rotation, a second rotation with an angle $(\pm\pi)$ around the $\eta^1$-axis is defined to both boundary edges of the mid surface in $\eta^2$-direction.

Therefore, a further inhomogeneous Dirichlet boundary condition arises.

The transport and the rotation of the two edges as well as the rotation of the outer normals are simulated at once. Due to that, we have twice as much increments as in all examples before, applying the full prescribed displacement vectors to the two boundaries. Using 20 increments, for the mid surface of the plate after the first Newton iteration we get the slightly deformed mid surface.

To guarantee the convergence of all Newton iterations during the computing process, we apply two mesh refinements. So, in Figure 7.24 the slightly deformed mid surface approximated with 256 elements is displayed.
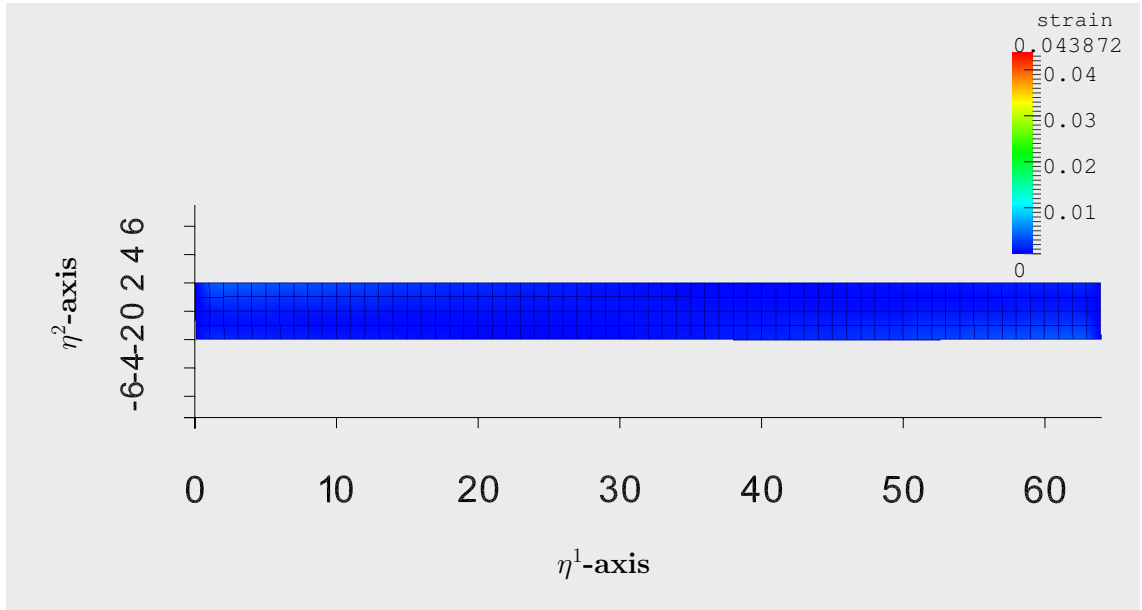


Figure 7.24:  Deformed mid surface, 256 elements, first increment.

After applying all increments we achieve the fully deformed mid surface, approximated with 256 elements in Figure 7.25.
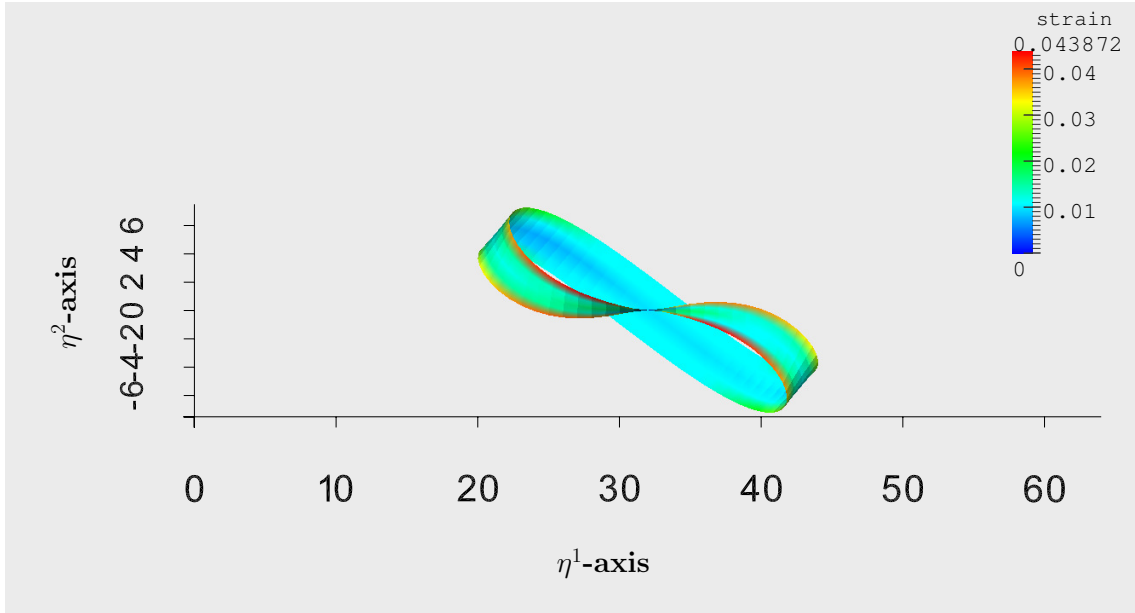
Figure 7.25: Deformed mid surface, 256 elements, full force applied.

Subsequently, three further refinements are carried out. In Figure 7.26 we can see that the computed mid-surface strain is very small over the whole plate.
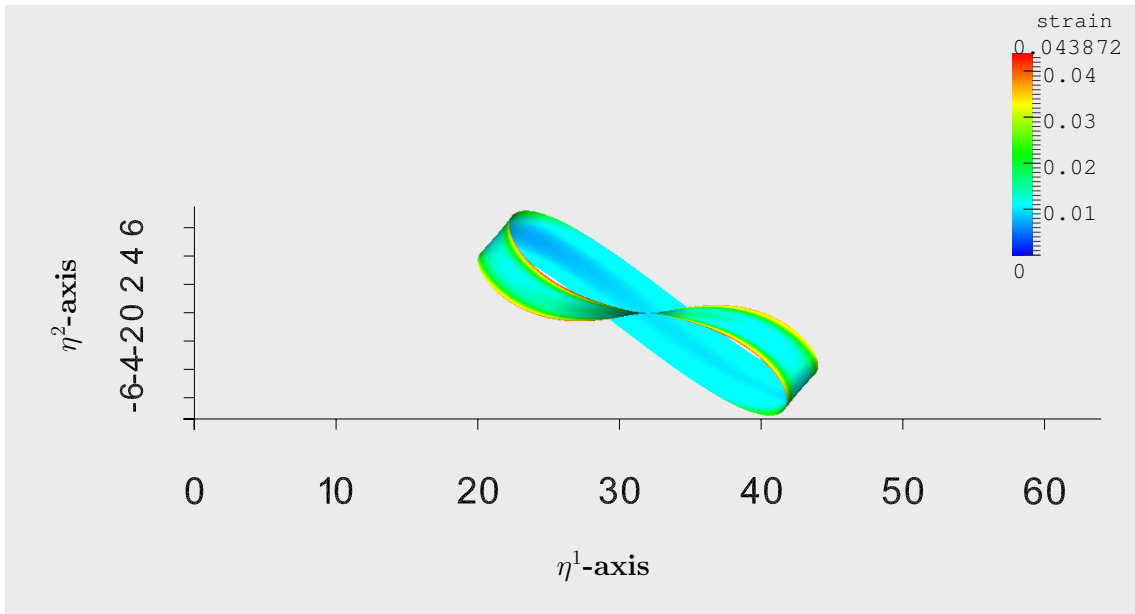


Figure 7.26: Deformed mid surface, 16.384 elements.

Although we apply the transport as well as both rotation angles for the edges in $\eta^2$-direction at the same time, it seems that the simulation does not need more Newton steps per Newton iteration prior reaching the stopping criterion as in the examples before. Certainly, the smaller increments have a positive influence on the

75

number of Newton steps per Newton iteration. Because we have chosen a mesh, which was twice refined before the incrementation takes place, we have a very fast convergence in the refinement stage as can also be seen in the following Table 7.5.

| | |
|---|---|
| 1st increment, 256 elements : | 4 |
| 2nd increment, 256 elements : | 7 |
| 3rd increment, 256 elements : | 6 |
| 4th increment, 256 elements : | 6 |
| 5th increment, 256 elements : | 4 |
| 6th increment, 256 elements : | 4 |
| 7th increment, 256 elements : | 5 |
| . . . . . . . . . . . . . . . . . | |
| 15th increment, 256 elements : | 5 |
| 16th increment, 256 elements : | 4 |
| 17th increment, 256 elements : | 7 |
| 18th increment, 256 elements : | 3 |
| 19th increment, 256 elements : | 6 |
| 20th increment, 256 elements : | 11 |
| 3rd refinement, 1.024 elements : | 3 |
| 4th refinement, 4.096 elements : | 2 |
| 5th refinement, 16.384 elements : | 2 |

Table 7.5:  Example 7.2.1.3; number of Newton steps in the single periods.

At the end of this example we show the deformation progress in Figure 7.27, in that the approximated mid surface in all increment stages as well as the most refined mid surface is displayed.
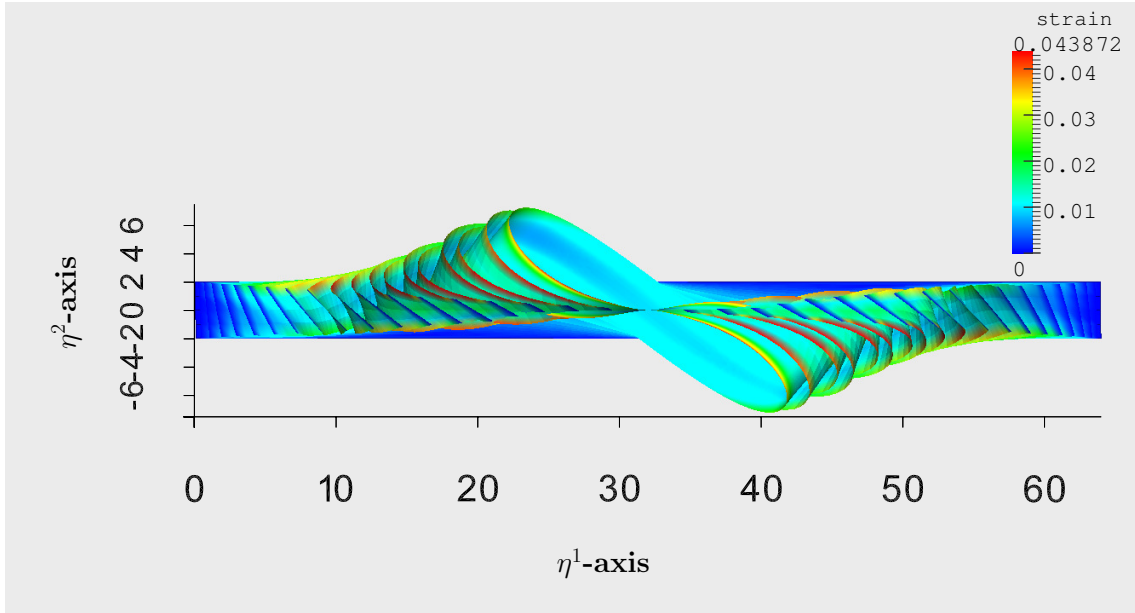
Figure 7.27: Möbiusstrip, deformation progress.

### 7.2.1.4 4th example: Plate with twisted edge

This example considers the same initial plate as it was considered in Example 7.2.1.3, before. But we change the boundary conditions. For the left edge of the mid surface the values for the boundary displacement vector and its derivatives are fixed to zero, except for its first component $U^{(1)}$, which is left free.
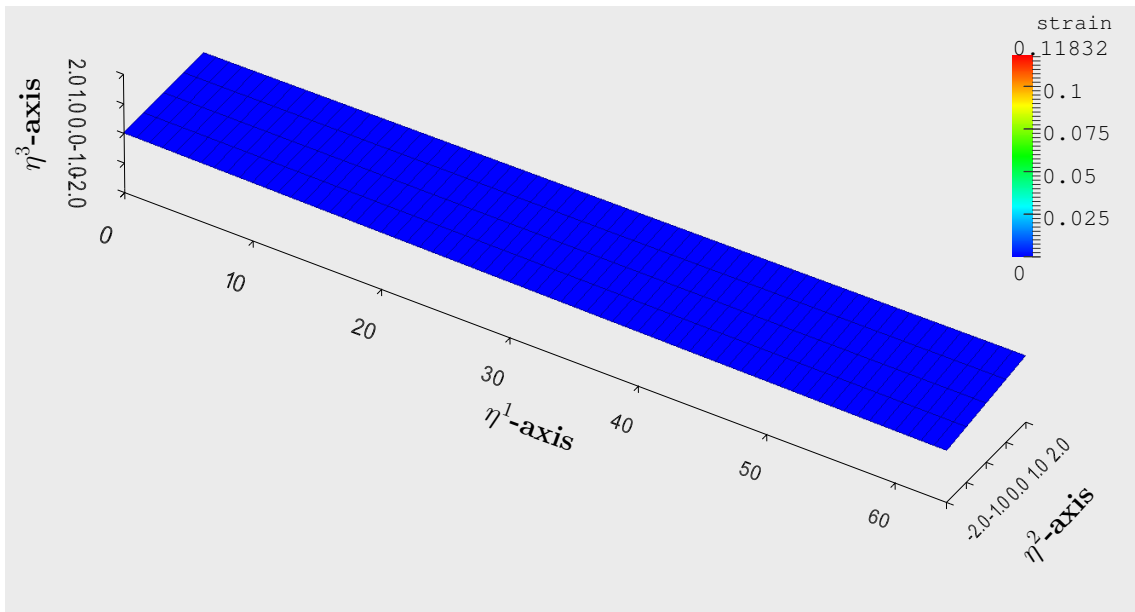


Figure 7.28: Deformed mid surface, 256 elements, first increment.

For the right boundary edge $(64, \eta^2, 0)$ of the mid surface we apply inhomogeneous Dirichlet boundary conditions so that a rotation around the $\eta^1$-axis until $4\pi$ is carried out.

This rotation is applied with 100 increments, which is much more than in all examples, above. The deformed mid surface approximated with again 256 elements in the first increment is displayed in Figure 7.28.
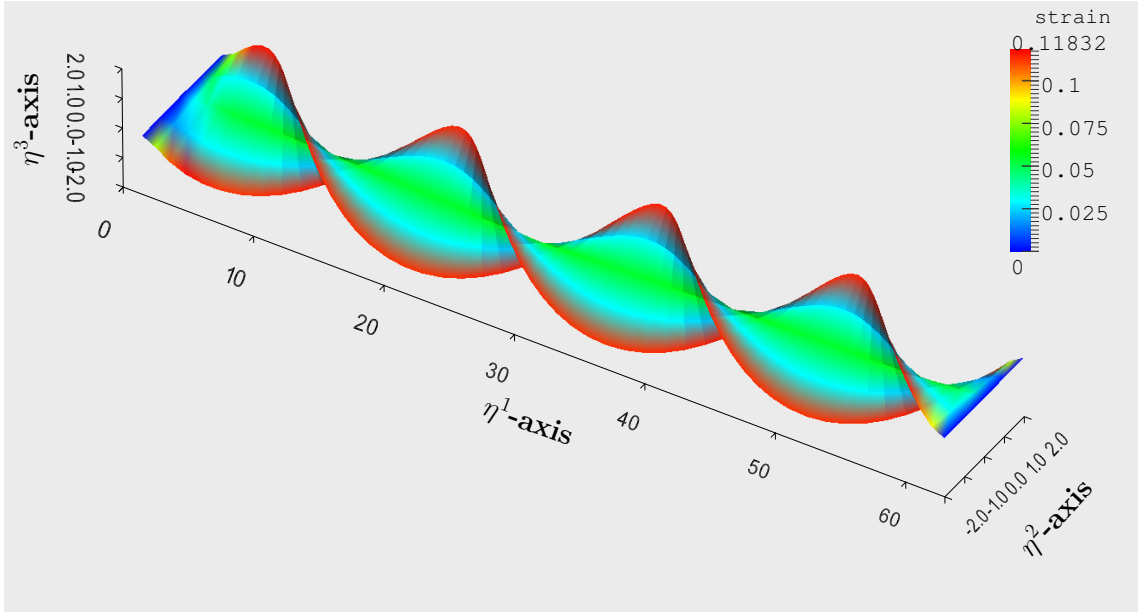


Figure 7.29: Deformed mid surface, 256 elements, full rotation of $4\pi$ applied.
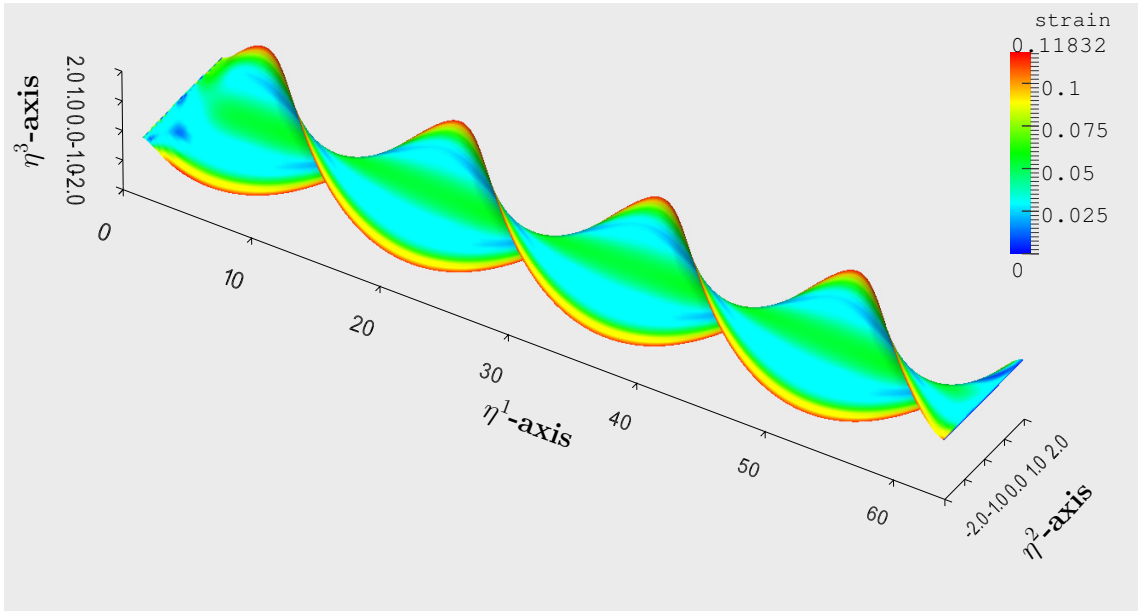


Figure 7.30: Deformed mid surface, 16.384 elements.

After the application of all increments the fully deformed mid surface, consisting of 256 elements, can be seen in Figure 7.29.

After further three refinements the deformed mid surface now is approximated with 16.384 elements. It is to be seen in Figure 7.30.

As before, we observe the norm of the strain tensor being small over the whole plate. However, the maximum of the strain tensor is nearly twice the corresponding value in the other bending-dominated examples. The largest strain is generated at the free boundary edges in $\eta^1$-direction. Expectedly, the left edge in $\eta^2$-direction is shifted around 1.5 in direction of the $\eta^1$-axis.

|  |  |
|---|---|
| 1st increment, 256 elements : | 4 |
| . . . . . . . . . . . . . . . . . | |
| $41st$ increment, 256 elements : | 4 |
| $42nd$ increment, 256 elements : | 5 |
| . . . . . . . . . . . . . . . . . | |
| 66th increment, 256 elements : | 5 |
| 67th increment, 256 elements : | 4 |
| . . . . . . . . . . . . . . . . . | |
| 100th increment, 256 elements : | 4 |
| 3rd refinement, 1.024 elements : | 6 |
| 4th refinement, 4.096 elements : | 5 |
| 5th refinement, 16.384 elements : | 5 |

Table 7.6:   Example 7.2.1.4; number of Newton steps in the single periods.

The number of Newton steps per Newton iteration is relatively constant 4 or 5 in the incremental stage, as can be seen in Table 7.6, due to the large number of increments, we had to choose for applying the full rotation angle. The constant numbers of Newton steps in each mesh refinement may are indicators for heavier problems in computing a larger rotation of edges around a vector, which is not directed along the considered edge. In contrast to that, we could observe a decreasing number of Newton steps for at least the last two refinements to three or even two

in all examples before.

## 7.2.2 Approximation with FEM using reduced HCT-elements

### 7.2.2.1 1st example: Partly divided annular octagonal plate

Starting point for the approximation of the deformation for this example is the octagonal mid surface with a diameter of 2 in both, $\eta^1$- and $\eta^2$-direction. The initial triangulation of the mid surface consists of 12 elements as can be seen in Figure 7.31.
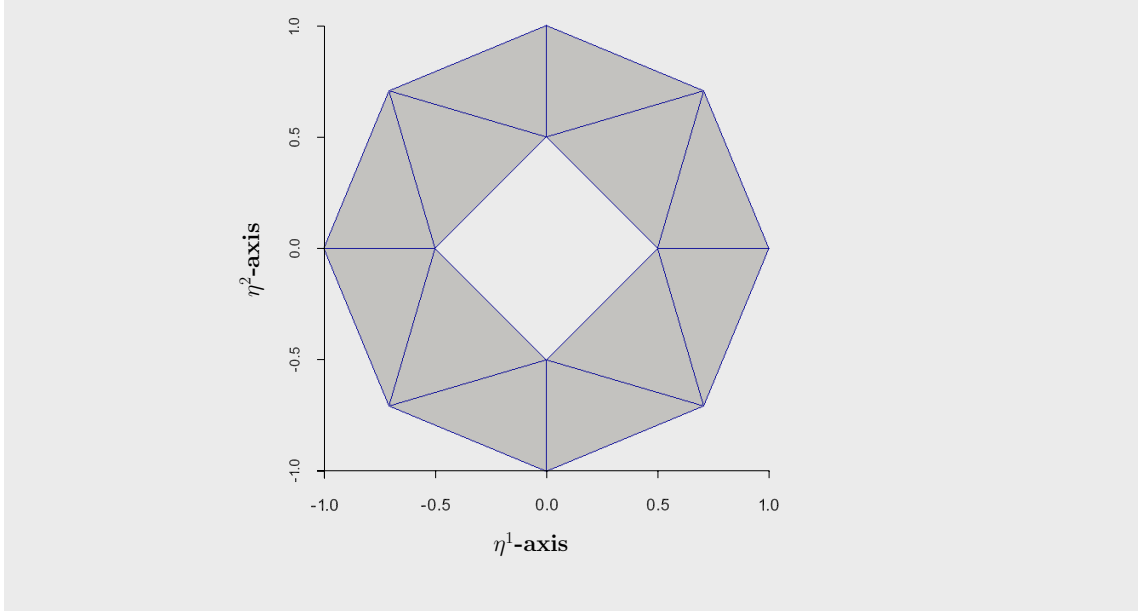


Figure 7.31: Undeformed mid surface, 12 elements.

The mid surface of the plate is cut along the edge from $(0, 0.5, 0)^\top$ to $(0, 1, 0)^\top$, yielding two edges with inhomogeneous Dirichlet type boundary conditions. Only the outer normals of these both boundaries are rotated throughout the simulation by

$$\boldsymbol{U}_{,1} = \left( \mp (1 - \cos t), 0, \pm \sin t \right)^\top \tag{7.3}$$

with the incremental parameter $t \in \left[ 0, \frac{\pi}{2} \right]$. The full rotation angle is applied in 10 incremental steps. The remaining edges are left free.

After applying the first increment, we get a slightly deformed mid surface, in that the outer normals of the emerged boundary edges have rotated a little bit. Due to that, the outer boundary is bending upwards. We have applied one mesh refinement in order to secure the convergence of Newton's method during the incremental stage. The mid-surface strain is very small in this stage, which can be seen in Figure 7.32.
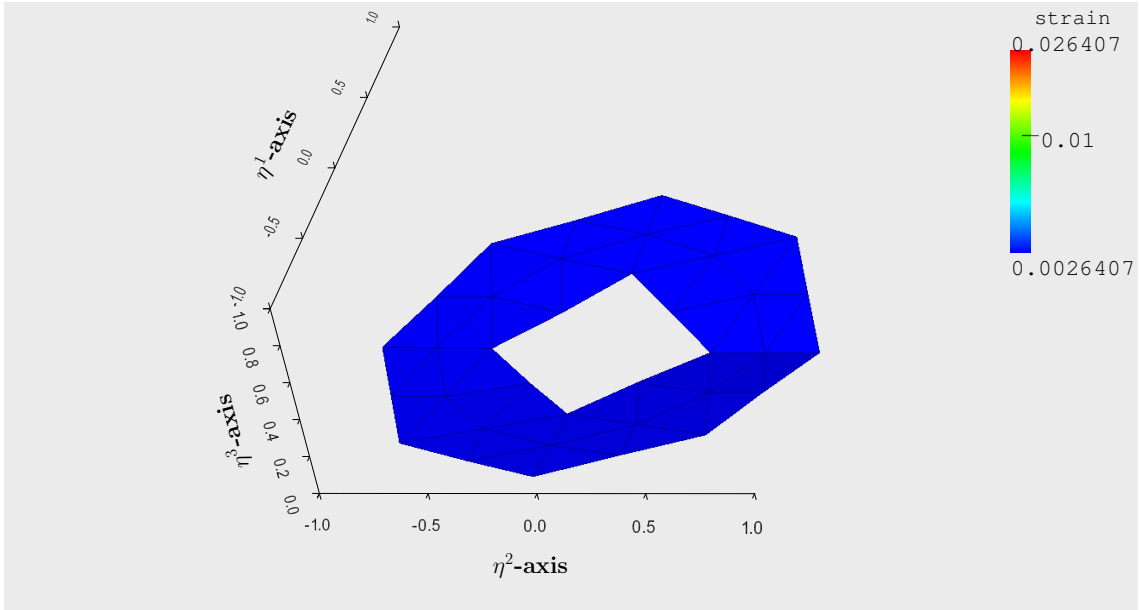
Figure 7.32:  Deformed mid surface, 48 elements, 1 increment.

Now we have to increase the increment until the full rotation angle is applied. In that way, we get a heavily deformed mid surface, which is displayed in Figure 7.33.
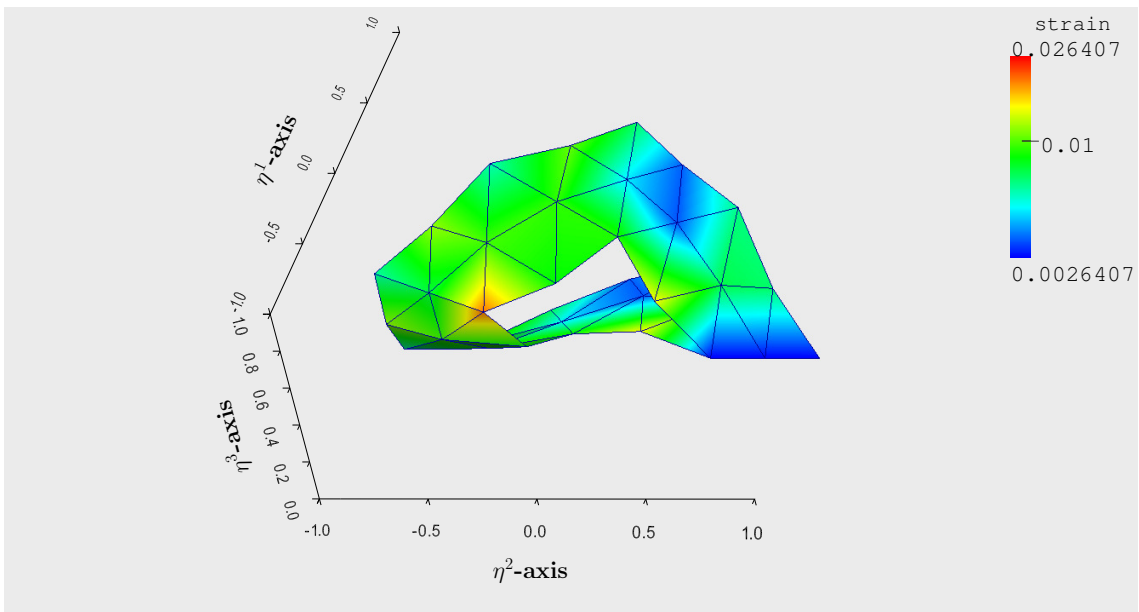


Figure 7.33:  Deformed mid surface, 48 elements, full force applied.

After three consecutive refinements we obtain a subdivided mid surface with 3.072 elements. As seen in Figure 7.34 the norm of the strain tensor is bounded by about 0.02.
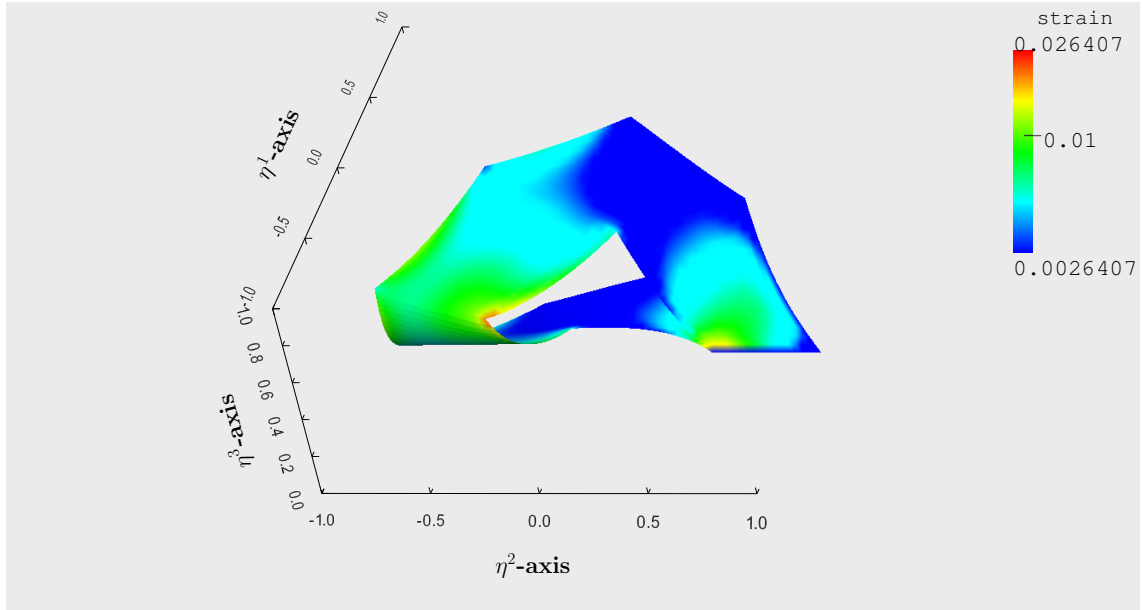
Figure 7.34:  Deformed mid surface, 3.072 elements, full force applied.

Another refinement step and a further solved Newton iteration yields the deformed mid surface, displayed with 12.288 elements in Figure 7.35.
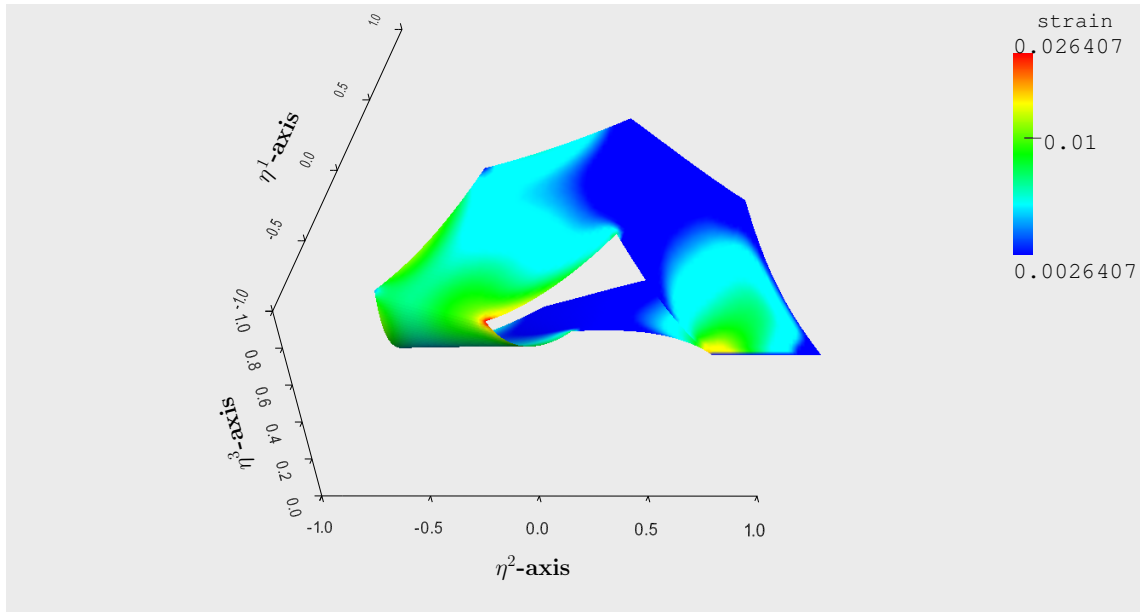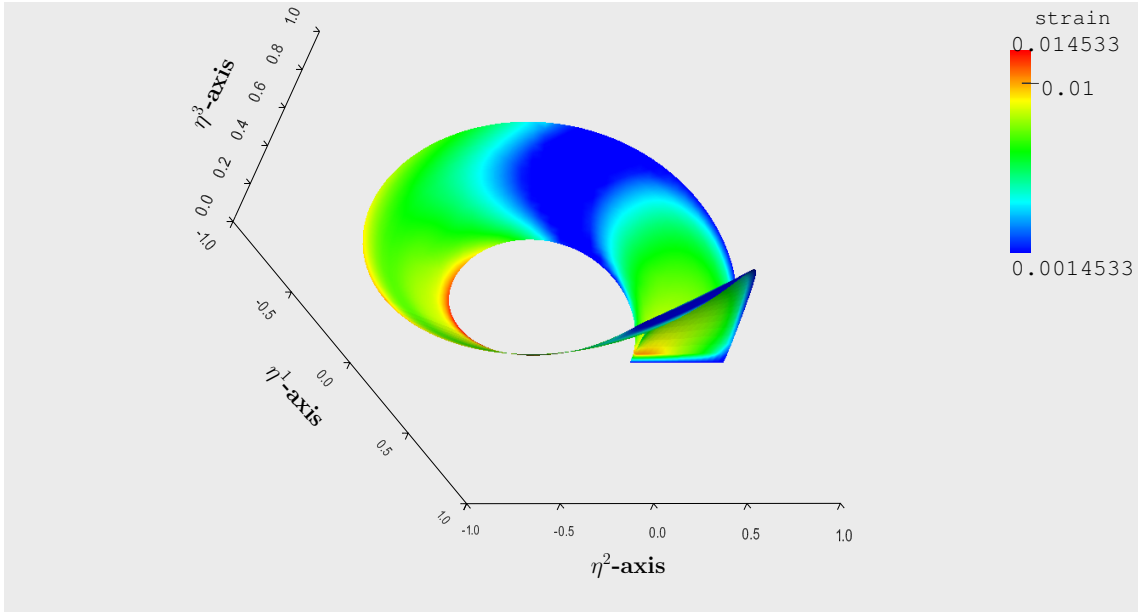


Figure 7.35:  Deformed mid surface, 12.288 elements, full force applied.

Here, the maximum of the norm of the strain tensor is about 0.0264.  This is much less than in the deflection example in Section 7.1.2.

For the approximation progress the following numbers of Newton steps were needed for the Newton iteration in every incremental and every refinement stage.

| | |
|---|---|
| 1st increment, 12 elements : | 12 |
| 1st increment, 48 elements : | 8 |
| 2nd increment, 48 elements : | 7 |
| 3rd increment, 48 elements : | 6 |
| 4th increment, 48 elements : | 6 |
| 5th increment, 48 elements : | 5 |
| 6th increment, 48 elements : | 5 |
| 7th increment, 48 elements : | 5 |
| 8th increment, 48 elements : | 4 |
| 9th increment, 48 elements : | 4 |
| 10th increment, 48 elements : | 6 |
| 2nd refinement, 192 elements : | 8 |
| 3rd refinement, 768 elements : | 8 |
| 4th refinement, 3.072 elements : | 4 |
| 5th refinement, 12.288 elements : | 3 |

Table 7.7:  Example 7.2.2.1; number of Newton steps in the single periods.

For this example, the number of Newton steps is similar to the numbers in the second example for bending problems using BFS-elements, Example 7.2.1.2, although the rotation angle here is only one third the rotation angle in the named example, respectively.

Obviously, using HCT-elements may be more problematic than using BFS-elements, due to the discussion in section 6.5, which is seen in the relatively high number of Newton steps for the second and for the third refinement.

### 7.2.2.2 2nd example: Divided annulus with rotated edge normals

For the last example we consider an annulus. This is similar to the plate in Example 7.2.2.1, above, but with a curved inner and outer boundary. The diameter is 2 again and the annulus is cut at the same edge, as the octagonal plate, before. The two new edges have inhomogeneous Dirichlet boundary conditions. All other edges are left free.

The undeformed mid surface looks alike the respective one in the example above, displayed in Figure 7.31.

The outer normals of the two arose straight edges are rotated in the same way as in the example before, applying equation (7.3).

For this rotation a serious problem occurs. The incrementation was successfully done for 80 or more increments. Unfortunately, after the full rotation angle was applied, the Newton iteration fails for the first refinement, due to both, the special refinement technique and the curved boundary.

A way out was changing the procedural method. So, first we apply four refinements in the first incremental stage. After that, we get a slightly deformed mid surface approximated with 3.072 elements, displayed in Figure 7.36.
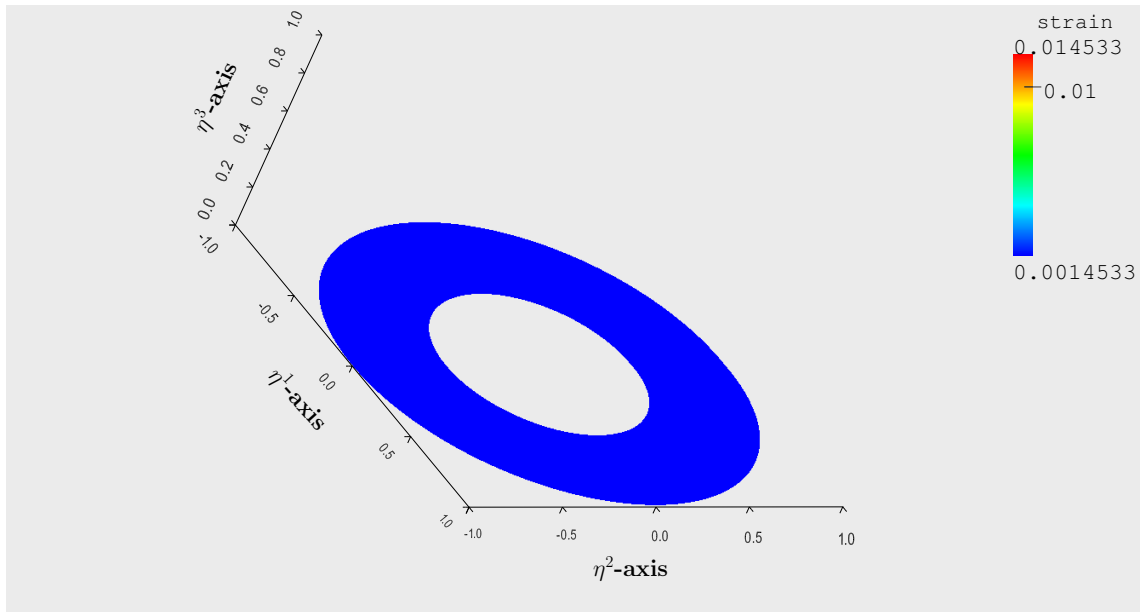


Figure 7.36: Deformed mid surface, 3.072 elements, 1 increment.

From the same reason as discussed in section 6.5, here the incrementation starts at a more refined mesh than before. The result can be seen in Figure 7.37.

Figure 7.37:  Deformed mid surface, 3.072 elements, full force applied.

The maximum of the norm of the strain tensor is about 0.0145. This is a little bit shorter than in Example 7.2.2.1 using 12.288 elements (Figure 7.35). It appears in the same region as in the example, above. Unfortunately, the computing time is much higher than in the example before, due to the large number of increments and the change of the sequence of incrementation and refinement.
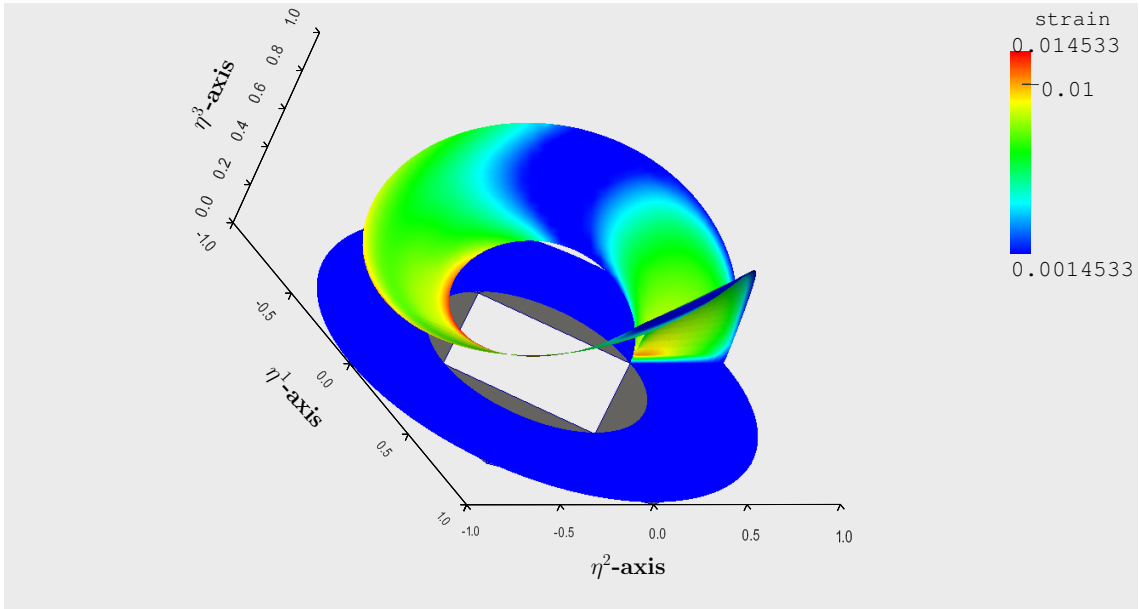


Figure 7.38:  Cut slab, deformation progress, 3.072 elements.

In Figure 7.38 the mid surface is displayed in the undeformed state using 12

elements and in the first incremental stage as well as in the refined period with 3.072 elements, respectively, for the imagination of the deformation progress.

The number of Newton steps for each stage of the simulation is shown in the following Table 7.8.

| | |
|---|---|
| 1st increment, 12 elements : | 6 |
| 1st increment, 48 elements : | 6 |
| 1st increment, 192 elements : | 5 |
| 1st increment, 768 elements : | 5 |
| 1st increment, 3.072 elements : | 5 |
| . . . . . . . . . . . . . . . . | |
| 4th increment, 3.072 elements : | 5 |
| 5th increment, 3.072 elements : | 4 |
| . . . . . . . . . . . . . . . . | |
| 10th increment, 3.072 elements : | 4 |
| 11th increment, 3.072 elements : | 3 |
| . . . . . . . . . . . . . . . . | |
| 80th increment, 3.072 elements : | 3 |

Table 7.8:  Example 7.2.2.2; number of Newton steps in the single periods.

Due to the problems discussed in section 6.5, here it was necessary to perform more mesh refinements in the beginning, before the incrementation starts. Unfortunately, this enlarges the total operating expense drastically. Nevertheless, the number of Newton steps is not much higher for one Newton iteration as in the examples before.

In summary we can determine that in the examples for BFS-elements we have a smaller number of Newton steps per Newton iteration than in the examples for the reduced HCT-elements. This effect is observable, due to the nested function spaces for the form functions. Unfortunately the BFS-elements are only usable for examples with axis-parallel edges.

Contrary, the HCT-elements are more flexible and can also be used for curved boundaries. But due to the discussion in section 6.5 there occur other problems to overcome. Because of the many different demands to a finite element, one would never find an element, which is the best for all the examples, at the same time.

# 8 Outlook and open questions

The main focus of this work is on the numerical simulation of large deformations of thin plates. Therefore, we consider a non-linear plate theory with a non-linear material law. Additional simplifications have been set aside. The displacement vector function is derived from a non-linear system of equations, which emerges from the equilibrium of forces. The reduction of dimension to the mid surface requires a plate assumption. Here, we use the Kirchhoff hypothesis, where no change in thickness direction is allowed during the deformation process. The basic principle for the simulation is the minimization of the energy functional over the deformed plate. This implies that the first derivative of this energy functional vanishes. For solving this non-linear system of equations Newton's method is applied, which necessitates the calculation of the second derivative of the energy functional. Its calculation and the efficient use in the F.E.-simulation was one of the most difficult parts within this work. As a result of each Newton iteration we obtain a correction term for the displacement vector function. Some examples for plates of different sizes and for different kinds of deformation are presented.

One starting point for additional research can be the weakening of the Kirchhoff hypothesis. Therefore let us consider the deformed plate as

$$\boldsymbol{x}(\eta) = \boldsymbol{Y}(\eta^1, \eta^2) + \boldsymbol{U} + h\tau\boldsymbol{d}$$

with an arbitrary direction vector $\boldsymbol{d}$ independent of $\boldsymbol{U}$, which is no longer restricted to be perpendicular to the deformed mid surface. In linear elasticity such a model is known as Mindlin-Reissner plate. Additionally, the straight line $h\tau\boldsymbol{d}$ can be replaced by non-linear curves depending on $\tau$, which is known as hierarchical shell models. For both approaches more degrees of freedom have to be taken into account. Unfortunately, new difficulties for the Finite-Element-practice arise.

Another research issue is the development of an adaptive approach for the FEM. For that an error estimator is needed. In [20] a basis for an error functional in the linear and in the non-linear case is provided for the full 3D theory. At present, the development of an error estimator for shells and plates and linear problems is in progress. In future, potential results have to be transferred to the non-linear case.

# Bibliography

[1] S. S. Antman. *Nonlinear Problems of Elasticity.* Springer, Berlin, Heidelberg, New York, 2nd edition, 2005.

[2] Y. Basar and W. Krätzig. A Consistant Shell Theory for Finite Deformations. *Acta Mechanica*, 76:73–87, 1989.

[3] M. Bischoff, W. A. Wall, K.-U. Bletzinger, and E. Ramm. Models and Finite Elements for Thin-walled Structures. *Encyclopedia of Computational Mechanics*, 2:59–137, 2004.

[4] J.P. Boehler. Applications of Tensor Functions in Solid Mechanics. *International Center for Mechanical Science (CISM Courses)*, 292, 1987.

[5] D. Braess. *Finite Elements: Theory, Fast Solvers and Applications in Solid Mechanics.* Cambridge University Press, Cambridge, 3rd edition, 2007.

[6] I. H. Bramble, J.E. Pasciak, and J. Xu. Parallel Multilevel Preconditioners. *Mathematics of Computation*, 55:1–22, 1990.

[7] D. Chapelle and K.-J. Bathe. *The Finite Element Analysis of Shells - Fundamentals.* Springer, Berlin, Heidelberg, 2003.

[8] P. G. Ciarlet. An Introduction to Differential Geometry with Application to Elasticity. *Journal of Elasticity*, 78-79:1–215, 2005.

[9] P. G. Ciarlet and P. Dstuynder. A Justification of a Nonlinear Model in Plate Theory. *Computer Methods in Applied Mechanics and Engineering*, 17/18:227–258, 1979.

[10] P.G. Ciarlet. *The Finite Element Method for Elliptic Problems.* North-Holland, Amsterdam, 1978.

[11] P.G. Ciarlet. *Mathematical Elasticity Volume I: Three Dimensional Elasticity.* North-Holland/Elsevier, Amsterdam, 1988.

[12] P.G. Ciarlet. *Mathematical Elasticity Volume II: Theory of Plates.* North-Holland/Elsevier, Amsterdam, 1997.

[13] W. Dahmen, P. Oswald, and Shi Xi-Quan. $C^1$-Hierarchical Bases. *Journal of Computational and Applied Mathematics*, 51:37–56, 1994.

[14] V. V. Eliseev and Y. M. Vetyukov. Finite Deformation of Thin Shells in the Context of Analytical Mechanics of Material Surfaces. *Acta Mechanica*, 209:43–57, 2010.

[15] Ch. Großmann and H.-G. Roos. *Numerical Treatment of Partial Differential Equations.* Springer, Berlin, Heidelberg, New York, 2007.

[16] M. Jung and U. Langer. *Methode der Finiten Elemente für Ingenieure – Eine Einführung in die Numerischen Grundlagen und Computersimulation.* Teubner, Stuttgart, Leipzig, Wiesbaden, 2001.

[17] H. Matthes. *Die nichtüberlappende Gebietszerlegungsmethode zur Parallelisierung und Vorkonditionierung iterativer Verfahren zur Lösung von Platten- und Schalenproblemen.* PhD thesis, TU Chemnitz, Chemnitz, 1996.

[18] A. Meyer. Efficient Preconditioners for Special Situations in Finite Element Computations. *Lecture Notes in Computational Science and Engeneering (LNCSE)*, 52:67–85, 2006.

[19] A. Meyer. Grundgleichungen und Adaptive Finite-Elemente-Simulation bei „Großen Deformationen". *Chemnitz Scientific Computing Preprints*, 02:1–6, 2007.

[20] A. Meyer. Error Estimators and the Adaptive Finite Element Method on Large Strain Deformation Problems. *Mathematical Methods in the Applied Sciences*, 32:2148–2159, 2009.

[21] A. Meyer. The Koiter Shell Equation in a Coordinate Free Description. *Chemnitz Scientific Computing Preprints*, 02:1–4, 2012.

[22] A. Meyer. A Simplified Calculation of Reduced HCT-Basis Functions in a Finite Element Context. *Computational Methods in Applied Mathematics (CMAM)*, 12(04):486–499, 2012.

[23] A. Meyer and J. Rückert. $C^1$-continuous FEM for Kirchhoff Plates and Large Deformation. *Journal of Applied Mathematics and Mechanics, (ZAMM), submitted*, 92, 2012.

[24] A. Meyer and J. Rückert. Kirchhoff Plates and Large Deformation. *Chemnitz Scientific Computing Preprints*, 01, 2012.

[25] A. Meyer and J. Rückert. Large Deformation and Plates. *Proceedings in Applied Mathematics and Mechanics (PAMM)*, 12:669–670, 2012.

[26] P. Oswald. Hierarchical Conforming Finite Element Methods for the Biharmonic Equation. *Siam Journal Numerical Analysis*, 29(6):1610–1625, 1992.

[27] M. Thess. Parallel Multilevel Preconditioners for Thin Smooth Shell Finite Element Analysis. *Numerical Linear Algebra with Applications*, 5:401–440, 1998.

[28] M. Thess. *Parallel Multilevel Preconditioners for Thin Smooth Shell Problems*. PhD thesis, TU Chemnitz, Chemnitz, 1998.

[29] H. Yserentant. Two Preconditioners Based on the Multilevel Splitting of Finite Element Spaces. *Numerical Mathematics*, 58:163–184, 1990.

# Notation

| | |
|---|---|
| $\eta = (\eta^1, \eta^2, \eta^3)$ | coordinate system |
| $\eta^i$ | $i$-th coordinate |
| $\tau = \eta^3$ | thickness coordinate |
| $\Omega_0$ $(\Omega)$ | domain of a undeformed (deformed) shell/plate |
| $\Omega_0^m$ $(\Omega^m)$ | domain of the mid surface of a undeformed (deformed) shell/plate |
| $\partial\Omega_0$ $(\partial\Omega)$ | boundary of a undeformed (deformed) shell/plate |
| $\Gamma_{0,N}$ | Neumann boundary part of the undeformed shell/plate |
| $\Gamma_D$, $\Gamma_N$ | Dirichlet and Neumann boundary part of the deformed shell/plate |
| $\boldsymbol{X}(\eta)$ $(\boldsymbol{x}(\eta))$ | material point of the undeformed (deformed) domain |
| $\boldsymbol{Y}(\eta^1, \eta^2)$ $(\boldsymbol{y}(\eta^1, \eta^2))$ | material point of the undeformed (deformed) mid surface |
| $\boldsymbol{G}_i$, $\boldsymbol{G}^i$ $(\boldsymbol{g}_i, \boldsymbol{g}^i)$ | covariant and contravariant tensor base of the undeformed (deformed) domain |
| Grad (grad) | gradient operator in the undeformed (deformed) domain |
| div | divergence operator |
| $\boldsymbol{U}, \boldsymbol{V}, \boldsymbol{U}^{KH}, \boldsymbol{\delta U}$ | vector functions |
| $\mathcal{F}$ | deformation gradient |
| $(\underline{C}, \underline{c},)\, \mathcal{C}, \widehat{\mathcal{C}}$ | (matrix of the) right Cauchy-Green deformation tensor |

| | |
|---|---|
| $I_{\mathcal{C}}, II_{\mathcal{C}}, III_{\mathcal{C}}$ | principal invariant of the right Cauchy-Green deformation tensor |
| $a_i, \quad i = 1, 2, 3$ | functions of the principal invariants of the right Cauchy-Green deformation tensor |
| $(\underline{E}, \underline{e},) \mathcal{E}, \widehat{\mathcal{E}}$ | (matrix of the) Lagrangian strain tensor |
| $\boldsymbol{A}_i (\boldsymbol{a}_i)\ i = 1, 2$ | tangential vectors of the undeformed (deformed) mid surface |
| $\boldsymbol{A}_3 (\boldsymbol{a}_3)$ | normal of the undeformed (deformed) mid surface in thickness direction |
| $\underline{A}, \underline{B}\ (\underline{a}, \underline{b})$ | matrix of the first end second fundamental forms in the undeformed (deformed) domain |
| $\overset{1}{\mathcal{T}}, \overset{2}{\mathcal{T}}$ | first and second Piola-Kirchhoff stress tensor |
| $\overset{2}{\underline{T}}$ | matrix of the second Piola-Kirchhoff stress tensor |
| $\mathcal{I}, \mathfrak{I}$ | identity tensor of 2nd and of 4th order |
| $\mathfrak{C}$ | 4th order tensor, material tangent |
| $\sigma$ | Cauchy stress tensor |
| $\rho$ | material density |
| $p$ | outer acceleration |
| $l'(\boldsymbol{U}; \boldsymbol{V})$ | Fréchet derivative of functional $l(\boldsymbol{U})$ in direction of $\boldsymbol{V}$ |
| $l''(\boldsymbol{U}; \boldsymbol{\delta U}, \boldsymbol{V})$ | Fréchet derivative of functional $l'(\boldsymbol{U}; \boldsymbol{V})$ in direction of $\boldsymbol{\delta U}$ |
| $\boldsymbol{\mathcal{N}} (\boldsymbol{n})$ | normal vector of the undeformed (deformed) domain in the 3D-theory |
| $a(\boldsymbol{U}; \boldsymbol{V}),\ f(\boldsymbol{V})$ | $a$-form and force vector for the variational formulation |
| $\mathcal{L}(\boldsymbol{V})$ | special defined differential operator applied on $\boldsymbol{V}$ |

| | |
|---|---|
| $\mathbb{T}_h$ | FE-mesh of the mid surface |
| $T$ | finite element |
| $\mathbb{V}_h$ | finite function space of the actual mesh $\mathbb{T}_h$ |
| $\boldsymbol{U}_h$, $\boldsymbol{V}_h$, $\boldsymbol{\delta U}_h$ | finite dimensional vector functions from $\mathbb{V}_h$ |
| $\underline{u}$, $\underline{v}$, $\underline{\delta u}$ | coefficients of the corresponding vector functions |

# Theses

(1) We introduce the 3D-theory for large deformations and describe the common non-linear shell theory. We restrict us to the plate, a shell, which is flat in the initial state. Both theories combined with the Kirchhoff hypothesis lead to a strain tensor $\mathcal{E}$ of lower rank 2 and to the non-linear weak formulation of the boundary value problem.

(2) The numerical solution of the non-linear boundary value problem obtained in the weak formulation requires both a Newton-linearization and a Finite Element-approximation. For a correct Newton iteration the second derivative of the energy functional has to be established. Its implementation in generating the element matrices after the F.E.-discretization is the main difficulty for obtaining an efficient simulation.

(3) For the F.E.-discretization the BFS-element as well as the reduced HCT-element have been considered, which both satisfy the special requirements for a $C^1$-continuous treatment.

(4) A collection of various examples illustrates the flexibility of the considered approach. The plate deflection examples are given for the validation of the code in comparing with small strain and for displaying the fast convergence of the method. The individual bending-dominated examples were the principal reason for this research and display the potential as well as the limits of the method. Some limits of the finite elements used are discussed additionally.

(5) This work can be used as a starting point for additional research. For example, the use of other $C^1$-continuous elements or a non-conformal approach could be investigated. Additionally, the weakening of the Kirchhoff hypothesis would require $C^0$-continuous elements only, but implies other numerical difficulties. Furthermore, an error estimator would allow adaptive mesh refinement, which increases the total efficiency.

# List of Figures

# List of Tables